Eye Tracking with EEG life-style

By

Mohammad Reza Haji Samadi

A Thesis Submitted to
The University of Birmingham
for the Degree of
Doctor of Philosophy

School of Electronic, Electrical
and System Engineering
College of Engineering
and Physical Sciences
The University of Birmingham
September 2015

Abstract

Innovative human-computer interaction paradigms with minimum motor control provide realistic interactions and have potential for use in assistive technologies. Among the human modalities, the eyes and the brain are the two modalities with minimum motor requirements. Most of the existing assistive technologies based on tracking the eyes (such as electrooculography and videooculography) are intrusive, limited to the laboratory environment and restrictive or are not accurate enough for real-life applications. The same limitations apply to brain activity monitoring systems such as electroencephalography (EEG).

In this research, the objective is to employ a less-intrusive, consumer-grade EEG headset designed for mobile applications to track the user's eyes and reliably estimate focus of foveal attention (FoA). To this end, signal processing approaches are proposed in order to classify different types of eye movements and estimate FoA. The FoA estimation is then improved using the brain responses to flickering stimuli recorded in EEG data. Afterwards, the FoA estimation is again improved by proposing an automated method to remove eye-related artefacts from brain responses to the stimuli. Finally, the FoA estimation is best improved by extracting eye-movement classification and brain-response detection features from EEG data projected into independent sources. A matched set of videooculography/EEG data is recorded to evaluate the proposed signal processing approaches. The work envisages eye-tracking technologies that utilise non-facially intrusive EEG brain sensing via dry contact scalp-based electrodes, an approach that has found various applications in EEG signal processing and eye tracking.

To Imam Muhammad al-Baqir (PBUH)

Acknowledgements

I praise God for all His mercy and grace, and the chance that he has given us to discover its laws. I would like to thank Dr. Neil Cooke, the supervisor of this research, for the scientific and moral guidance of this work. I would like to thank my parents, for all their support and encouragement throughout my life. I would like to thank my beloved wife Marziehsadat for all her love and patience. I would like to thank my sisters, for all their support. I would like to thank all the teachers and professors that I have had throughout my life. I would also would like to thank my dear friends and colleagues, especially Zohreh, Farzad, Masoud and Yasin who helped me through completion of my work.

Contents

List of Figures

List of Tables

List of Abbreviations

BA Balanced-Accuracy

BSS Blind Source Separation

CC Cross Correlation

EEG Electroencephalography

EOG Electrooculogram

ERP Event Related Potentials

Ex-Info Extended-Infomax

FoA Focus of Foveal Attention

ICA Independent Component Analysis

IC Independent Component

KNN K Nearest Neighbour

NB Naive Bayesian

PCC Pearson product-moment correlation coefficient

PSD Power Spectral Density

RBF Radial Basis Function

RMSE Root Mean Square Error

SSVEP Steady-State Visual Evoked Potentials

SVM Support Vector Machine

VOG Video-oculography

"A good question is [already] half of knowledge."

Hasan ibn Ali (PBUH)

1 Introduction

In recent years, there has been a significant increase in the development of assistive technologies and innovative interfaces based on human modalities such as the eye (gaze) [1], touch[2], speech[3] and the brain[4]. Thus, traditional computer inputs are being supplemented or replaced by others that promise richer, more realistic human-computer interaction (HCI) schemes for both healthy people and those with severe disabilities.

Generally, all HCI systems are challenging in terms of ensuring the user's acceptance of the interaction apparatus and achieving accurate performance from both the hardware and the signal processing mechanism. Users prefer to use HCI methods that are affordable, comfortable, less intrusive, highly portable and non-restrictive. The methods should also require minimal personal calibration and operate with sufficient accuracy and speed.

Among the new interaction methods, eye-tracking systems and brain-computer interfaces (BCI) can be considered as the final frontiers, and they are gaining more interest in recent HC researches [5, 4]. This is due to the minimum motor control requirement of BCI and eye-tracking systems, which makes the interaction possible for both healthy people and those with limited motor control or severe disabilities.

The brain is the centre of the human nervous system; it exerts control over the other organs of the body and all human actions and cognitive states [6]. Humans use their eyes to gain information about their environment. As a result, the underlying patterns in both brain activity and eye movement can distinguish among activities [7, 8].

1.1 Eye Tracking

Occurrence of different types of eye movements and estimating the focus of foveal attention (FoA) are main aspects that are used in eye-based interactions. To date a variety of techniques have been developed for eye-tracking [9]. The common peripherals to use eyes in an interaction system are Electrooculogram (EOG) and videooculography (VOG). Both methods are mostly limited to laboratory setups or are socially intrusive and their users feel inconvenienced when use them.

1.2 Electroencephalography

The brain activities are usually detected by measuring electrical activity of the brain over the scalp using electroencephalography (EEG). Brain signal processing via EEG provides two additional sources of eye movement information: Oculomuscular movements via EOG and the brain's response to flickering stimuli - the Steady-State Visual Evoked Potential (SSVEP) [10]. SSVEP is the electrical response of the brain to a flickering stimulus and provides a means to detect a person's FoA without the use of an eye tracker. The quality of EEG signals is usually contaminated by different types of artefacts. The EOG activity resulting from eye movements and blinking is the main source of artefacts which degrade

the quality of the EEG signal.

The Blind Source Separation (BSS) technique Independent Component Analysis (ICA) has been successfully applied on EEG data to separate such artefacts [11]. Although it can estimate independent components/sources it does not label them. Automatic labelling of artefactual components for omission from the EEG signal reconstructed from components is a current research topic [12] [13]. In addition to the artefacts, when users are exposed to prolonged flashing stimuli there is a gradual decrement in their SSVEP response and thus SSVEP detection - an effect known as *habituation* [14].

1.3 EEG Apparatus

Although EEG-based BCIs have been studied for more than 40 years [15], most BCI research efforts remain at the stage of laboratory demonstration. Most studies in EEG and EOG signal processing are motivated by Neuroscience and BCI rather than eye tracking; eye movement is seen as an unwanted artefact. They normally use laboratory grade EEG devices with a high number of channels (e.g. 64), each channel being sensed by a wet-contact electrode. Scalp-based electrodes are normally complemented by others on the face and chest to assist with artefact rejection. Consequently, such systems are costly and not suited for wearable applications.

To bridge this gap and use EEG devices in real-life applications some important issues need to be addressed; the performance must be reliable - between person variation and signal artefacts must be adequately handled by the signal processing techniques. The device should also be affordable and easy to use. Because of growing interest in using BCI for gaming and other consumer applications, several manufacturers are currently offering commercial portable EEG devices [16]. The emergence of these new compact and wireless commercial EEG recording systems, measuring brain activity is no longer limited to research and laboratory demonstration. In the long term, such BCI systems might be even more convenient and accessible than remote controls, joysticks or phones.

1.4 Research Questions

EEG artefact removal and developing low-cost, consumer-grade eye-tracking apparatus for daily life applications are still active topics of research [17, 18, 19]. To reap the potential benefits of the BCIs and eye-tracking systems in daily human-computer interaction, the development of a signal processing method for removing artefacts from EEG signals and of affordable and robust eye-tracking systems is necessary. Additionally, fusion of brain signals and eye movements has the potential to lead to a more robust method for attention detection and human activity recognition. In this work we are trying to answer the following research questions:

- Can we use affordable consumer-grade EEG devices to reliably detect a subject's focus of foveal attention?
- What type of information can be extracted from EEG signals?
- Do the consumer-grade EEG devices collect real cerebral signals?
- How can we use the EEG signals for eye-tracking?
- How can we use cerebral information to improve eye-tracking?
- How eye-tracking information can be used to improve SNR of cerebral information in the EEG signals?
- Is EEG artefact removal the optimum way to improve SNR of cerebral information in the EEG signals?

1.5 Contributions

The work described in this thesis provides original contributions to EEG signal processing and reveals the potential benefits of using consumer-grade EEG devices to estimate the focus of foveal attention. The major contributions can be summarised as follows:

- Assessment of the integrity of an affordable and non-intrusive consumer-grade EEG device for BCI applications.
- Introduction of a novel VOG-EEG dataset specifically recorded for the purpose of removing EOG artefacts arising from saccade and smooth pursuit eye movement as well as for reducing the habituation effect.
- Proposal of a signal processing approach to classify blink, fixation saccade and smooth pursuit eye movements, as well as to classify saccade amplitude and eye movement direction.
- Proposal of a hybrid method which ulitises eye movement classification and SSVEP detection to improve FoA estimation.
- Proposal of 'Blink BVOG-ICA', an ICA-based EEG artefact removal method which employs optical eye-tracking information to detect ICA components corresponding to blink and eye movements.
- Exploration of the effect of subject habituation on the amplitude of SSVEP responses.
- Improvement of eye movement classification, EEG pattern classification and FoA estimation using the features extracted from ICA components rather than EEG channels.

1.6 Thesis Structure

The thesis consist of eight chapters. While the next chapter provides necessary background, the main contributions of this research are presented in Chapter 3 to Chapter 7, and a conclusion is made in Chapter 8. Figure 1.1 depicts the conceptual links between different chapters of the manuscript. In the following, a brief overview of each chapter is given.

1.6.1 Chapter 2 - Background Knowledge

This chapter provides a background review of techniques used to detect a person's focus of foveal attention. The chapter begins by defining the eye-tracking problem and reviewing some of the early eye-tracking experiments. This is followed by presenting the electrophys-

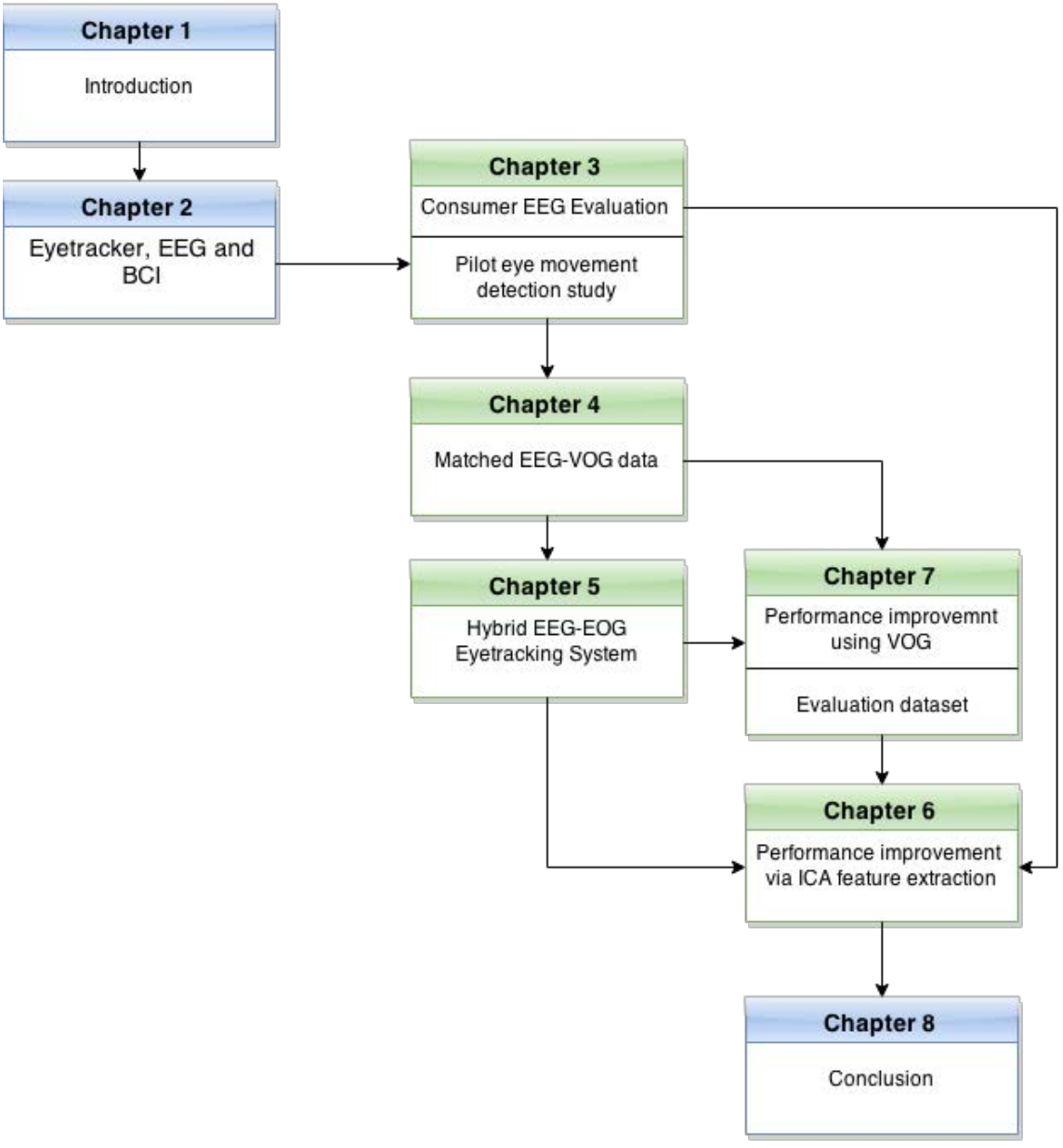

Figure 1.1: The hierarchical thesis structure.

iology of the eyes and categorising different types of eye movements. Then, some of the major signal processing methods used for eye tracking, including noise removal, feature extraction and eye-movement classification, are outlined. In addition to conventional eye tracking, EEG-based BCI is described as a means to detect the focus of foveal attention; eye movement is introduced as a source of artefacts, exploiting EEG. This is followed by an outline for some of the major noise removal methods, feature sets and classifiers used for classification of the patterns in the EEG signals corresponding to different types of activity. Finally, ICA is introduced as the most successful eye-related artefact removal method, and the feasibility of using ICA as a feature extraction method, in addition to artefact removal, is discussed.

1.6.2 Chapter 3 - Consumer-grade EEG Device Evaluation

In this chapter, the feasibility and reliability of employing commercial EEG recording devices for routine BCI are assessed via evaluating integrity of a consumer-grade EEG headset, Emotiv Epoc. The device is employed for recording EEG during three common BCI experiments. The limitations of the device and recommendations on processing signals from the device are discussed. Additionally, a pilot study is performed to evaluate the changes in the patterns of EEG signals originated by eye movements and blinking, which are among the main sources of biological artefacts. In the pilot study, the performance of the EEG device in classifying EEG signals arising from eye blinks and eyes moving in different directions is assessed. This way, the feasibility of using the EEG headset to detect point of gaze in addition to eye-related artefacts is evaluated.

1.6.3 Chapter 4 - Matched VOG-EEG Datasets

In this chapter, a matched EEG-VOG dataset, recorded using consumer-grade EEG and VOG apparatus, is introduced. EEG and VOG data are simultaneously recorded during four different experiments. Additionally, the details of another matched EEG-VOG dataset, recorded using laboratory-grade apparatus by [13], are described. The datasets

are later employed in the experiments described in Chapter 5 and 6.

1.6.4 Chapter 5 - Hybrid EEG-EOG Eye-Tracker

A signal processing approach to classify blink and different types of eye movements, including fixation, saccade and smooth pursuit, is presented in this chapter. The method is also used to classify saccade amplitude and direction of eye movements. In addition, the focus of foveal attention is estimated using a hybrid approach of eye movement direction classification and SSVEP detection. The datasets described in Chapter 4 are used to evaluate the proposed signal processing approach.

1.6.5 Chapter 6 - Performance Improvement by VOG-based EOG Artefact Removal

In this chapter, the FoA estimation is improved by proposing an EEG artefact removal method based on ICA, thus improving SSVEP detection accuracy. Optical eye-tracking information is used to detect and remove eye-related artefacts from EEG data and to improve the accuracy of SSVEP detection. Additionally, the effect of subjects' habituation on SSVEP detection performance is explored. Similar to the previous chapter, the datasets described in Chapter 4 are employed for evaluation of the proposed method.

1.6.6 Chapter 7 - Performance Improvement by Extracting Features From Independent Sources

This chapter demonstrates that employing the independent sources estimated by ICA can be beneficial for feature extraction, leading to improved eye movement and EEG pattern classification. All the experiments conducted in Chapter 3 to 6 are repeated; however, features are extracted from independent components rather than normal (raw or cleaned) EEG channels. The datasets described in Chapter 3 and 4 are used to evaluate the ICA-based feature extraction method.

1.6.7 Chapter 8 - Conclusion

The final chapter provides a summary of the thesis, summarises the major results and draws a conclusion of the thesis in addition to anticipating the future directions of the work.

1.7 Summary

In this chapter, the motivations of the study, the research questions and thesis contributions are discussed. The chapter is finished by providing the thesis structure and a brief summary of each chapter.

"The most learned of men is one who collects bits of knowledge from others and thus enhances his own knowledge."

Prophet Muhammad (PBUH)

2

Background Knowledge

2.1 Introduction

The aim of this thesis is to develop signal processing approaches that are capable of tracking the eyes, based on information obtained from recorded EEG data, captured using an affordable, non-intrusive, consumer-grade EEG device. This chapter provides a brief overview/background of eye-tracking and EEG signal processing methods. It begins by introducing the characteristics of eye tracking, EEG and their applications. We also outline different methods used in the literature for the classification of EEG patterns and different types of eye movements, elicited during different activities. Extant EEG artefact handling methods are discussed, followed by an introduction to the well-known artefact

removal method, ICA, in detail.

2.2 Eye Tracking

The eye-tracking problem is defined as estimating a person's point of gaze in his or her visual field, or simply estimating his or her focus of foveal attention [20]. In the field of human activity recognition and cognitive state detection, it also extends to other elements such as analysing eye blinking rate and the repetition of specific patterns in the eye movements [9, 21], or detecting different types of eye movements (e.g., saccade, fixation, etc.) [22].

2.2.1 Eye Movements and Blinking

When a person participates in activities or looks at different scenes, his or her eyes do not move in a smooth and steady pattern. The process involves different eye movement types. To be able to use eye-tracking information, it is crucial to understand different types of eye movements. Eye movements can be categorised as saccade, fixation, smooth pursuit and blinking.

Saccade

Simultaneous and rapid movement of the eyes for redirecting the visual axis is known as a saccade. The angular distance the eyes travel during saccade is called the saccade amplitude. A typical saccade amplitude varies from 20 to 30 degrees and lasts from 10 to 100ms [23, 24]. Vertical and horizontal movements of the eyes on a visual scene can be modelled using saccades.

Fixation

Fixation is the steady state of the eyes when the eyes remain still and are fixed on a single location in the visual scene. Usually, fixation is defined as the duration between

each saccade, and it might last from tens of milliseconds to several seconds. However, the average fixation duration lies between 100 and 200ms[7, 9].

Smooth Pursuit

Movement of the eyes for tracking moving targets is known as smooth pursuit eye movement. The smooth pursuit eye movements are not generally under voluntary control; the presence of a moving target is required.

Blinking

Regular openings and closings of the eyelids are called blinks. Blinks are the response to irritation of the eyes, and they clean and lubricate the eyes by spreading tears across the cornea [22]. The typical blinking rate is 12 to 19 blinks per minute, and each blink lasts for 100 to 400ms [9]. In many lines of research, blinking is also considered as an eye movement type.

2.2.2 Eye Tracking Techniques

A variety of techniques have been developed for eye tracking. Broadly speaking, they can be classed as either optical (video-based) or non-optical (non-video-based). Non-optical methods mostly rely on measuring potential changes in the eye movements (electrooculography or EOG) [25, 9]. These methods are relatively cumbersome and can quickly become uncomfortable or tiresome for the subjects. Moreover, the methods are usually limited to laboratory experiments, and they cannot be employed in daily life and mobile circumstances. Alternatively, the optical or videooculography (VOG) eye-tracking systems record a sequence of images of a subject's eye, using high-resolution cameras. They rely on the software processing system to obtain the subject's gaze position [26, 9]. Apart from the signal processing aspect of VOG eye trackers, the accuracy of these trackers greatly depends on the resolution of the images they record.

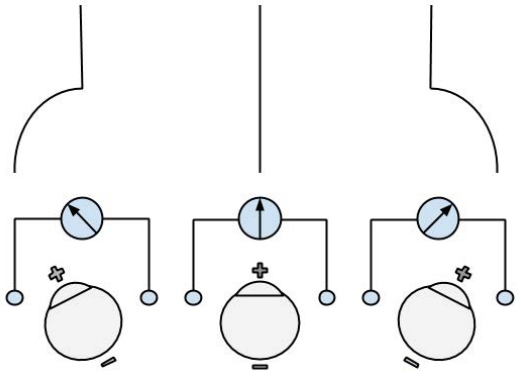

Figure 2.1: The dipolar model of the eyes.

Electrooculography

The eye can be modelled as a dipole in which the cornea is the positive pole and the retina is the negative pole. EOG is a method for sensing eye movements based on measuring changes in the steady corneo-retinal potential difference [25]. If the eye moves from its steady state position (centre position) toward one side, the positive pole of the eye (cornea) moves to one of the electrodes while the negative pole (retina) approaches the opposite electrode (see Figure 2.1).The resulting change in dipole orientation causes a change in the EOG signal amplitude. Blinks or eyelid movements also cause a change in the EOG signals. Analysis of these EOG changes provides a means for tracking eye movements and detecting blinks. EOG signal amplitudes are typically in the range of 50 to 200μV, with a frequency range of about 0 to 30Hz. EOG has applications in HCI, behavioural and perceptual research. Different types of eye movements (Section 2.2.1) that are captured by EOG signals can be used for human-computer and human-robot interfaces which are intended to be used by people with disabilities [27, 28, 29].

Video-oculography

VOG or video-based eye trackers usually use corneal reflection or pupil tracking [9], to capture horizontal and vertical movements of the eyes. Generally, there are two approaches for VOG eye tracking: (1) remote eye tracking, in which the tracking cameras are stationary with narrow visual field; and (2) head-mounted eye tracking, in which cameras

capture a close-up shot of the eyes [30]. Since VOG eye trackers are video-based, there is no need for direct contact with eyes, making them more comfortable and less intrusive. However, in both types of VOG eye-tracking approaches, there are some challenges: remote eye-trackers limit the visual field and mobility of the users, whereas head-mounted trackers require users to wear cumbersome devices, which limits users' physical activity. VOG has been widely used in scientific research and cognitive science [31].

2.3 Brain Activity Measurement

The brain is the most complex unit in the human body, and it is the centre of the nervous system. The nervous system is the command centre of the body; it sends and receives signals every moment. The basic units of communication in the nervous system are nerve cells, also known as neurons [32]. There are three types of neurons: *sensory neurons*, which send information from the skin or other organs toward the central nervous system; *motor neurons*, which send information from the central nervous system to muscles; and *association neurons*, which make the connection between sensory and motor neurons.

Neurons transmit information using electrochemical signals. The neurons in certain regions of the brain are activated unconsciously when a person perceives a specific external stimulus or voluntarily, following an internal cognitive process or the performance of a mental task. Generally, the brain is divided into two nearly symmetrical halves called the right hemisphere (RH) and the left hemisphere (LH). Each hemisphere contains four lobes: frontal, parietal, occipital and temporal. Areas within the brain lobes oversee all forms of conscious experience, including perception, thought, planning and emotion, along many unconscious emotional and cognitive processes. The frontal lobe assists in motor control and cognitive activities, such as making decisions, planning, etc. The parietal lobe assists in sensory processes, attention, language comprehension and spatial interpretation. The occipital lobe processes visual information and passes its conclusions to the temporal and parietal lobes. The temporal lobe assists in language comprehension, visual

recognition and auditory perception. Therefore, measuring neural activity at different locations of the brain can reveal the activities in which a person is involved. There are a variety of techniques to measure brain activity. The non-invasive electroencephalography (EEG) is the most extensively investigated and commonly used brain activity measuring system, for both medical and HCI applications. Because EEG has a high temporal resolution (i.e. changes in the functional activity of the brain can be measured after a couple of milliseconds), is durable and more cost effective than other bulky and expensive brain activity monitoring methods such as functional magnetic resonance imaging (fMRI), positron emission tomography (PET) and magnetoencephalography (MEG) systems [33].

2.3.1 Electroencephalography-EEG

The variation of the surface potential distribution over the scalp results from neural activity and reflects functional activities of the brain [34]. This surface potential variation can be recorded by placing a set of electrodes (sensors) over the scalp and measuring the voltage differences between pairs of these electrodes. Typically, EEG signals vary between $10\mu V$ to $100\mu V$ in amplitude, and lie within the frequency range of about 1 to $100Hz$ [35, 36].

EEG electrodes are generally placed on the scalp and named according to a standard mode - namely, the $10-20$ international system [37]. The international $10-20$ system provides meaningful letters and numbers for positions in the brain. The letters are the first letter of the brain lobes to which an electrode is attached (e.g., O for occipital lobe). The odd and even numbers correspond to electrode locations on the left and right hemisphere of the brain, respectively. For example, $O2$ corresponds to an electrode located over the right side of the occipital lobe.

EEG measurement can be either invasive or non-invasive. In the invasive measurements, signals are obtained by surgically placing probes (electrodes) within the brain (i.e., under the skull). In non-invasive recordings, electrodes are placed outside the head - for instance, on the scalp. The invasive approach produces the highest possible signal-to-

noise ratio for measuring brain signals, but it is usually unacceptable because it requires surgery and carries the risk of infection or brain damage. Non-invasive recordings are less intrusive, less complex, easy to wear and much cheaper; however, the electrodes can read brain signals less effectively. Through the acquisition of EEG signals, analogue signals are amplified and converted into digital data. A filtering scheme is needed to reduce the effects of the different sources of noise (e.g., $50Hz$ mains interference) from the signal. Because data resolution is important in terms of transferring and processing, the sampling rate and the total number of electrodes are crucial parameters in EEG acquisitions [38].

Previous studies have revealed that a variety of information can be extracted from EEG electrodes (sensors). This includes slow cortical potentials (SCP) [39], patterns associated with different mental tasks [40], event-related desynchronisation (ERD) [41], steady-state visual evoked potential (SSVEP) [10], and the P300 event-related potential (ERP) [42]. The information extracted from EEG signals is dependent upon the application. However, the ERP and SSVEP have become popular because they need less training, have less between-person variation and are more feasible for use in real-life applications.

2.3.2 Event-related Potential

The ERP is the brain's response to an external stimulus. The ERP response can be characterised by positive or negative deflections in the EEG signal from 100 to $900ms$ after exposing a subject to a stimulus [43]. The ERP responses are stronger over electrodes positioned at the vertex of the scalp. ERP responses are mostly used for brain spellers, in which subjects are stimulated with flashing letters at certain times and their choices are detected by detecting ERP response time-locked to the stimuli.

2.3.3 Steady-State Visual Evoked Potential

The SSVEP is an electrical response in the brain when the retina is stimulated by a flickering visual stimulus at a frequency higher than $6Hz$ [44]. SSVEP responses are oscillations in the EEG signals at the same frequency as the visual stimulation. By

analysing the spectral content of the EEG signal, the SSVEP can be detected reliably and without consideration of between-person difference. The SSVEP enables a person's focus of attention (FoA) to be estimated, providing the focus/stimulus is flickering. Thus, augmenting the presentation of a focus with a flickering luminosity enables detection of visual attention without the use of VOG.

EEG Wave Groups (Brain Rhythms)

Due to the large amount of information coming from each EEG electrode, the analysis of continuous EEG signals is complex. Therefore, signals coming from each electrode are usually divided into different waves with respect to their oscillation frequencies [45, 35]. The frequency bands of alpha ($8 - 12Hz$), beta ($13 - 30Hz$), delta ($0.5 - 4Hz$), theta ($4 - 7Hz$) and gamma (above $30Hz$) are conventionally used to describe brain waves (brain rhythms). Sometimes, another rhythm called the mu (or sensorimotor rhythm) is measured which lies in the same frequency range as the alpha rhythm. However, the mu rhythm occurs in the motor cortex, in contrast to the alpha rhythm, which occurs mostly over the visual cortex at the back of the scalp. Alpha is the most prominent wave and can be utilised to measure the level of relaxation [46]. Alpha waves appear mainly over posterior regions of the head and are usually found over the occipital lobe of the brain [47]. They are best seen when the subject's eyes are closed and he or she is in a wakeful, relaxed state. It has also been demonstrated that preparation for movements or the imagination of different motor actions, such as right- or left-hand movements, results in a decrease in mu and/or beta rhythms in the contra-lateral side (i.e., right or left) of the brain hemisphere for which movement is planned [48].

2.3.4 EEG Artefacts

EEG signals are always contaminated by artefacts, degrading the quality of EEG signals and potentially making them unusable. There are two categories of artefacts: biological and environmental [45].

Biological artefacts are electrical activities which affect signal readings from the scalp, but they have non-cerebral origins. The most common biological artefacts are electrical activities produced by muscles (captured by means of electromyography or EMG) and eye-induced artefacts or EOG.

Environmental artefacts originate from outside the body. Some common environmental artefacts are the misplacement of electrodes (resulting in spikes due to change in the impedance of an electrode), poor grounding of the EEG electrodes (causing $50Hz$ or $60Hz$ artefacts, depending on the local power system's frequency) and conductivity between two electrodes due to sweat.

2.4 EEG Signal Processing

The brain activity signals, recorded by EEG, are highly complex and random in nature. Several signal processing methods have been proposed to extract hidden information from these signals [35]. EEG signal processing usually consists of three major steps: artefact handling, feature extraction and classification. Each step is explained in the following sections.

2.4.1 Artefact handling methods

Most of the environmental artefacts are usually avoided by proper filtering and shielding. However, in the case of biological artefacts, filtering performance may be compromised, because EOG or EMG artefacts lie in the same frequency range as brain signals. There are three approaches for handling biological artefacts: avoidance, rejection and removal [49].

- *Avoidance:* The basic approach to handling biological artefacts is to avoid their occurrence by instructing the subjects to remain as still as possible and asking them to avoid blinking or rolling their eyes. However, eye and body movements can be involuntary.

- *Rejection:* In the rejection approach, EEG data contaminated with artefacts are detected manually or automatically. The segments including artefacts can be excluded from the EEG data. The drawback of this method is that there would be substantial loss of data due to the rejection of the contaminated segments.

- *Removal:* Another method for ensuring that the EEG data are as clean as possible is artefact removal. Artefact removal tries to remove the effects of the artefacts from the EEG signals while keeping the related neurological data intact.

Of the three artefact-handling methods, artefact removal is gaining more interest in EEG research, due to the fact that there is less information loss compared to artefact rejection and that the method is more reliable and feasible than artefact avoidance. Numerous methods have been proposed to remove EEG artefacts. Many of these existing methods are based on regression models and attempt to regress out reference signals recorded by electrodes placed around the eyes [50, 51]. However, regression-based artefact removal has some major drawbacks. The EEG and EOG activities mix bidirectionally [52], and consequently regressing out EOG results in removing some neural information in addition to the EOG activities. Additionally, the regression methods do not work in the absence of reference electrodes placed around the eyes. More recently, ICA has been used successfully to remove EEG artefacts [53, 54, 55], and it has been demonstrated to be more reliable than other artefact-removal methods [56].

2.4.2 Feature Extraction

EEG signal properties include non-Gaussianity, non-stationarity and non-linearity. The goal of feature extraction is to find an appropriate representation of the data that enables classification of different brain patterns. There are three main sets of features for raw EEG signal processing [57], [35]: temporal, frequential and time-frequency.

- Temporal: these features are particularly adapted to describe EEG signals with precise time signatures. For example, in ERP paradigms, the visual attention of the

users is detected by monitoring amplitude deflections in EEG signals, time-locked to certain stimuli [56].

- Frequential: as mentioned earlier, EEG signals are composed of a set of specific oscillations known as brain waves. Performing a given mental task (such as movement imagination [58]) makes the amplitude of these waves vary. Subsequently, it appears as natural to exploit the frequential information embedded in the EEG signals, such as EEG waves' band power.

- Time-frequency: these features are adopted to catch relatively sudden temporal variations of the signals, while still keeping frequential information. For example, in SSVEP paradigms, a short-time Fourier transform can extract information about the times when a subject attended to stimuli flickering at a certain frequency [44].

2.4.3 Classification

The main aim of the feature classification is to distinguish and classify the extracted features associated with different activities and/or mental states. There is a wide range of classification algorithms used in EEG studies, such as K-nearest neighbour (KNN) [59], support vector machine (SVM) [60], Linear Discriminant Analysis (LDA) [61], neural networks (NN) [62], hidden Markov models (HMM) [63] and naive Bayesian (NB) classifiers [64]. They can generally be classified into discriminative classifiers (e.g., SVM) and generative classifiers (e.g., NB). Generative classifiers model the distribution of the data in order to categorise the signal, while discriminative classifiers make a classification decision based on the characteristics of the data [65]. The KNN, NB and SVM are the three common classification algorithms successfully used for classification of brain activity patterns reflected in the EEG signals. A complete review of the classification algorithms used for EEG pattern classification can be found in [66].

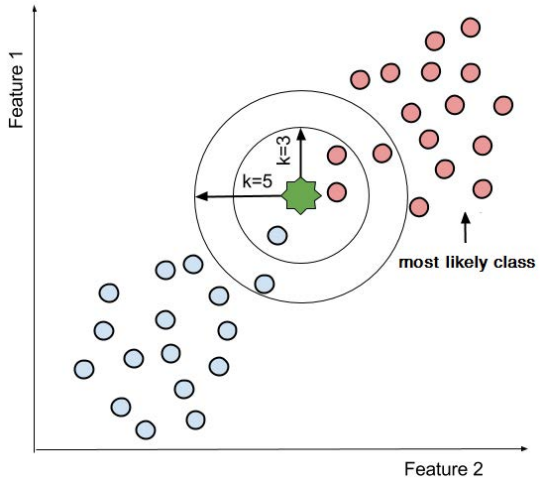

Figure 2.2: A typical example of a KNN classification for a two class problem (i.e. the "pink" and the "blue" circles) when the K parameter is set to "3" and "5". The green star represents a unseen sample point.

K-Nearest Neighbour

The KNN classifier is a relatively simple but robust, data-driven discriminative classifier. The classifier assigns a class label to an unseen point by comparing it to the K closest labelled points (nearest neighbours) in the training set [67]. The nearest neighbours are most commonly obtained by calculating the Euclidean distance. The value of K is normally defined manually. If the value of $K = 1$, then the unseen point is labelled according to the label of the closest labelled point in the training data. For $K > 1$, usually a majority voting rule is applied. In majority voting, each class takes a vote for each point in the K neighbours, which are labelled as that class. Then the unseen point is classified as the class with the highest number of votes (see Figure 2.2). This way, the classifier is less sensitive to outliers and it is robust to noisy and mislabelled training data.

Naive Bayesian

NB, the simplest and most widely used (generative) probabilistic classifier, is based on Bayes' theory [67]. NB is a simplified Bayesian probability and works under the naïve assumption that the features are independent, so that the effect of a particular feature's value on a given class is independent of the values of other features. NB aims to assign

an unseen point to a class with the highest posterior probability. Let $X = x_1, x_2, ..., x_n$ represent a sample point, with n values of the n independent features, $F_1, F_2, \cdots, F_n$; and there are k classes $(C_1, C_2, \cdots, C_k)$. According to the Bayes theorem, the probability of X belonging to class C_k can be calculated as follows:

$$p(C_k|X) = \frac{p(C_k)p(X|C_k)}{p(X)} \tag{2.1}$$

where,

- $p(C_k|X)$ is the posterior probability of class C_k given predictor X
- $p(C_k)$ is the prior probability of class C_k, or probability of occurrence of class C_k in the training set.
- $p(X|C_k)$ is the likelihood or the probability of predictor X, given class C_k.
- $p(X)$ is the prior probability of predictor X, or probability of occurrence of X in the training set.

Given X, the NB classifier predicts that X belongs to the class with highest posterior probability, conditioned on X, $p(C_i|X)$. Therefore, it is desired to find the class which maximises $p(C_k|X)$. Because $p(X)$ is constant for all the classes, only $p(C_k)$ $p(X|C_k)$ needs to be maximized. According to the joint probability model,

$$p(C_k)p(X|C_k) = p(C_k, x_1, x_2, \cdots, x_n) \tag{2.2}$$

and

$$p(C_k, x_1, x_2, \cdots, x_n) = p(C_k)p(x_1|C_k)p(x2|C_k, x_1), \cdots, p(x_n|C_k, x_1, x_2, \cdots, x_{n-1})$$

Now based on the naïve assumption, each feature F_i is independent of every feature F_j;

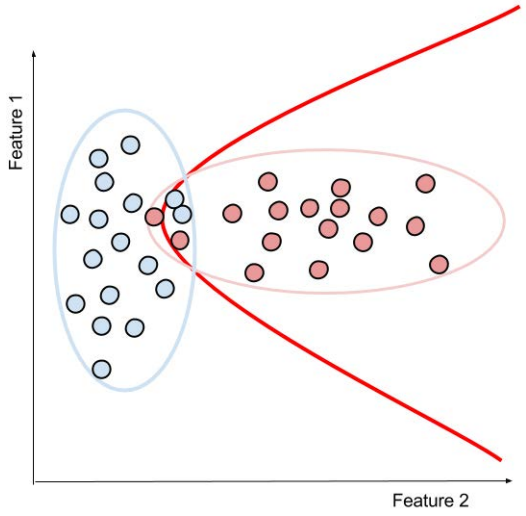

Figure 2.3: A typical example of a 2D binary classification with NB. A density contour is plotted for the Gaussian model of each class (i.e. "blue" and "pink" contours) and the decision boundary is shown in red.

for $j \neq i$, given class C_k. Consequently,

$$p(x_i|C_k, x_1) = p(x_i|C_k)$$
$$p(x_i|C_k, x_1, x_2, \cdots, x_{n-1}) = p(x_i|C_k)$$

Mathematically this means that,

$$p(C_k|X) \propto p(C_k)\prod_{i=1}^{n} p(x_i|C_k) \tag{2.3}$$

which can be easily estimated using the training set. In order to classify the unseen point X, the posterior probability for each C_k is calculated, and the class which maximizes $p(C_k|X)$ is assigned to the X (see Figure 2.3).

Support Vector Machine

The SVM proposed by [68] is a discriminative parametric classifier and is popular due to its good generalisation performance and computational efficiency. Given the labelled training set, the SVM constructs and uses a discriminant hyperplane to identify classes. The

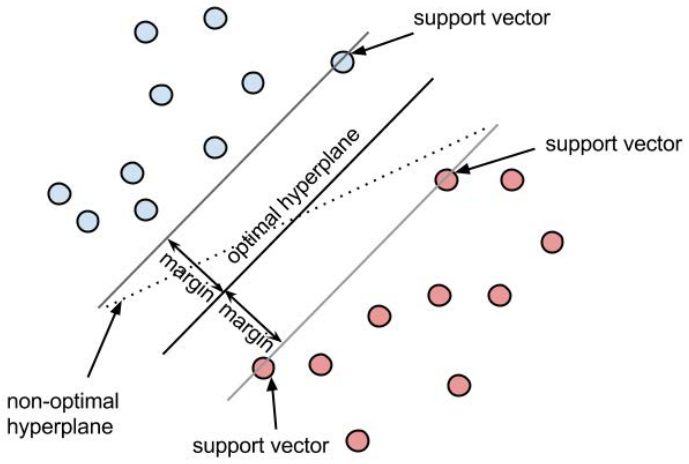

Figure 2.4: SVM finds an optimal hyperplane which separates tow classes: the "pink" and the "blue" circles.

hyperplane with maximum distance to the nearest training data samples (i.e., maximum margin) of any class is selected for discrimination of the classes. A larger margin leads to better generalisation capabilities (see Figure 2.4). The trade-off between maximum margin size and misclassification error is determined by a free regularisation parameter, C. Suppose we have a training set with N data points, where each D dimensional X_i ($X_i \in \Re^D$) belongs to a predefined class y_i, $\{y_i, X_i\}_{i=1}^N$. An SVM aims to construct a classifier based on the decision function $f(X)$ as follows:

$$f(X) = \text{sgn}\left(\sum_{\text{i=1}}^{N} y_i \alpha_i \Psi(X, X_i) + b\right) \tag{2.4}$$

where X is a test vector and α_i and b are positive and real constants, respectively. $\Psi(X, X_i)$ is the kernel function.

The kernel function is a computationally efficient method to obtain the projection of input data into a higher-dimensional space. The kernel function is suitable for cases where the points belonging to different classes are not linearly separable. There are multiple choices for the kernel function; however, the radial basis function (RBF) is the most widely used and has performed well in EEG signal processing.

The performance of the RBF-SVM is highly dependent on the choice of two hyperparameters: C (regularisation parameter) and σ (RBF width or kernel parameter). More details on SVM can be found in [67].

2.5 Independent Component Analysis

ICA is a blind source separation (BSS) [69] technique and is widely used for analysis of EEG data. ICA is chiefly applied to separate neural activities from artefacts. ICA assumes that the observed EEG signals from N electrodes, $x_1, x_2, \cdots, x_N$, are a linear mixture of N independent source signals (components), $s_1, s_2, \cdots, s_N$, that build them;

$$x_j = a_{j1}s_1 + a_{j2}s_2 + \cdots + a_{jN}s_N, \text{ for all } j \ (j = 1, 2, \cdots, N). \tag{2.5}$$

Where a are mixing coefficients. Let us define X as a vector whose elements are $x_1, x_2, \cdots, x_N$, and define S as a vector whose elements are $s_1, s_2, \cdots, s_N$. Additionally, let us define A as a matrix with elements a_{ij}. Therefore, the equation 2.5 can be written as

$$X = AS \tag{2.6}$$

where A is the mixing matrix, and source signals $S(t)$, are assumed to be independent, non-Gaussian and stationary. The ICA objective is to estimate a time-invariant, invertible mixing matrix A so that a set of non-gaussian and independent source signals, $S(t)$, can be reconstructed; using only the observations $X(t)$. Then, after estimating A, the "unmixing" matrix W is obtained by computing the inverse of matrix A ($W = A^{-1}$), and the ICs are simply obtained:

$$S = WX \tag{2.7}$$

Although ICA can estimate independent sources, it does not label them. Additionally, ICA does not guarantee the sign of the estimated sources and does not recover the exact amplitude of the sources. There are many ICA implementations which differ on the inde-

pendence of the components and estimation of the mixing matrix, such as Infomax [70], Extended-Infomax [71] and FastICA [72]. Many studies have compared the reliability of the estimated sources by different ICA algorithms [73, 74]. In the most recent study, researchers found that there is no significant difference between the performance of ICA algorithms; further, they found that the reliability of estimated sources by ICA is highly dependent on the pre-processing steps (e.g. proper filtering of raw EEG) applied to data prior to ICA rather than the type of ICA algorithm [75].

2.5.1 ICA-based Artefact Removal

As mentioned in Section 2.4.1, ICA is the most commonly used EEG artefact-removal method. In order to use ICA, usually the cerebral and artefactual sources are assumed to be biologically separate (and independent) processes. Therefore, ICA is used to separate cerebral and artefactual sources. After obtaining the ICs, those sources which are attributed to artefacts can be identified and removed; therefore, EEG signals can be reconstructed without the identified artefact components. The main drawback of ICA is that it does not label its estimated sources. Several attempts have been made to automatically label the artefactual sources by employing the temporal, frequential and spatial stereotyped characteristics of artefacts. For example, ADJUST [12], one of the most popular IC labelling techniques, uses a combination of temporal and spatial features to detect different types of EEG artefacts.

2.6 Summary

This chapter reviewed the basic concepts of eye-tracking and EEG techniques that are employed for the rest of this thesis. Different signal processing methods used for classification of EEG patterns were outlined. ICA, a successful EEG artefact-removal method that can separate cerebral and non-cerebral sources from EEG observations, was also introduced.

"Wisdom never attains perfection except by following the truth."

Hussain ibn Ali (PBUH)

3

Consumer-grade EEG Device Evaluation

3.1 Introduction

The development of consumer-grade EEG devices is accelerated by the ability of using BCI as an assistive technology for people with physical impairments [76] and the growing interest in using BCI in gaming and virtual reality applications [77]. The availability of low-cost EEG devices affords the possibility of widespread use of brain signals in HCI. However, in practice the uptake is hindered by limitations due to the low sampling rate, the low number of channels to cover the whole scalp, the low SNR due to artefacts and the unreliability of processed information.

In this chapter, the performance of a commercially available EEG device is evaluated

for BCI paradigms for which it is most suited: cognitive load, motor imagery and SSVEP. The study employs a portable, wireless, low-cost EEG device (i.e., the Emotiv EPOC) and integrates it with a Python software platform to capture brain activity. The goal of this chapter is to demonstrate the integrity of the Emotiv EPOC, and evaluate the feasibility and reliability of employing commercial EEG recording devices for routine BCI use. An additional objective of this study is to evaluate the changes in the patterns of EEG signals originated by eye movements and blinking which are among the main sources of biological artefacts. Thus, a pilot study was performed to assess performance of the EEG device for classification of blink and eye movement artefacts. The pilot study also assessed the feasibility of using the EEG headset to classify movements of eyes in different directions. The evaluation results are demonstrated and we discuss recommendations on processing signals from this EEG device.

3.2 Related Works

From the beginning of this research several researchers employed Emotiv EPOC consumer EEG device in different EEG paradigms. Table 3.1 summarises some of the recent studies evaluating the EEG headset with the obtained results.

Table 3.1: The obtained performance of different classification paradigms, in terms of balanced accuracy, when Emotiv EPOC is employed to record EEG.

Experiment	**Results**
ERP Classification	88.88% [78] 89.66% [79]
SSVEP Classification	73.5% [80] 75% [81] 95.83% [82]
Mental State Detection	68% [83] 64% [84]
Imagery movement Classification	82% [85] 76.92% [86] 82% [87]

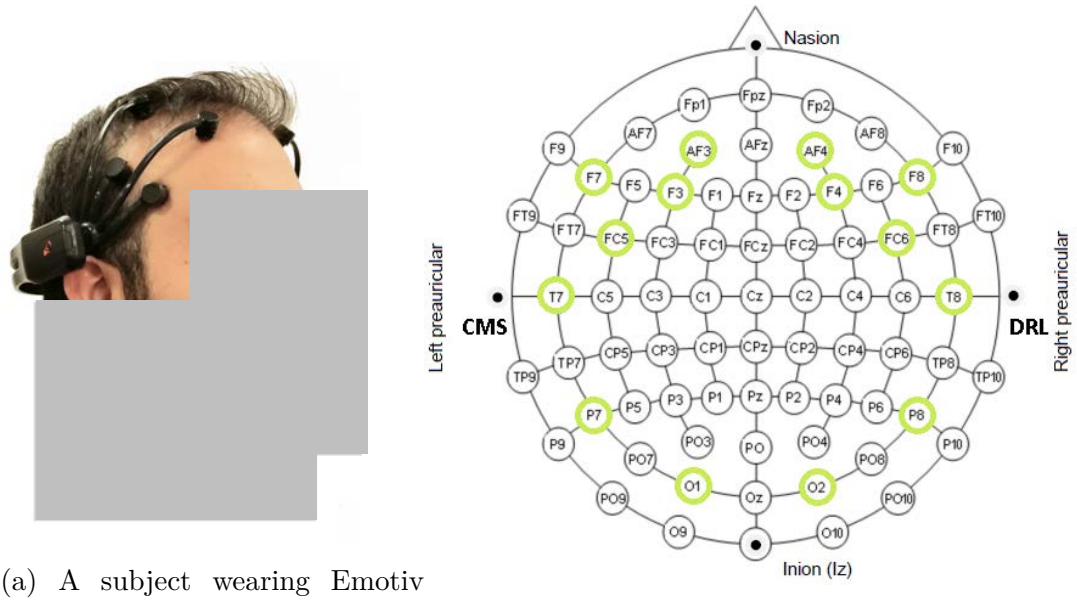

(a) A subject wearing Emotiv EPOC EEG headset.

(b) Electrode positioning.

Figure 3.1: Illustration of Emotiv EPOC EEG headset (a) in use and (b) its electrode locations based on the international $10-20$ system.

3.3 Apparatus

For the purpose of recording EEG, an Emotiv EPOC consumer-grade EEG headset was employed (Figure 3.1a). The headset's fixed array of electrodes makes it easy to fit and portable. Because it connects wirelessly to any PC, the user maintains a full range of motion. Instead of applying conductive gel or paste, EPOC simply requires that the users wet its felt-tipped electrodes with contact lens solution prior to each use. This device also comes with an embedded, two-dimensional gyroscope sensor that can be utilised for head-movement detection. The headset has 14 EEG electrodes (channels) located at the positions $AF3$, $F7$, $F3$, $FC5$, $T7$, $P7$, $O1$, $O2$, $P8$, $T8$, $FC6$, $F4$, $F8$, and $AF4$ on the scalp, in accordance with the international $10-20$ system, as shown in Figure 3.1b. There are two additional reference electrodes located above the subject's ears (CMS/DRL), for the electrodes on the left and the right hemispheres of the head. The data sampling rate is $128Hz$. The sampled EEG signals are transmitted wirelessly to a PC in the frequency of $2.4GHz$.

3.4 Methodology

Three BCI experiments were conducted in order to evaluate the integrity of the Emotiv EPOC EEG headset. Performance of the EPOC was measured using the obtained accuracies of the EEG signal classification through each experiment.

3.5 Data Collected

The dataset contains data recorded during three cue-based non-feedback (screening) paradigms - namely, *Cognitive Load* ($Experiment1$), *Motor Imagery* ($Experiment2$) and *Steady-State Visual Evoked Potential* ($Experiment3$). All subjects (described in section 3.5.1) participated in all the experiments. The same experimental set-up was applied to all. All the experiments were performed in one session.

3.5.1 Subjects

EEG data were recorded from 10 subjects (3 females, 7 males; age range $19-29$, mean 23.10; 2 left-handed). The subjects had normal or corrected-to-normal vision and had no history of neurological disorders. Written informed consent was obtained from all subjects prior to their participation in the study. The study was approved by the University of Birmingham ethics committee.

3.5.2 Experimental set-up

The participants were positioned in a comfortable chair at a distance of about $70cm$ from a $15-inch$ liquid crystal display (LCD) panel, with a $60Hz$ vertical refresh rate, inside a sound-attenuated recording booth. The screen was positioned at eye level. Subjects were instructed to relax and remain as placid as possible, to avoid the contamination of EEG signals with muscle artefacts. The entire preparation process took less than 5 minutes. In

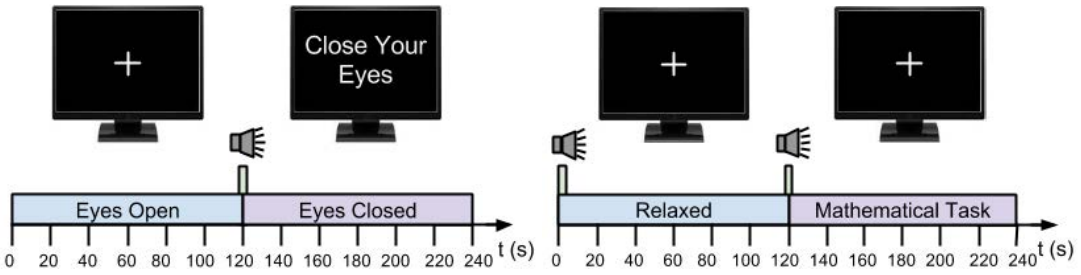

(a) Eyes-open vs. eyes-closed (b) Relaxation vs. active thinking

Figure 3.2: Timing scheme of the cognitive load experimental paradigm.

order to make participants feel more comfortable, they were given the chance to try the EEG headset on beforehand.

Two Python-based applications were implemented, one for capturing the raw EEG data and the other one for stimulus presentation. Both of the applications were launched on a single PC and were fully synchronised. To check the quality of the synchronisation, the machine's CPU time was recorded using both applications. The recording application ran first and started capturing EEG data points and CPU time, 128 times per second. Then stimulus presentation application ran, and it recorded the machines CPU time at the occurrence of each event and at the start and end of the stimulation.

3.5.3 Experiment 1: Cognitive Load

The screening paradigm in this experiment (Figure 3.2) consisted of three tasks: eyes-open relaxed ($class1$), eyes-closed relaxed ($class2$) and eyes-closed mathematical task ($class3$). Each subject participated in one screening session. The session consisted of 2 runs of $120s$ each and 2 classes of tasks. This resulted in recording $240s$ of EEG data per run and $480s$ of EEG data per session.

The first run started with the appearance of a fixation cross in the middle of the screen ($t = 0$). Subjects were asked to relax and fix their gaze on the fixation cross. After $120s$ ($t = 120s$), with the presentation of a visual cue (*close your eyes*) and hearing of a signalling tone ($1kHz$, $100ms$), the subjects closed their eyes and remained relaxed for another $120s$ (see Figure 3.2a). Figure 3.3 depicts the power spectral density (PSD)

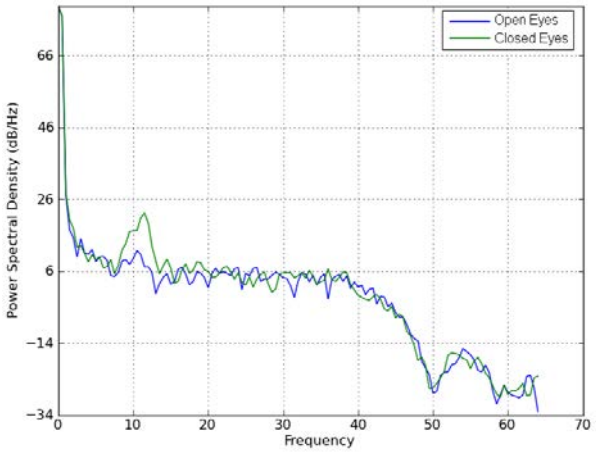

Figure 3.3: A typical PSD of a subject's EEG data, recorded at O_1 channel, during eyes-open and eye-closed task.

pattern of the recorded EEG data, recorded at a channel placed on the visual cortex, when a subject was relaxed and performed eyes-open and eye-closed tasks.

The second run started with presentation of a fixation cross and a signalling tone ($t = 0$), instructing the subjects to relax and close their eyes. After $120s$ ($t = 120$), on the hearing of a signalling tone, the subjects started to conduct a mathematical task (e.g., multiplication of 555 and 14), for another $120seconds$ (see Figure 3.2b). During the eyes-open condition, subjects were instructed to fix their gaze on a fixation cross to reduce contamination of EEG signals with artefacts arising from eye movements.

3.5.4 Experiment 2: Motor Imagery

The screening paradigm in this experiment (Figure 3.4) consists of two tasks: motor imagery of the right hand ($class1$) and the left hand ($class2$). Each subject participated in one screening session. The session consisted of 10 runs of $14s$ each and 2 classes of task. This resulted in 20 motor imagery trials ($280s$ of EEG data) per session.

Each run started with presentation of a fixation cross in the middle of the screen ($t = 0$). After 2 seconds ($t = 2$), the fixation cross was overlaid with an arrow pointing either to the right ($class1$) or the left ($class2$). The cue (arrow pointing to the right or the left) remained on the screen for $12s$. Presentation of the arrow prompted the subjects to

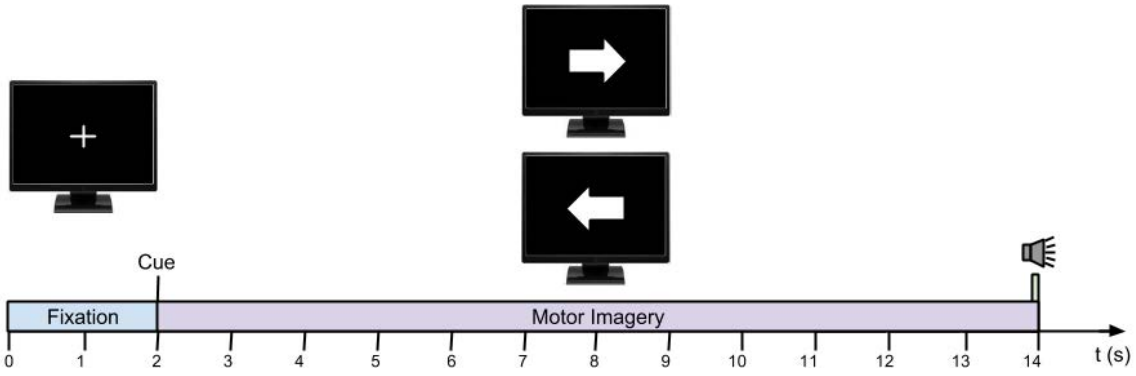

Figure 3.4: Timing scheme of the motor imagery experimental paradigm.

close their eyes and imagine a right- or left- hand movement, depending on the direction of the arrow. At second 14 ($t = 14$), the subjects were informed the run was finished, by hearing a signalling tone.

3.5.5 Experiment 3: SSVEP Classification

This experiment consisted of three tasks: attending to a fixation cross, which was $0Hz$ stimulation ($class1$), and visual stimulus flickering in $7Hz$ ($class2$) and $10Hz$ ($class3$). Each subject participated in one screening session. The session consisted of 14 runs of $10s$ each and 3 classes of tasks. This resulted in recording $20s$ of EEG data per run and $280s$ of EEG data per session. In this experiment, users were presented with $7Hz$ and $10Hz$ flickering visual stimuli (Figure 3.5).

Each run started with presentation of a fixation cross in the middle of the screen ($t = 0$). Subjects were instructed to remain relaxed and fix their gaze on the fixation

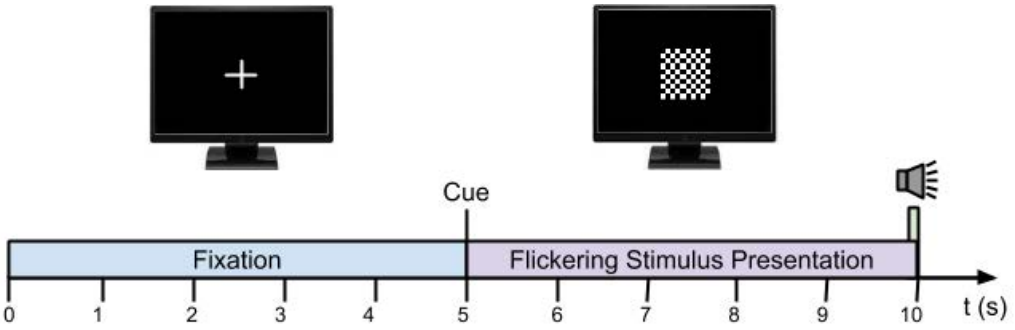

Figure 3.5: Timing scheme of the SSVEP classification experimental paradigm.

cross for $5s$ ($class1$). At time $t = 5$, a 10×10 checkerboard flickering in $7Hz$ or $10Hz$ (corresponding to one of two classes, $class2$ or $class3$) covered the fixation cross and remained for $5s$. During the presentation of the flickering stimuli, subjects focused on them. There was a $5s$ gap between each run.

3.6 Data Analysis

The captured data were used to classify the EEG patterns associated with different tasks included in each experiment. First, the EEG data were preprocessed and DC drift and high frequency noise were removed from the data. Then, ICA was used to remove artefacts and clean EEG data. Different sets of features were extracted from EEG data recorded during each experiment. Finally, the extracted features were fed into different classifiers to perform the classification tasks.

3.6.1 Preprocessing

The EEG data recorded outside the time range of the screening paradigms (data recorded before the start of the first run and after the end of the last run) in each experiment were excluded from the data. In order to remove the slow drifts and high-frequency noise from the recorded data, signals were band-pass filtered (bandwidth $1 - 40Hz$). The filtering was done by applying a zero phase forward/backward FIR filter.

3.6.2 ICA-based Artefact Removal

In order to separate and remove sources associated with artefacts from EEG, three commonly used ICA algorithms - FastICA, Infomax and Extended-Infomax - were applied to the data, and the performances of the algorithms in artefact removal were compared. Previous studies have shown that eye-related artefacts are the main source of biological artefacts and explain more than 90% of data variance, when compared to other types of artefacts [12]. Consequently, we only considered EOG artefact removal, and the sources

corresponding to EOG artefacts were manually labelled by visually inspecting their time-course, PSD and scalp map.

3.6.3 Feature Extraction

Features were extracted from the pre-processed EEG data channels. The EEG readings of each channel were split into epochs of window lengths of 1.0, 1.5 and 2.0 seconds, with different overlaps ranging from $100ms$ to $900ms$ with steps of $100ms$. The larger the window size, the lower the temporal resolution of the system.

In the first two experiments, a set of frequential features were extracted obtained by a 256-point fast fourier transform (FFT). In Experiment 1 (cognitive load) and Experiment 2 (motor imagery), the sum of the squared amplitude of frequencies lying in delta ($1-4Hz$), theta ($4-8Hz$), alpha ($8-13Hz$) and beta ($13-20Hz$) bands and relative intensity ratio of each band were considered as the features.

For Experiment 3 (SSVEP), the squared amplitude of the stimulation frequencies ($7Hz$and$10Hz$) and their second harmonics ($14Hz$ and $20Hz$) were extracted from the spectrum of the signal and considered as the feature.

For each experiment, the corresponding features are extracted from each single EEG channel separately, then they are concatenated together to make the final feature vector.

3.6.4 Classification

A classifier was trained on a subset of data to distinguish different task-related patterns in the EEG signal. In this study, RBF-SVM, NB and KNN classifiers were employed. The distance metric used in KNN classifier was Euclidean distance and the consistency of the classifier's performance was optimised by varying the K value between 1 to 9. For the RBF-SVM classifier, an optimal regularisation parameter C and a kernel parameter σ were identified using grid search [88]. The parameter's effectiveness was evaluated by 10-fold cross-validation.

For each experiment, classifiers were trained using a set of features, extracted from

epochs with different window and overlap length. A 10−fold cross validation method was used to evaluate the performance of the trained classifiers. In the 10−fold cross-validation procedure, extracted features were divided into 10 subsets, each corresponding to the data from one of 10 subjects. The classifiers were trained using 9 of 10 subsets, and the remaining subset was used for testing. This procedure was repeated 10 times, giving each feature instance an equal chance of being the training or test data.

3.7 Evaluation

The performance of the consumer EEG device was evaluated by measuring the classifiers' performance for each experiment. The performance criterion for the three classifiers was the accuracy of correctly classified instances in each experiment, averaged over 10 subjects. Additionally, the effect of varying window size and overlap on the performance of the classifiers was assessed.

3.8 Results

Figures 3.6, 3.7 and 3.8 illustrate the effect of varying window and overlap size on the performance of the employed classifiers for classification of the tasks in the cognitive load (*Experiment1*), motor imagery (*Experiment2*) and SSVEP classification (*Experiment3*) experiments, respectively.

Generally, the results indicate that there is a notable change in the performance of all the classifiers in all the experiments, when window and overlap length vary. In most of the cases, the classification performance is improved by increasing the percentage of window overlaps.

Increasing the overlap results in increasing the number of training samples; therefore, results suggest that there were not enough training samples in the short overlap sizes and that the classifiers' boundaries were not accurate enough. Consequently, the classifiers' performance was improved by increasing the percentage of overlap, thus increasing the

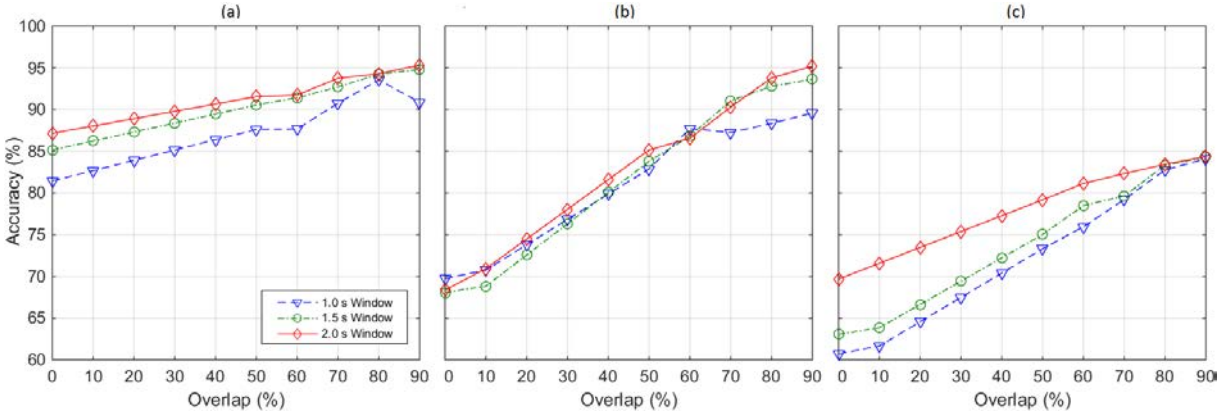

Figure 3.6: Performance of (a) Support Vector Machine, (b) Nearest Neighbour and (c) Naive Bayesian classifiers when features are extracted from variable window and overlap size, in Cognitive Load experiment (*Experiment1*).

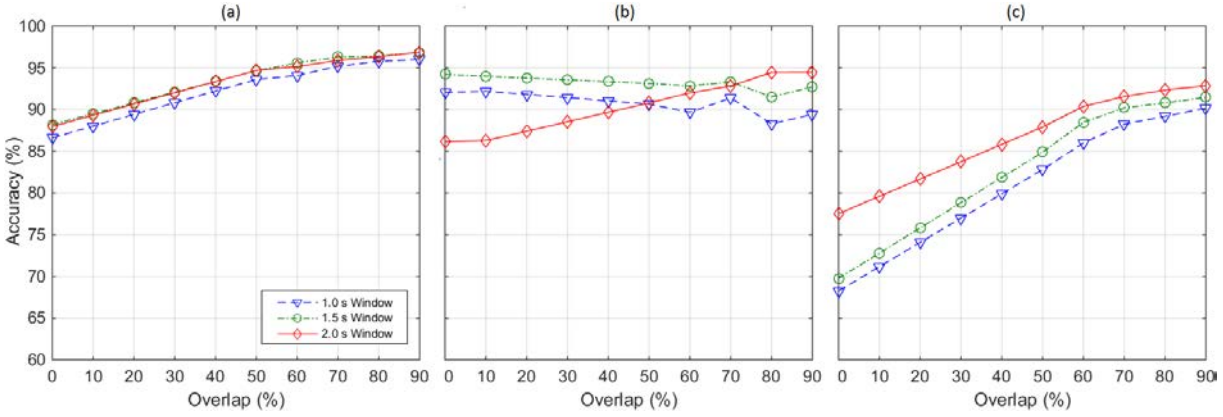

Figure 3.7: Performance of (a) Support Vector Machine, (b) Nearest Neighbour and (c) Naive Bayesian classifiers when features are extracted from variable window and overlap size, in Motor Imagery experiment (*Experiment2*).

number of training samples.

In the cognitive load experiment (Figure 3.6), increasing the overlap size resulted in approximately 15%, 26% and 25%, improvement in the performance of the SVM, KNN and NB classifiers, respectively. This suggests that the KNN and NB classifiers benefited more from increasing the overlap, than did the SVM classifier. However, Figure 3.7 indicates that in the motor imagery experiment both the SVM and KNN classifiers achieved similar levels of performance improvements (10%) from increasing the overlap size, and the NB classifier benefited considerably more (20% improvement) from increasing the overlap size.

In the SSVEP classification experiment (Figure 3.8), increasing the overlap resulted in

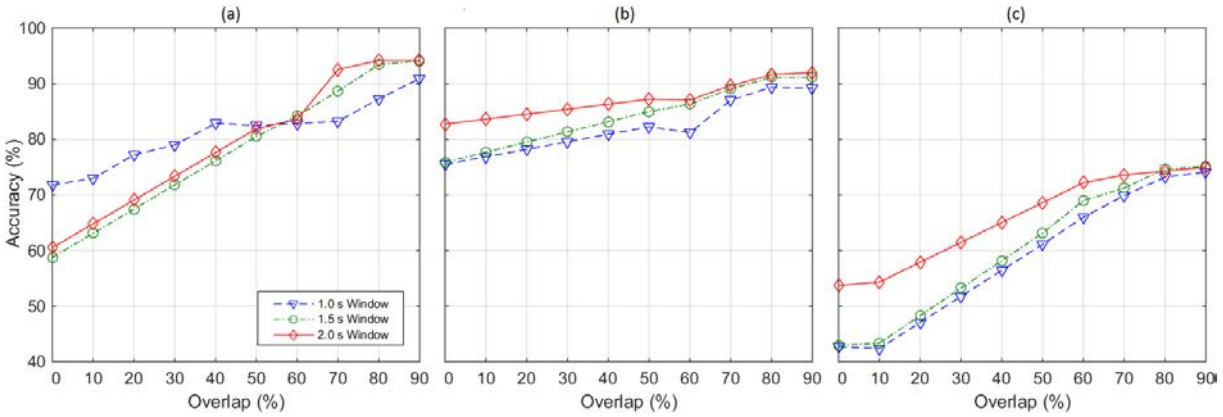

Figure 3.8: Performance of (a) Support Vector Machine, (b) Nearest Neighbour and (c) Naive Bayesian classifiers when features are extracted from variable window and overlap size, in SSVEP classification experiment (*Experiment3*).

approximately 35%, 15% and 33%, improvement in the performance of the SVM, KNN and NB classifiers, respectively. In contrast with the two previous experiments (*Experiment1* and *Experiment2*), in this experiment the SVM classifier benefited from increasing the overlap more than the other two classifiers did, and the performance of KNN tended to be more stable across varying overlaps than were the performance of the two other classifiers. When comparing the results obtained in all three experiments, the performance of the NB classifier was more sensitive to the variation of overlap size (and number of training samples) than were the SVM and KNN classifiers; in all cases, the highest performance of the classifiers was obtained when 90% overlap was used.

Table 3.2 highlights the results obtained by the three classifiers when $1.0s, 1.5s$ and $2.0s$ windows with 90% overlap were used for feature extraction. In terms of window size,

Table 3.2: The percentage (%) accuracy of the SVM, kNN and NB classifiers to classify tasks in the Cognitive Load, Imagery Movement and SSVEP classification experiments through various window sizes. The best obtained result for each experiment is highlighted in bold.

Window Size	**Experiment1**			**Experiment2**			**Experiment3**		
	SVM	**kNN**	**NB**	**SVM**	**kNN**	**NB**	**SVM**	**kNN**	**NB**
1.0 sec	90.86	89.58	84.11	96.01	89.42	90.16	90.94	89.20	74.12
1.5 sec	94.17	93.65	84.20	96.83	92.71	91.45	94.12	89.42	75.00
2.0 sec	**95.33**	95.20	84.33	**96.86**	94.46	92.85	**94.23**	93.13	75.10

the highest and lowest performance of the classifiers were obtained when 2.0s and 1.0s windows were used, respectively. In all three experiments, a set of frequential features were extracted for task discrimination; therefore, although increasing the window size resulted in poor time resolution and fewer training samples, this resulted in better frequency resolution, and thus more effective frequential features with more discrimination power were extracted. Overall, the highest performance of all classifiers was obtained in the case of 2.0s window size and 90% overlap. When comparing the classification methods, the two discriminative classifiers SVM and kNN achieved similar performance in all three experiments and outperformed NB, which is a generative classifier.

The result, represented in Table 3.2, also suggests that SVM and NB classifiers were less sensitive to the varying window size than was the KNN, and the kNN classifier benefited more from larger window size than did the other two classifiers.

Table 3.3 illustrates the performance of the classification methods before and after applying FastICA, Infomax and Extended-Infomax ICA algorithms for artefact removal. In all of the experiments, there was an increase in the performance of the classifiers when an ICA algorithm was employed to remove artefacts. In all the experiments, the NB classifier benefited more from ICA-based artefact removal than did SVM and kNN classifiers. NB performance improved up to 5.24%, 4.44% and 13.47% after applying ICA in *Experiment1*, *Experiment2* and *Experiment3*, respectively.

When comparing the performance of the three ICA algorithms based on classification

Table 3.3: The percentage (%) accuracy of the SVM, kNN and NB classifiers for different experiments, prior applying ICA (NO-ICA) and after applying FastICA, Infomax and Extended-Infomax ICA algorithms for artefact removal. The best obtained result for each experiment is highlighted in bold.

ICA Algorithm	**Experiment1**			**Experiment2**			**Experiment3**		
	SVM	**kNN**	**NB**	**SVM**	**kNN**	**NB**	**SVM**	**kNN**	**NB**
NO-ICA	95.33	95.20	84.33	96.86	94.46	92.85	94.23	93.13	75.10
FastICA	96.75	96.65	89.43	97.20	97.20	96.03	96.24	96.24	87.83
Infomax	**97.65**	**97.65**	89.57	97.63	97.57	97.00	96.87	96.87	88.23
Extended-Infomax	**97.65**	**97.65**	89.57	**98.99**	98.87	97.29	**97.22**	**97.22**	88.57

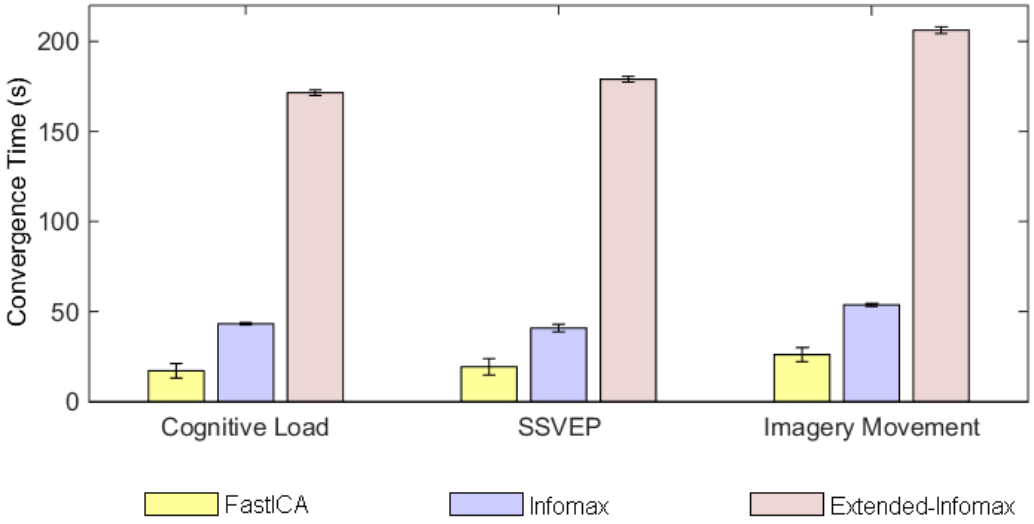

Figure 3.9: Time taken by FastICA, Infomax and Extended-Infomax ICA algorithms to converge, averaged over 10 subjects, through Cognitive Load (*Experiment1*), Motor Imagery (*Experiment2*) and SSVEP (*Experiment3*) experiments.

accuracy, there was no considerable difference between the algorithms. However, the highest classification accuracies were obtained when Extended-Infomax was applied for artefact removal. Although, when the ICA algorithms are compared based on the CPU time, they tended to estimate the independent sources and separate artefactual sources from non-artefacts, Extended-infomax took considerably more time than did the other algorithms (Figure 3.9). The shortest CPU time was obtained for fastICA.

Here, our main focus was to obtain best classification performance, not the shortest processing time. Figure 3.10 shows the performance of the classification methods, averaged over 10 subjects, after applying the best-performing ICA algorithm (Extended-Infomax) to remove artefacts. In terms of classification methods, the SVM and kNN classifiers almost achieved the same results and outperformed the NB classifier. Table 3.4 depicts the obtained p-values when t-test is performed to compare the performance of the three classifiers through all the experiments. In *Experiment1* and *Experiment3*, the SVM and KNN classifiers achieved significantly higher accuracy (approximately 8%) than did the NB classifier. In *Experiment2* they achieved approximately 2% more accuracy than did the NB classifier, however this difference is not statistically significant. The error bars in Figure 3.10 suggest that performance of the kNN classifier through different subjects was

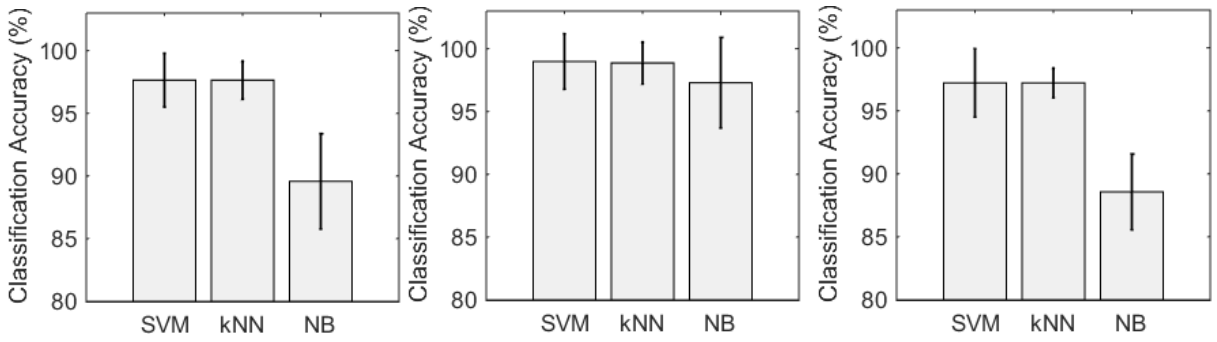

(a) Experiment1 (b) Experiment2 (c) Experiment3

Figure 3.10: Accuracy of the SVM, kNN and NB classifiers (averaged over 10 subjects) after applying Extended-Infomax algorithm is applied to remove artefactual sources from EEG data. The error bars represent standard errors.

more consistent than the performance of the SVM and NB classifiers, especially in the SSVEP classification (*Experiment3*).

Overall, in the cognitive load experiment(*Experiment1*), the result demonstrates that using the commercial EEG headset, the differences in the EEG patterns in three conditions - opened-eyes relaxed, closed-eyes relaxed, closed-eyes while solving a math task - were detected with accuracy of about 97.65%. The imaginary right- and left-hand movements performed by subjects (*Experiment2*) were detected with accuracy of 98.99%. In the SSVEP classification (*Experiment3*), the accuracy of detecting whether or not subjects were looking at a stimulus flickering at $10Hz$ or $7Hz$ was 97.22%. The results demonstrate comparable performance to other studies that used laboratory-based EEG devices (see Figure 3.5). They also, demonstrate that all three experiments were successful and that the commercial headset proved its integrity over a range of BCI applications.

3.9 Pilot Study: Consumer EEG for Blink and Eye-movement Direction Classification

This experiment is designed to assess the feasibility of using the EEG headset for eye-tracking applications via classification of blinking and movements of the eyes in different directions. The experiment consists of five tasks: fixation ($class1$) and moving the eyes to

Table 3.4: Obtained p-values after performing t-test on the results presented in Figure 3.10. Performance of all the classifiers are compared pairwise. In the cases where there is a significant difference (i.e. p-value<0.05) between performance of different classifiers, in each experiment, the p-values are highlighted in red. To avoid confusion the cells with repeated results are left blank.

	Experiment 1			Experiment 2			Experiment 3		
	SVM	KNN	NB	SVM	KNN	NB	SVM	KNN	NB
SVM	-			-			-		
KNN	1	-		0.80	-		1	-	
NB	**6**$\times 10^{-7}$	**4**$\times 10^{-6}$	-	0.08	0.09	-	**3**$\times 10^{-7}$	**1**$\times 10^{-6}$	-

Table 3.5: The results (balanced accuracy) obtained for classification of different tasks, when laboratory EEG devices used to capture brain activity. The tasks include (T1) relaxation (baseline), (T2) right motor imagery, (T3) left motor imagery, (T4) performing mathematical task, (T5) opening the eyes, (T6) closing the eyes, (T7) looking at different SSVEP stimuli.

Experimental Paradigm	**Classification Accuracy**
T1 + T4	91.4%[89], 95%[90]
T1 + T2 + T3	71%[91], 84%[92]
T2 + T3	87.4%[93], 89.3%[94], 90%[95]
T5 + T6	87%[96]
T7	90.50[97], 93.57[98], 94.4[99]

the right($class2$), left ($class3$), up ($class4$) and down ($class5$). Each subject participated in one session. The session consisted of 2 runs, blinking and eye movements. The first run contained $30s$ of EEG data recorded during blinking (approximately 30 blinks per run). The second run consisted of 10 repartitions of the eye movement tasks ($class1 - class5$). This resulted in recording $30s$ of EEG data associated to blinking and $50s$ of EEG data associated to five eye-movement types (10 repartitions for each eye-movement type) per session. The first run started with the appearance of a fixation cross. Subjects were asked to fix their gaze on the fixation cross and blink approximately once a second for $30s$. The next run started with the presentation of a fixation cross as well, and then after $1s$ an arrow pointing to the right, left, up or down covered the fixation cross for $1s$ (Figure 3.11). During this run, subjects were instructed to fix their gaze on the fixation cross ($class1$) or move their gaze from the fixation cross (centre of the screen) to the cued direction

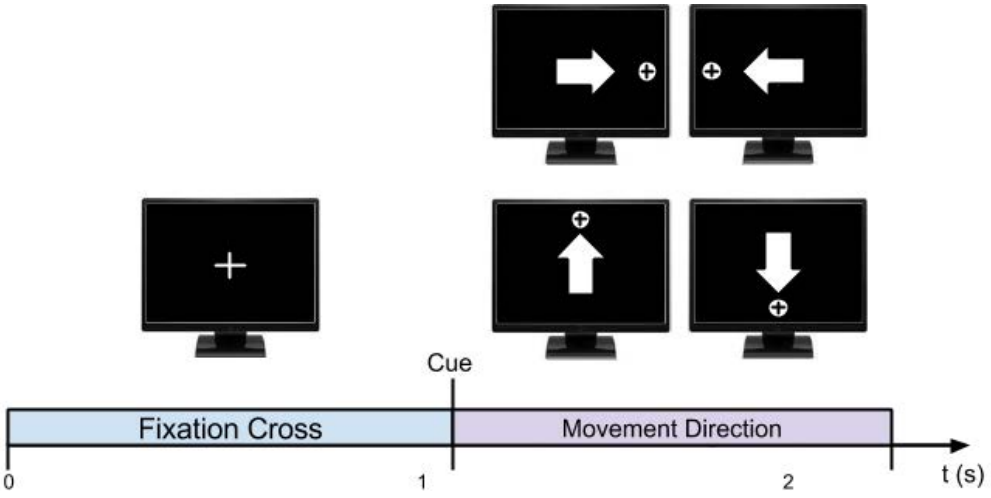

Figure 3.11: Timing scheme of the pilot study on gaze direction detection.

($class2-5$), depending on the direction of the arrow. This procedure was repeated 10 times for each of the four directions (i.e., right, left, up and down).

3.9.1 Data Analysis

The preprocessing method described in Section 3.6.1 was also applied to the data collected in this experiment. For blink classification, average power of EEG time-course and minimum and maximum amplitudes occurring in a $500ms$ moving window with 50% overlap were extracted from each channel as features. For eye-movement direction classification, the time samples of the signal within a window, extracted from each channel, were considered as features. Features were extracted from $1000ms$ epochs of the pre-processed data channels, time-locked to the stimuli. The final feature vectors were created by concatenating the time samples of all channels. The three classifiers described in section 3.6.4 (RBF-SVM, KNN and NB classifiers) were used for classification of the movements of the eyes in different directions. Similar to section 3.6.4, a 10-fold cross validation method was used to evaluate the performance of the three classifiers.

3.9.2 Results

Figure 3.12a depicts time series of EEG data, recorded from a subject during the blinking task. As shown in the figure, blinking produced rapid and high amplitude deflections; based on the blinking task, the duration between blinks was approximately 1 second.

Figure 3.13a and Figure 3.13b illustrate performance of the SVM, kNN and NB classifiers, in terms of balanced-accuracy, in classification of blinking and eye movements into different directions, respectively. According to Figure 3.13a, blinks were classified with approximately 89% accuracy using both the SVM and kNN classifiers. The NB classifier classified blinks with approximately 84% accuracy and achieved the worst classification performance. Table 3.6 shows the confusion matrix of the blink classification, averaged over all subjects. As shown in the table, 92.35% of the blink instances were correctly pre-

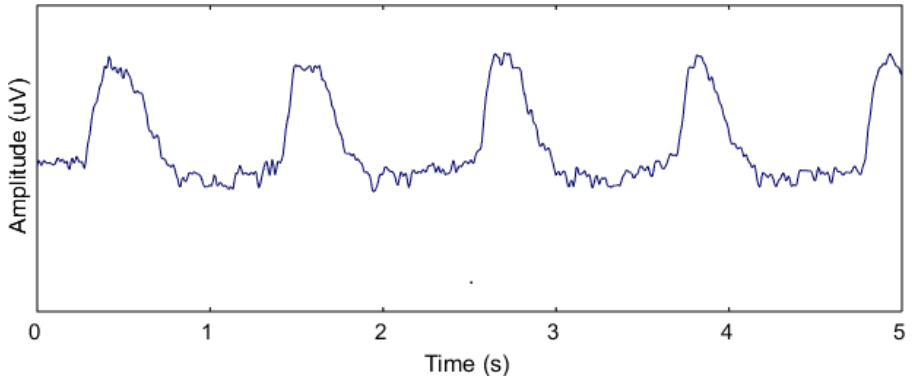

(a) Blinking

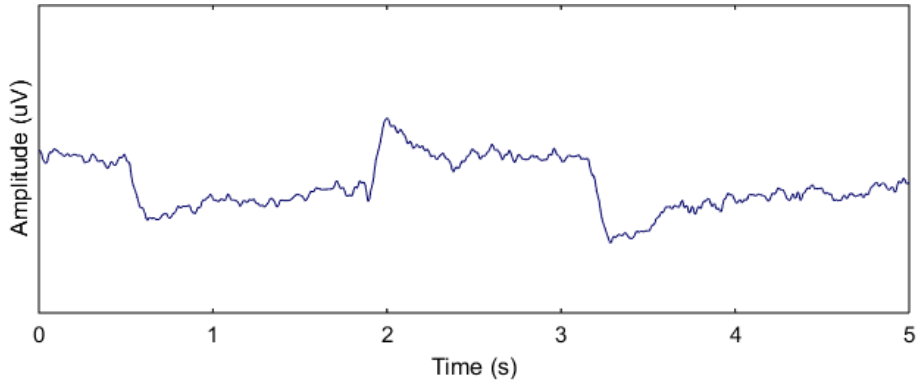

(b) Eye movements

Figure 3.12: Time series of EEG data captured at (a) $AF3$ channel, when a subject performed the blinking task and (b) $F7$ channel, when a subject moved his eyes to the right corner of the screen.

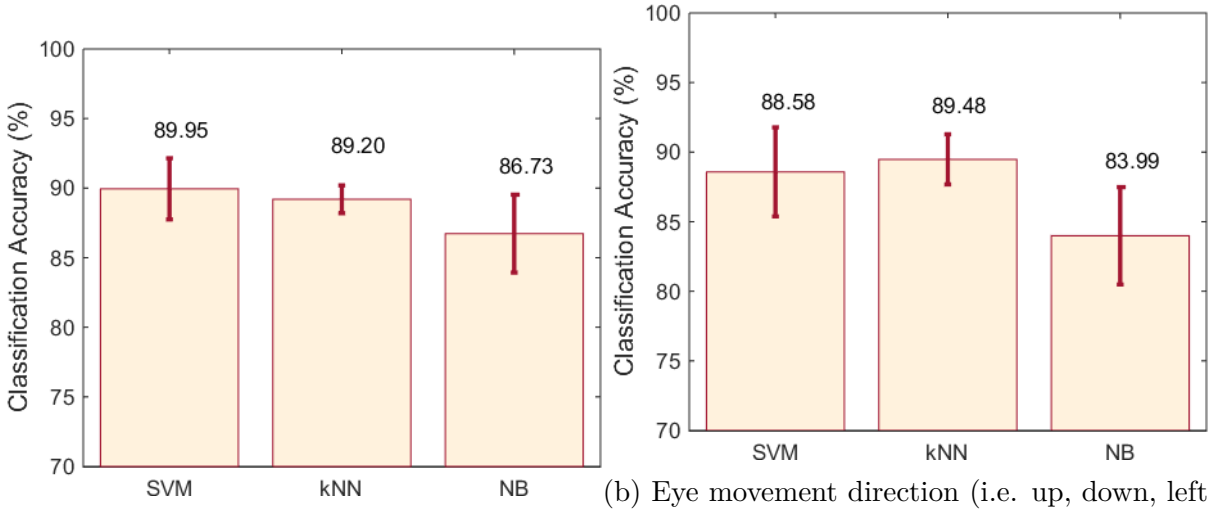

(a) Blink and fixation classification

(b) Eye movement direction (i.e. up, down, left ,right and fixation) classification.

Figure 3.13: Accuracy of SVM, kNN and NB classifiers (averaged over all subjects) in (a) Blink and (b) eye movement direction classification. The error bars represent standard errors.

dicted (classified) as blinks; however, only 86.05% of all fixation instances were correctly classified as fixation. This could be due to the fact that blinking happens involuntarily in the fixation durations as well; additionally, there could be other types of activity, e.g. electrode movements, can produce amplitude deflections similar to blinking.

Figure 3.12b shows a typical example of EEG data when a subject performed the eye movement task. As shown in the figure, the eye movements produced a large amplitude deflection similar to blinking; however, the duration of eye movements was longer than blinking. Figure 3.13b shows the accuracy of the proposed method to classify eye movements in different directions. As shown in the figure, eye-movement directions were classified with accuracy of more than 89% using the KNN classifier, followed by the SVM

Table 3.6: Confusion matrix of blink classification, averaged over 10 subjects. The numbers denote result of classification of EEG patterns, corresponding to blinking and fixating the gaze.

		Prediction	
		Blink	Fixed
Truth	Blink	92.35%	7.65%
	Fixed	13.95%	86.05%

Table 3.7: Confusion matrix of eye movement direction classification, averaged over 10 subjects. The numbers denote result of classification of EEG patterns, corresponding to eye movements into different directions and fixating the gaze.

		Prediction				
		Right	Left	Up	Down	Fixed
Truth	Right	95.28%	0%	3.10%	1.62%	0%
	Left	0.50%	93.35%	1.15%	2.30%	2.70%
	Up	5.00%	1.07%	85.23%	8.70%	0%
	Down	5.16%	2.60%	11.80%	78.34%	2.10%
	Fixed	0%	3.77%	0%	1.00%	95.23%

classifier (approximately 88%). Similar to the blink classification, the lowest accuracy was obtained when the NB classifier was employed (3% lower than KNN and SVM).

The error bars in Figures 3.13a and 3.13b suggest that the performance of the KNN classifier was more consistent across subjects than was the performance of the other two classifiers, for both blink and eye-movement direction classification. Additionally, kNN achieved the highest performance in blink classification and performed similarly to the SVM classifier in eye-movement direction classification.

Table 3.7 illustrates the confusion matrix of the kNN classifier for eye-movement classification, averaged over all subjects. The diagonal elements of the confusion matrix are observably dominant, indicating high classification quality. As shown in the table, the best performance was achieved for classification of eyes moving to the right, 95.28%, followed by fixation classification, 95.23%, which are only significantly (p-value$<$0.05) higher than downward and upward eye movements. The weakest performance was achieved for downward eye-movement classification (approximately 78%). As shown in Figure 3.1a, there were no electrodes placed below the eyes, and the effect of downward eye movements could be observed predominantly on the electrodes placed on the forehead (on top of the eyes). Thus, almost 11% of the downward eye movements were erroneously classified as upward eye movements (see Table 3.7). However, the difference between upward and downward eye movements is not statistically significant (p-value$>$0.05).

Overall, the result demonstrates the reasonable potential of Emotiv EPOC to be em-

ployed as a tool for blink and eye-movement direction classification, despite the fact that the lack of electrodes placed below the eyes limits the device's ability to detect downward eye movements as accurately as movement of eyes in other directions. Additionally, the performance of the simple KNN classifier for blink and eye-movement direction classification, was compared to more advanced classifiers such as SVM. The KNN classifier performed eye-movement and blink classification more consistently across different subjects than did the NB and SVM classifiers.

3.10 Summary

A series of experiments were performed to evaluate the integrity of a commercial EEG device (i.e. Emotiv EPOC) to be utilised in BCI applications. Additionally, a pilot study was performed to evaluate the feasibility of using the Emotiv EPOC to classify eye blinks and eye movements in different directions. The result demonstrated comparable performance of the device to similar studies which employed standard laboratory based EEG devices. Given its low cost, the consumer EEG device showed remarkable performance in cognitive load, mental state and SSVEP classification, confirming integrity of the device for use in BCI applications. It was also demonstrated that selecting appropriate window and overlap length and applying artefact removal methods have a considerable effect on the performance of the classifiers in BCI paradigms. Optimum window and overlap size for different BCI paradigms, using the Emotiv EPOC were reported and the best-performing ICA algorithm for artefact removal was introduced. The device also showed reasonable performance for classification of blink and eye movement in directions, suggesting the feasibility of using the Emotiv EPOC in eye tracking applications.

"The believer is not believing unless he is afraid and hopeful, and he is not afraid and hopeful unless he put into practice what he is hopeful and afraid of."

Ja'far al-Sadiq (PBUH)

4

Matched VOG-EEG Dataset

4.1 Introduction

In the next experimental chapters of this thesis, different methods are proposed to classify eye-movement types and remove EOG artefacts from EEG data. In this chapter, we introduce a matched EEG/VOG dataset collected during four experiments specifically designed for our study. The data are used to evaluate the proposed eye-movement classification and EOG artefact removal methods. Details of the designed experimental paradigms, and specification of the EOG and VOG recording apparatus are also described.

The first two experiments (described in section 4.2.5 and 4.2.6) are designed to study the EOG activity during saccadal eye movement. During the experiments, subjects are

asked to fixate or produce saccades based on the visual cues presented on the screen. The last two experiments are designed to investigate the effect of EOG activity due to smooth pursuit eye movements, on SSVEP response detection, and explore the potential benefits of SSVEP response detection for the focus of foveal attention estimation. In the latter experiment, the brain response to a flickering stimulus and EOG activity due to eye movement are produced at the same time by exposing the subject to flickering stimuli moving in different directions.

During all the experiment, EEG and VOG data are captured simultaneously using consumer-grade EEG and VOG apparatus. Both EEG and VOG apparatus are wearable, non-intrusive and designed for mobile (wireless) situations outside of laboratory settings.

Additionally, in section 4.3 we describe a similar matched EEG/VOG dataset recorded using laboratory EEG and VOG equipment. This dataset (named Plöchl), is recorded by [13] to use VOG information for removing EOG artefacts and improving SNR of ERP responses. Here, the dataset is used for benchmarking and evaluating the proposed EOG artefact removal method.

4.2 Simultaneously Recorded VOG/EEG Dataset

This dataset contains data recorded during four cue-based non-feedback (screening) paradigms namely, short saccade (*experiment*1), long saccade (*experiment*2), fixed SSVEP (*experiment*3) and pursuit SSVEP (*experiment*4). All subjects (described in section 4.2.1) participated in all of the experiments and the same experimental set-up is applied on all.

4.2.1 Subjects

This dataset contains EEG data recorded from seven subjects (all male; age range $23-30$, mean 26.05; 2 left-handed). The subjects have normal or corrected-to-normal vision and have no history of neurological disorders. Informed consent is obtained from all subjects. The study is approved by the University of Birmingham ethics committee.

Figure 4.1: A subject wearing EEG and VOG recording devices.

Figure 4.2: Emotiv EPOC EEG headset.

Figure 4.3: Tobii glasses, a head mounted eye tracker.

4.2.2 Experimental set-up

Experimental set-up is similar to the one described in section 3.5.2, with some minor differences. The subjects are positioned in a comfortable chair at a distance of about $100cm$ from a squared $19inch$ liquid crystal display (LCD) panel with $60Hz$ vertical refresh rate. The screen is positioned at eye level. Subjects are instructed to relax and remain as still as possible, to avoid the contamination of EEG signals with muscle artefacts. There are four cue-based experiments included in the dataset; each experiment is performed in one session.

4.2.3 Apparatus

EEG and VOG are captured using two non-intrusive consumer-grade recording apparatus designed for mobile situations outside of laboratory settings. Figure 4.1 shows a subject wearing the EEG and the VOG recording devices together.

EEG signals are recorded using the 14 electrode wireless Emotiv EPOC EEG headset described in section 3.3 (Figure 4.2), at the sampling rate of $128Hz$.

VOG data is captured using Tobii Eye Glasses (Figure 4.3), a head-mounted eye-tracker, sampling at $30Hz$. The glasses are a monocular eye-tracker that uses dark pupil detection for tracking the subject's right eye, with reported accuracy of 0.5°.

In addition to the eye-tracking data, the eye-tracker records visual angles up to 56°

horizontally and 40° vertically, using a $1.3 MegaPixels$ camera. Before each recording, a 9-point calibration procedure, to correctly map the eye-tracking data to the scene video, is done. Calibration details can be found in the eye-tracker's manual. In order to avoid miscalibration, subjects are asked to not move the eye-tracking glasses during the experiments.

Python applications described in section 3.5.2 are used for EEG recording and stimulus presentation. In the stimulus presentation paradigm, the start and end of the stimulation and stimulus presentation times are timestamped and displayed on the LCD. Timestamps are captured by the eye-tracker's scene camera. Exact time of all timestamps are labelled in the VOG data using Tobii Studio software and used for synchronisation of EEG data, the stimulus presentation paradigm and eye-tracking data.

4.2.4 Synchronisation

Since EEG and VOG data are recorded at different sampling rates, using different recording apparatus, we need to synchronise the recorded data. For the aim of synchronisation, in all of the VOG-EEG experiments, a set of time stamps are displayed on the stimulus presentation screen and captured by the eyetracker's scene camera. Synchronisation is performed in three steps. First, the scene camera recordings are visually inspected to label the stimulation start and end as well as the events displayed on the screen. Afterwards, VOG data between the start and end of the stimulation is up-sampled to match the EEG sample rate with linear interpolation [100]. Finally, the shared events between VOG and EEG recordings are identified for checking the quality of the synchronisation. Knowing that the exact time of all the events in the stimulation paradigm are automatically timestamped in the EEG data, the latency difference between corresponding events in the EEG and the VOG data can be used as a measure to investigate the synchronisation error (in samples).

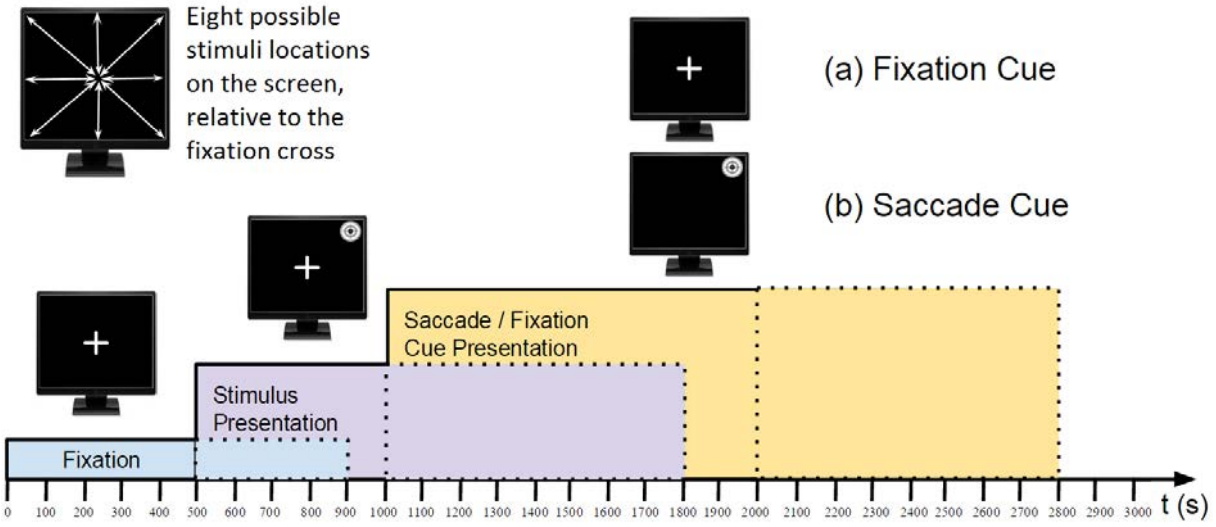

Figure 4.4: Timing scheme of the Short Saccade experimental paradigm (*Experiment1*).

4.2.5 Experiment 1: Short Saccade

The screening paradigm in this experiment consists of nine tasks namely, fixation ($class1$), short horizontal saccades to the right ($class2$) and the left ($class3$), short vertical saccades to the up ($class4$) and the down ($class5$) and short diagonal saccades to the up right($class6$), the up left ($class7$), the down right ($class8$) and the down left ($class9$). Each subject participated in one session. The session consists of one run including 112 repetitions for the fixation task ($class1$) and 112 repetitions of the saccade tasks ($class2-9$). This resulted in recording approximately $600s$ of EEG data per session.

Referring to Figure 4.4, users are presented with a black square display and there are 8 possible stimulus locations around the screen edge. Sessions start with the appearance of a white fixation cross in the centre of the screen ($t = 0$). After a random time between $500ms$ and $900ms$ ($t = 500 - 900ms$), the stimulus is presented at one of the nine edge locations. In the saccade trials, the fixation cross disappears at a random interval between $500ms$ to $900ms$ after stimulus presentation ($t = 1000 - 1800ms$), which provides the cue for subjects to make a saccade to the stimulus location. Stimuli are presented for a further $1000ms$ after presentation of the cue. In the fixation trials, the fixation cross remains on the screen and the stimuli presented at the edge disappear at a random interval between

$500ms$ to $900ms$ after its presentation ($t = 1000 - 1800ms$). Subjects should fix their gaze on the fixation cross while it is presented on the screen. The fixation cross remains on the screen for a further $1000ms$ after its presentation.

4.2.6 Experiment 2: Long Saccade

The paradigm in this experiment is similar to the *Short Saccade* experimental paradigm described in section 4.2.5; however, in this experiment fixation cross appears at one of the 8 edge locations rather than centre of the screen.

The screening paradigm in this experiment consists of nine tasks namely, fixation ($class1$), long horizontal saccades to the right ($class2$) and the left ($class3$), long vertical saccades to the up ($class4$) and the down ($class5$) and long diagonal saccades to the up right($class6$), the up left ($class7$), the down right ($class8$) and the down left ($class9$). Each subject participated in one session. The session consists of a run including 112 repetitions of the fixation task ($class1$) and 112 repetitions of the saccade tasks ($class2-9$). This resulted in recording approximately $600s$ of EEG data per session.

Referring to Figure 4.5, users are presented with a black square display and there are 8 possible stimulus locations around the screen edge. Sessions start with the appearance of a white fixation cross at one of the edge locations ($t = 0$). After a random time between $500ms$ and $900ms$ ($t = 500 - 900ms$), the stimulus is presented at one of the eight remaining edge locations. In the saccade trials, the fixation cross disappears at a random interval between $500ms$ to $900ms$ after stimulus presentation ($t = 1000 - 1800ms$); which provides the cue for subjects to make a saccade to the stimulus location. Stimuli are presented for a further $1000ms$ after presentation of the cue. In the fixation trials, the fixation cross remains on the screen and the stimuli presented at the edge disappear at a random interval between $500ms$ to $900ms$ after its onset ($t = 1000 - 1800ms$). Subjects should fix their gaze on the fixation cross while it is presented on the screen. The fixation cross remains on the screen for a further $1000ms$ after its presentation.

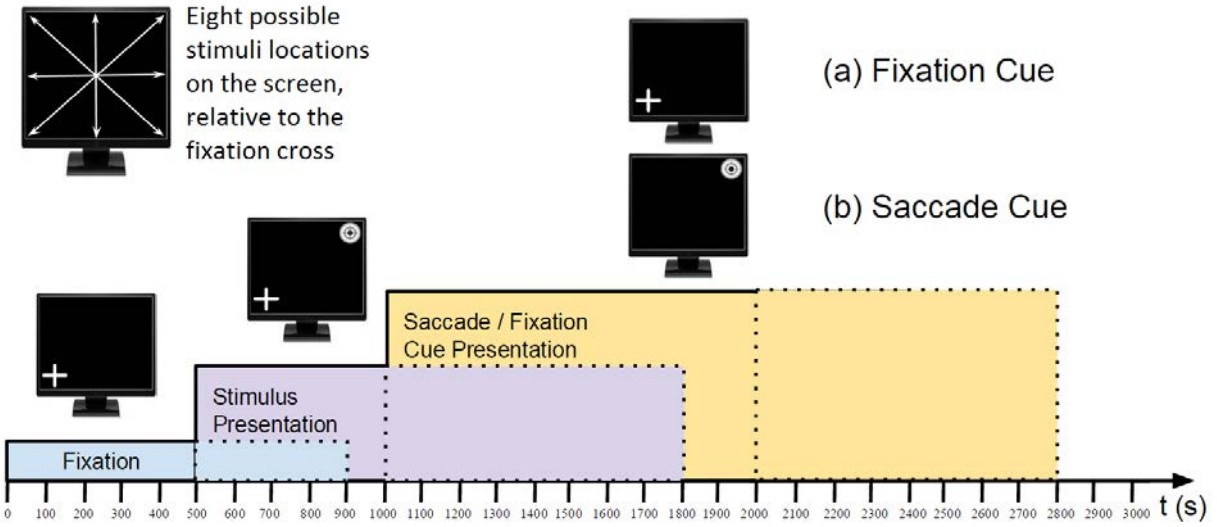

Figure 4.5: Timing scheme of the Long Saccade experimental paradigm (*Experiment2*).

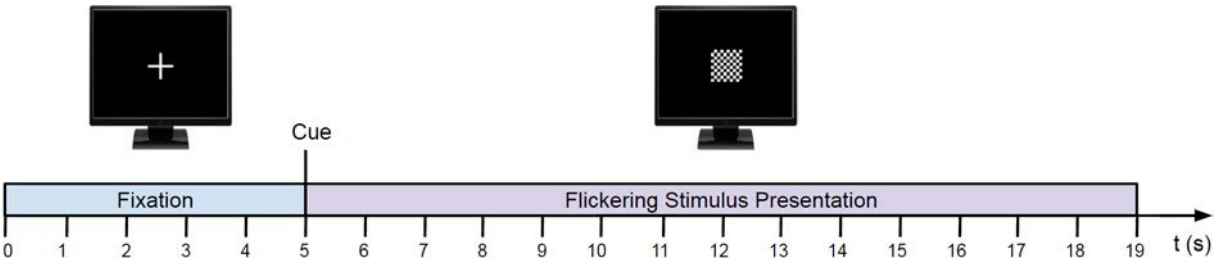

Figure 4.6: Timing scheme of the Fixed SSVEP experimental paradigm (*Experiment3*).

4.2.7 Experiment 3: Fixed SSVEP

This experiment consists of three tasks, attending to a visual stimulus flickering at $7Hz$ ($class1$), $10Hz$ ($class2$) and $12Hz$ ($class3$). Each subject is participated in one screening session. The session consists of 8 runs of $19s$ each and 3 classes of task. This resulted in recording $57s$ of EEG data per run and $456s$ of EEG data per session. In this experiment users are presented with $7Hz$, $10Hz$ and $12Hz$ flickering visual stimuli. Referring to Figure 4.6, each run starts with presentation of a fixation cross in the middle of the screen ($t = 0$). Subjects are instructed to remain relaxed and fix their gaze on the fixation cross for $5s$. At time $t = 5$, a 10×10 checkerboard flickering at $7Hz$, $10Hz$ or $12Hz$ (corresponding to one of three classes, $class1$, $class2$ or $class3$) overlays the fixation cross and remains still for $14s$. During the presentation of the flickering stimuli subjects should focus on them.

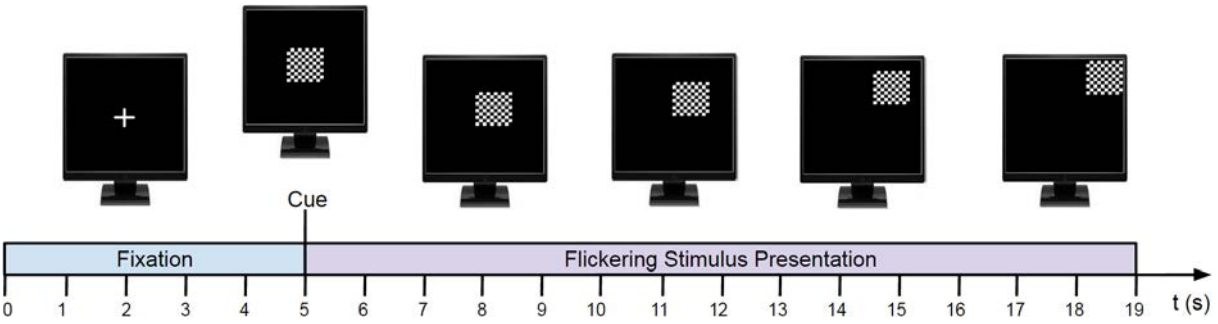

Figure 4.7: Timing scheme of the Pursuit SSVEP experimental paradigm (*Experiment4*).

4.2.8 Experiment 4: Smooth Pursuit SSVEP

This experiment consists of 24 tasks, attending to visual stimuli smoothly moving towards one of the eight locations around the screen edge each flickering at $7Hz$ ($class1-8$), $10Hz$ ($class9-16$) and $12Hz$ ($class17-24$). Each subject participated in one screening session. The session consists of a $19s$ run and 24 classes of tasks. This resulted in recording $456s$ of EEG data per session.

Participants are instructed to perform the tasks illustrated in Figure 4.7: The screen is a black square which is divided into 8 possible locations which a stimulus can move towards. The trials start with appearance of a white fixation cross on the centre of the screen ($t = 0$). After 5 seconds ($t = 5$), a 10×10 checkerboard (the stimulus) flickering at one of the three different frequencies ($7Hz$, $10Hz$ or $12Hz$) covers the fixation cross. The stimulus moves from centre towards one of the 8 edge locations on the screen for $14s$. There are also 8 trials for flickering stimuli moving in different directions.

4.2.9 Data file description

All EEG recordings are stored in *.set* and *.fdt* formats, readable by the EEGLAB toolbox [101]. The *.fdt* file contains raw EEG data and the *.set* file contains header files and meta-information (e.g. sampling frequency, referencing method, event markers, etc.). Data files can be loaded using EEGLAB which is an open-source interactive MATLAB toolbox, available for free at `http://sccn.ucsd.edu/eeglab/`. VOG recordings are stored in

MATLAB's *.mat* file.

Overall, there are two files for the datasets described in Chapter 3, and three files for the dataset described in section 4.2, per subject per experiment.

4.3 Plöchl Dataset

The Plöchl dataset was originally collected using laboratory apparatus, to identify and characterise eye movement artefacts and remove them from EEG data. In this study, the dataset is used for evaluation of the proposed signal processing approaches described in Chapter 5, 6 and 7, and comparing the obtained results with the data collected using consumer-grade apparatus (described in section 4.2). The dataset contains simultaneously recorded EEG and VOG data, during a cue-based non-feedback (screening) paradigm. All subjects (described in section 4.3.1) participated at least in two runs of the experiment and the same experimental set-up is applied on all.

4.3.1 Subjects

EEG and eye movements are simultaneously recorded from 14 subjects (7 male, 7 female; age range $20 - 31$ years). The subjects have normal or corrected-to-normal vision and have no history of neurological disorders. Informed consent is obtained from all subjects.

4.3.2 Experimental set-up

The subjects were positioned at a distance of about $60cm$ from a $30inch$ thin-film-transistor (TFT) LED monitor with $60Hz$ vertical refresh rate. Due to the limited tracking range of the remote eye tracker only a square region of 960×960 pixels in the center of the screen was used for stimulus presentation.

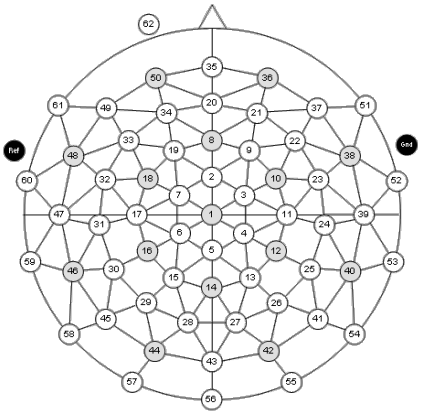

Figure 4.8: Electrode locations in the comparison dataset.

4.3.3 Apparatus

EEG was recorded using an ActiCap 64-channel active electrode system with a BrainAmp DC amplifier(Brain Products GmbH, Gilching, Germany). 61 of the electrodes are placed equidistantly on the scalp, in accordance with the international $10-20$ system (Figure 4.8). The other 3 electrodes are used for EOG recording; and were placed on the forehead, and on the left and right infraorbital rim, respectively. The EEG sampling rate was $1000Hz$, and data is online band-pass filtered between $0.016Hz$ and $250Hz$. A nose tip electrode is used as the reference for all the electrodes.

VOG was captured with Eyelink 1000, a remote eye tracker, sampling at $500Hz$ (Eyelink 1000, SR Research Ltd., Mississauga, Canada). The eye tracker system uses monocular pupil tracking to track the subject's left eye with averaged accuracy of $0.5°$. Prior to each recording, a 13-point grid is used to calibrate eye position.

4.3.4 Synchronisation

First, EEG data is down-sampled to $500Hz$ and low-pass filtered at $100Hz$, in order to match the sampling rate of VOG data. Then, EEG and VOG data are aligned using the shared events that are simultaneously sent to both, the EEG and eye tracking system.

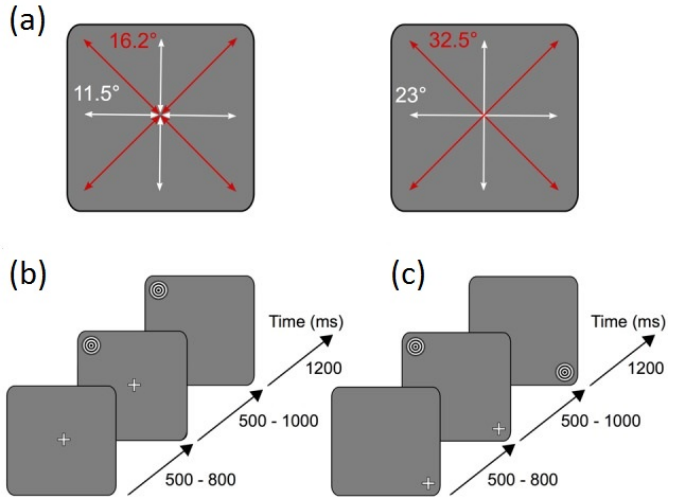

Figure 4.9: Possible stimulus locations and timing schemes of the comparison dataset [13].

4.3.5 Experimental Procedure

The screening paradigm in this experiment consists of eighteen tasks namely, fixation ($class1$), ERP ($class2$) short horizontal saccades to the right ($class3$) and the left ($class4$), short vertical saccades to the up ($class5$) and the down ($class6$) and short diagonal saccades to the up right ($class7$), the up left ($class8$), the down right ($class9$) and the down left ($class10$), long horizontal saccades to the right ($class11$) and the left ($class12$), long vertical saccades to the up ($class13$) and the down ($class14$) and long diagonal saccades to the up right($class15$), the up left ($class16$), the down right ($class17$) and the down left ($class18$). The session consists of a run including 480 repetitions of the fixation task ($class1$), 480 repetitions of the ERP task ($class2$) and 480 repetitions of the saccade tasks ($class3 - 17$). This resulted in recording approximately $3000s$ of VOG and EEG data per run. All subjects performed at least two runs of the experiment.

Referring to Figure 4.9, users are presented with a black square display and there are 8 possible stimulus locations around the screen edge. Sessions start with the appearance of a white fixation cross in the centre of the screen ($t = 0$). After a random time between $500ms$ and $800ms$ ($t = 500 - 800ms$), the stimulus is presented at one of the other eight remaining edge locations. In the short and long saccade conditions (Figure 4.9b

and Figure 4.9c, respectively), the fixation cross disappears at a random interval between $500ms$ to $1000ms$ after stimulus presentation ($t = 1000 - 1800ms$), which provides the cue for subjects to make a saccade to the stimulus location. In the fixation condition, the stimuli presented at the edge disappear and are replaced by the fixation cross at a random interval between $500ms$ to $800ms$ after its presentation ($t = 1000 - 1800ms$). Subjects should fix their gaze on the fixation cross while it is presented on the screen. In both conditions, the stimulus is presented for a further $1200ms$ after the disappearance of the fixation cross.

4.4 Summary

In this chapter, we introduced two matched EEG/VOG datasets. The first dataset is collected using wearable consumer-grade apparatus, while the latter dataset is recorded using intrusive laboratory equipment. The EEG/VOG datasets are used, to evaluate the proposed eye movement classification, EOG artefact removal and feature extraction methods described in the next experimental chapters of the thesis (Chapters 5, 6 and 7).

"There is no greater wealth than wisdom, no greater poverty than ignorance; no greater heritage than culture and no greater support than consultation."

Ali ibn Abi Talib (PBUH)

5

Hybrid EEG-EOG Eye Tracker

5.1 Introduction

Most studies in EEG signal processing are motivated by Neuroscience and BCI rather than eye tracking; eye movement is seen as an unwanted artefact. In this chapter, we propose a hybrid EEG-EOG eye tracking scheme, in which Oculomuscular movements via EOG and the brain's response to flickering stimuli - SSVEP, are used to estimate FoA.

First, we propose a signal processing method to classify blinks and different types of eye movements. This could be beneficial for researchers interested in human activity recognition based on number of blinks or eye movement types occurring during different activities. Then, the proposed method is used for saccade amplitude and eye movement

direction classification, leading to FoA estimation. The FoA estimation is then improved by using the brain responses to SSVEP stimuli as an additional source of information.

The dataset described in section 4.2 is used to evaluate the proposed method. The ultimate goal of the study is to assess the feasibility of employing non-intrusive and affordable EEG apparatus for real-life applications. Therefore, in contrast with normal EEG and EOG studies which use laboratory grade devices, the evaluation dataset is recorded using wearable consumer-grade apparatus. This way the feasibility of using off-the-shelf EEG devices for human activity recognition and eye-tracking is also assessed. Additionally, in order to prove the integrity of our method and for the aim of comparison, the method is applied on a VOG-EEG dataset recorded using laboratory-grade devices (dataset descried in section 4.3).

5.1.1 Related Works

Several studies have focused on employing EEG for FoA estimation and have proposed different algorithms for EEG-based FoA estimation [102, 103, 104]. However, most of the proposed algorithms are either computationally demanding or EEG data are recorded using intrusive laboratory-based apparatus. Some other studies attempted to use EOG data for eye-tracking and FoA estimation. In the most recent study, [105] exploited the nonlinearity of EOG and estimated absolute eye angle with an error less than 4°. Also, [7] used a SVM classifier to classify saccade, fixation and blinks with an average precision of 76.1%. Although EOG is a simple method for FoA estimation, it performed well in FoA estimation. Like EEG, it is intrusive and limits the visual field due to the electrodes placed around the eyes. Typically, EOG users feel discomfort.

There is much research stating that simultaneous use of EEG and EOG is not viable, especially in EEG researches, where EOG is seen as an unwanted source of artifacts that must be removed from the data. However, recently, [106] proposed an algorithm to extract EOG information from EEG data (recorded by laboratory apparatus) for classification of eye movements in four directions and obtained an average accuracy of 64%. In a more

recent study, [107] used a laboratory-based EEG apparatus with only two electrodes and achieved an average accuracy of 85.20% for classification of eye movements in five different directions.

The combined use of EEG and EOG has also gained interest in the research community, and some research has attempted to use EOG artefacts as an extra source of information to improve the performance of EEG paradigms [108, 109]. For example, in the most recent study, [109] proposed a hybrid EEG/EOG approach in which the eye movements detected using EOG (recorded using facial electrodes) are used along with ERP data extracted from EEG, for robot control. Also, [108] used the combination of EOG and EEG activity for asynchronous control of a wheelchair. All the described studies used methods that were intrusive and recorded data using laboratory-grade equipment or achieved low performance in eye-movement detection.

5.2 Methodology

A signal processing method for eye tracking based on the EEG integrated EOG information and detection of SSVEP responses is proposed. The proposed method is used to:

- Classify different types of eye movements- saccade, smooth pursuit and fixation.
- Classify direction and amplitude of eye movements, in case of saccade and smooth pursuit.
- Estimate the eye position in relation to the visual field from the SSVEP response detection and apriori knowledge of the positions of stimuli in the visual field.

Figure 5.1 illustrates the overall architecture of the proposed signal processing method. Input to the processing chain are the 14 channel EEG signal (including timestamps of all events) and the VOG signal capturing vertical and horizontal coordinates of the eyes.

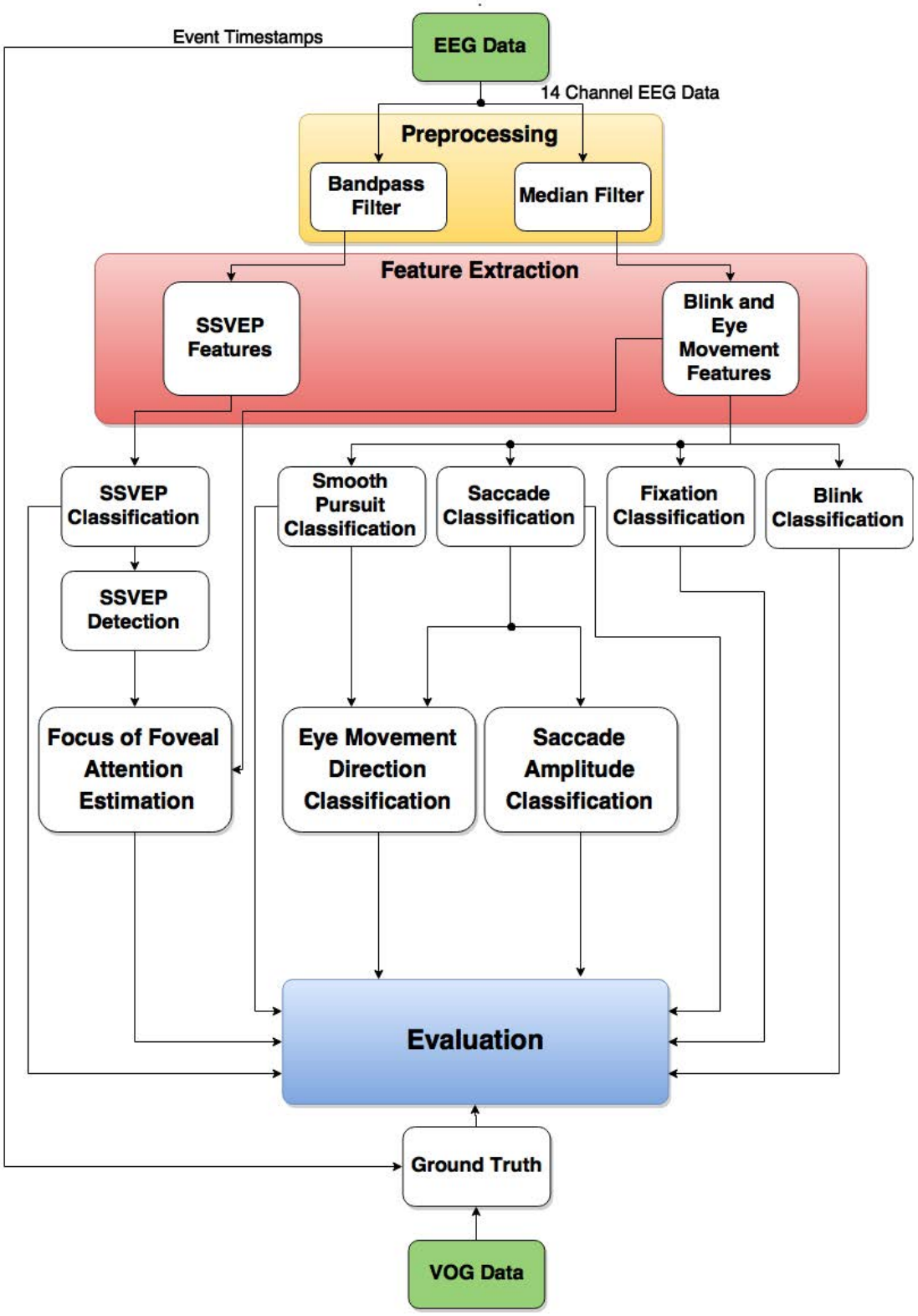

Figure 5.1: Architecture of the proposed eye movement classification and focus of foveal attention estimation system.

In the first step, as a preprocessing step, the 14 channel EEG data are filtered in order to remove the undesired frequency ranges and high frequency noise. In the next step, a set of features are extracted to classify blinks and three different types of eye movements from the processed data: saccade, smooth pursuit and fixation. Then, the amplitude and direction of the eye movements are classified. In parallel to eye movement classification, a SSVEP classification procedure is performed to find out whether a subject is attending to a flickering stimulus or not. In the last stage, the FoA is detected based on the results obtained in the directional eye movement classification and SSVEP classification results. The results are then evaluated using a Ground Truth generated from timestamped events within the EEG data and optical information from the VOG data.

5.2.1 Blink and Eye Movement Classification

Blink and eye movement classification consists of multiple steps; noise removal, feature extraction and classification. Details of each step are described in the following.

Noise Removal

EOG data (integrated with EEG) may be contaminated with noise originated from different sources, such as the power line noise, DC drift, electrode displacement, etc. Existing noises in the recordings, may spoil the eye movement analysis, thus it is crucial to remove noise from eye movement data.

In order to classify the eye movements, the EOG characteristics such as steepness of signal edges and signal amplitude, should be preserved after noise removal. Additionally, the de-noising filters should not introduce additional noise that may be misinterpreted as different types of eye movements. In order to identify optimum noise removal filters, a moving average filter and a median filter [7] are applied on the data and results are compared by visual inspection.

Figure 5.2 illustrates a comparison between the raw and filtered EEG signal during blinking, when median and moving average filters are applied for de-noising. Based on

the comparison, the median and moving average filters successfully preserved the signal amplitude and removed noise at the same time. A similar result is obtained for preserving the edge steepness of the signal (see Figure 5.2b). Comparing the two filters, both of them successfully removed noise and preserved eye movement characteristics at the same time; however, a smoother signal is obtained when the median filter is applied. Most of the small fluctuations which are removed using the median filter are actually micro-saccades. As it was described in Chapter 4, the employed VOG device is unable to record micro-saccades due to its low sampling frequency. Therefore, in this research we do no take into account the micro-saccades, and median filter is selected as the optimum filter. This confirmed the results obtained by [7] in which the median filter is selected as the optimum EOG noise removal filter. The choice of median filter's window size is really important, due to the fact that a very large window size could remove pulses such as blinks, of a width smaller than about half of the window size; and very short window sizes might not effectively remove noise from the signal. The window size of the median filter is empirically obtained and is set to $100ms$, which is large enough to preserve blink pulses [110].

Feature Extraction

Features are extracted from each of the cleaned EEG channels. To extract features, each channel is epoched into $400ms$ temporal windows with 50% overlap. The window and overlap size are empirically optimised based on the knowledge about duration of eye movements (described in section 2.2.1) and the empirical results obtained in the pilot study (described in section 3.9). Four features are extracted per window per channel- the mean, variance, maximum amplitude and minimum amplitude. All the extracted features are concatenated at the end. In total, 56 features (i.e. 4 features $\times$ 14 channels) are extracted from each temporal window.

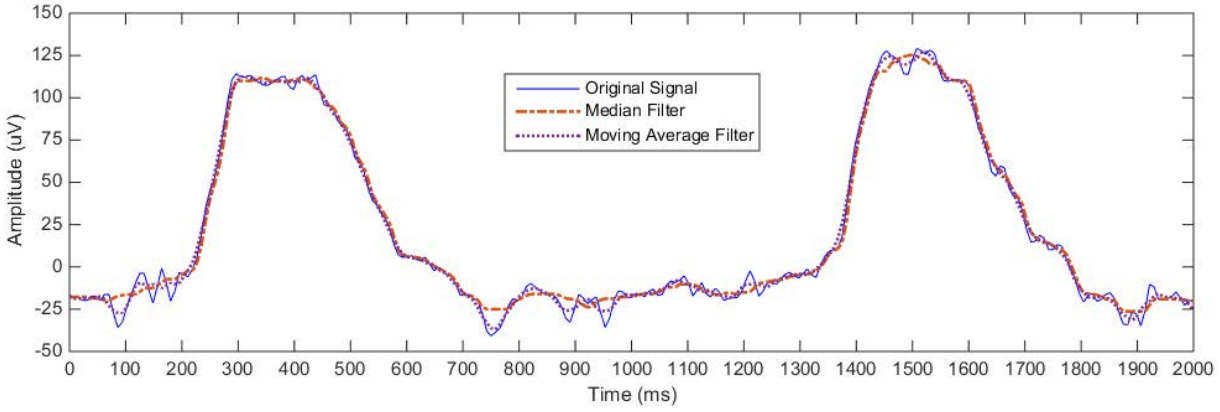

(a) Blink signal

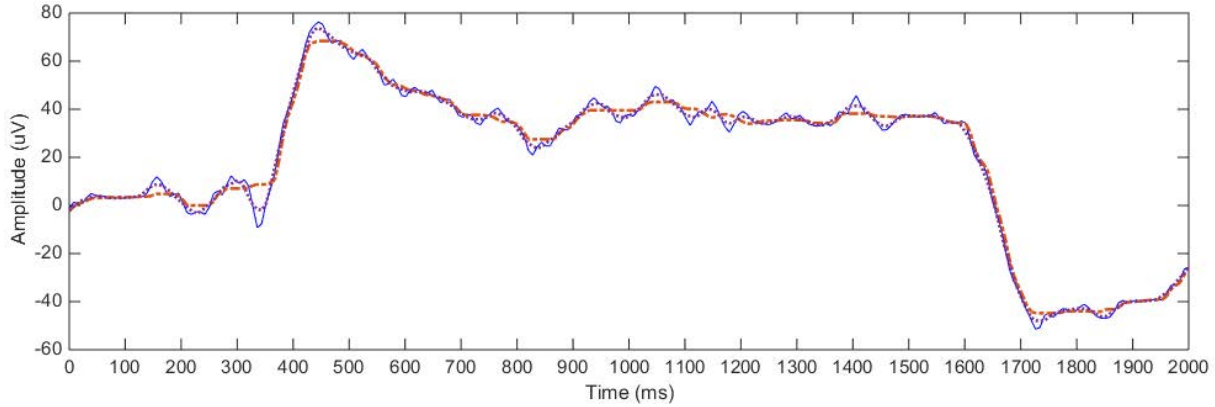

(b) Saccade Signal

Figure 5.2: Comparing performance of different filter types in removing noise while preserving different eye movement characteristics for (a) blink and (b) saccade.

Classification

For feature classification, a K-Nearest neighbour (kNN) classifier with Euclidean distance metric is employed. The value of k is set to 1 (i.e. 1-NN). The eye movement classification procedure consists of multiple stages. In the first stage, 4 separate classifiers are trained to distinguish blink from non-blink, fixations from non-fixation, saccade from non-saccade and smooth pursuit from non-smooth pursuit. In the next stage, the feature instances classified as saccades are inputted to two other classifiers for classification of amplitude and direction of saccadal eye movements. In Parallel, the feature instances classified as smooth pursuit are inputted to another classifier, to classify direction of smooth pursuit eye movements.

The classifiers in the first stage might not perfectly classify all instances, consequently, there is a possibility that the inputs to the classifiers used for eye movement direction and saccade amplitude classification might not be the correct saccade or smooth pursuit eye movements at all. Therefore, for the aim of comparison, 4 other classifiers are trained to classify saccade amplitude and direction of smooth pursuit, short saccade and long saccade eye movements.

5.2.2 SSVEP Frequency Classification and Stimuli Detection

The SSVEP classification process is similar to the one described in section 3.6. However, here the stimuli flicker at three different frequencies.

Preprocessing

EEG channels are band-pass filtered (1 –30Hz) to remove slow drift and high-frequency noise (e.g. mains hum and EMG artefacts), which contaminate the EEG data.

Feature Extraction

Features are extracted from each of the preprocessed EEG channels. To extract features, each channel is split into 2000ms temporal windows with 90% overlap. The window and overlap size is selected based on the results obtained in section 3.8. Based on the stimulation paradigm, 2 features per stimulus are extracted per channel - the spectral power at the stimuli frequencies (typically either 7Hz, 10Hz or 12Hz) and the second harmonics. The Power Spectral Density is estimated using Welch's method [111]. The extracted features from all channels are concatenated at the end to generate 84 features.

Classification

In order to detect whether subjects are attending to an SSVEP stimulus, the following SSVEP detection procedure is performed. First, $1 - NN$ classifier with a Euclidean distance metric is employed for SSVEP classification. The flickering frequencies of stimuli

are classified into 4 classes- $7Hz$ (C_{7Hz}), $10Hz$ (C_{10Hz}), $12Hz$ (C_{12Hz}) and fixation or $0Hz$ (C_{0Hz}) . Then, if a feature instance, f is classified as belonging to fixation class, C_{0Hz}, the output of the SSVEP detector, $SSVEP_{Stim}$, is set to 0 (no SSVEP stimulation), otherwise, there is SSVEP stimulation, and the output of the SSVEP detector is set to 1.

$$SSVEP_{Stim} = \begin{cases} 0 & \text{if } f \text{ belongs to class } C_{0Hz} \\ 1 & \text{otherwise} \end{cases} \tag{5.1}$$

5.2.3 Hybrid SSVEP-EOG for FoA estimation

The SSVEP response detection and apriori knowledge of the position of flickering stimuli in the visual field are used as extra information to improve the classification of directional pursuit eye movements, providing an estimation of the eye position in relation to the visual field. To this aim, first SSVEP detection is performed. Then, the SSVEP detection results are used as a new feature (with values 0 and 1) and is concatenated to the eye movement feature vectors. If the value of the new feature is 0 it implies that there is no smooth pursuit, and if the value is 1 it implies that there is smooth pursuit eye movement. The new feature vectors are input to a 1-NN classifier for gaze estimation.

5.3 Evaluation

With the aim of evaluation, the proposed system is applied on a matched VOG-EEG dataset captured during a screening paradigm. The system's classification output is compared to the Ground Truth (as described in section 5.3.3); and performance of the system is assessed using the True Positive Rate, True Negative Rate, Balanced Accuracy and Root Mean Square Error.

Table 5.1: Application of the data recorded in each experiment, for saccade, fixation, blink, smooth pursuit and FoA classification.

Experiment	Blink	Fixation	Smooth Pursuit	Saccade	Saccade Amplitude	Eye Movement Direction	SSVEP
Exp.1	x	x	–	x	x	x	–
Exp.2	x	x	–	x	x	x	–
Exp.3	x	x	–	–	–	–	x
Exp.4	x	x	x	–	–	x	x

5.3.1 Data description

The matched VOG-EEG dataset described in section 4.2 is used. The dataset contains data recorded during four experiments. In the first two experiments subjects are asked to perform short and long saccadal eye movements; and in the next two experiments subjects are asked to attend to flickering stimuli that are fixed on the screen, or move in different directions.

Table 5.1 shows what is the usage of data recorded during each experiment. As is illustrated in the table, fixation and blink classification is performed using the data from all experiments. The data captured in experiments 1 and 2 are used to classify the saccadal eye movements and amplitude of the saccade.

The data captured during experiments 1, 2 and 4 are used for classification of direction of the eye movements. Smooth pursuit eye movements are classified using the data captured during experiment 4. SSVEP frequency classification and stimulus detection is performed on the data captured in experiments 3 and 4. The dataset includes matched VOG-EEG recorded from 7 subjects. However, the VOG data of 2 subjects is not useful due to the large amount of missing data and large gaps in the VOG recording. Consequently, the data collected from these 2 subjects are not considered in this study.

5.3.2 Comparison Dataset - Plöchl

To evaluate the generalisability of the proposed blink and eye movement type and eye movement direction classification method over different datasets, the signal processing method wa applied to a comparison VOG-EEG dataset, recorded by laboratory equipment. Details of the dataset and experimental paradigm can be found in section 4.3. The dataset is used to classify blink, fixation, saccade, saccade amplitude and eye movement directions.

5.3.3 Ground Truth

In order to evaluate the performance of the proposed blink and eye movement classification system, a ground truth is needed. The system's classification output is compared to the labeled blinks and eye movements.

Eye movement labeling

All the eye movement events except blinks (i.e. saccade, fixation, smooth pursuit, direction of eye movements and saccade amplitude), are automatically timestamped in the recorded data, using the Python based stimulation paradigm described in section 3.5.2.

Blink labeling

Because the blinks occur involuntarily in the data, it is not possible to label the blink events using the stimulation paradigm. It is known that when blink occur, the optical eye-tracker cannot identify eyes, and gaps occur in the VOG data due to missing data samples. It is also known that, average blink duration varies between 100 and 400ms (see section 2.2.1). Therefore, the gaps in the VOG data which last between 100 to 400ms are labeled as blink events.

Figure 5.3 shows the histogram of the detected blinks' durations. The histogram shows that blink durations have a near-uniform distribution. However, the duration of

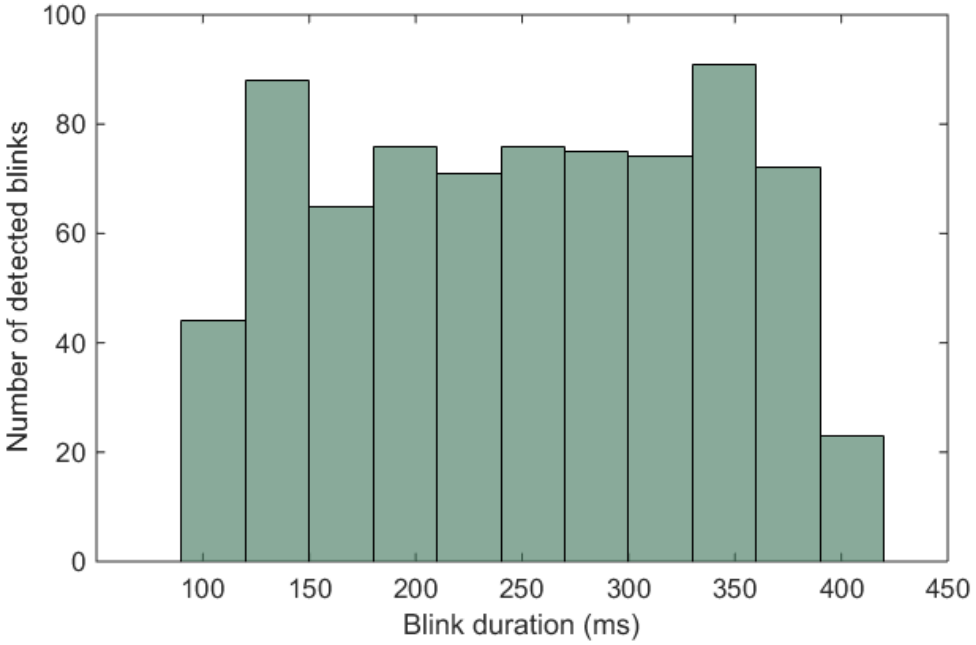

Figure 5.3: Distribution of the detected blink's duration.

most blinks is between $125ms$ to $375ms$; and less blinks lasted about $400ms$.

5.3.4 Performance measures

By matching system's classified blink and eye movement events with the annotated ground truth, true positives (TPs), false positives(FPs), true negatives (TNs) and false negatives (FNs) are calculated. Therefore, because the number of instances in all of the classes are not necessarily equal (e.g. number of blink is not known and may not be equal to non-blinks), Balanced Accuracy (BA), which is the average of True Positive Rate (TPR) and True Negative Rate (TNR), and is unaffected by imbalanced classes [112], is calculated.

$$BA = \frac{(TPR + TNR)}{2} \tag{5.2}$$

where,

$$TPR = \frac{TP}{TP + FN} \tag{5.3}$$

$$TNR = \frac{TN}{TN + FP} \tag{5.4}$$

The BA of the blink and different eye movement types are calculated separately; for each subject. The BA of the proposed system for classification of blink and all other eye movement types is obtained by averaging BA over all subjects. Additionally, performance of eye movement direction classification is assessed by the Root Mean Square Error (RMSE) of the difference between the detected angle and the real angle associated with the stimuli's position:

$$RMSE = \sqrt{\frac{1}{N}\sum_{t=1}^{N}(\theta_t - \hat{\theta}_t)^2} \tag{5.5}$$

where N is the time length, and θ_t, $\hat{\theta}_t$ are the real and estimated angular position of the stimuli at time t, respectively.

The performance of the classifiers is evaluated using a 5-fold cross-validation. The data is divided into 5 folds, and each fold corresponds to the feature vector extracted from data of 1 subject. There are 5 iterations in which during each iteration, the feature vector of 4 subjects (4 folds) are taken as training data and the feature vector of the remaining subject is taken as test data. The BA and RMSE (if applicable) are obtained on each iteration. The system's overall BA (and RMSE) is obtained by averaging the obtained BA (and RMSE) over all the 5 iterations and subjects.

5.4 Results and Discussion

The obtained results for blink and eye movement classification as well as SSVEP detection and hybrid FoA estimation are reported.

5.4.1 Blink and Eye Movement Classification

The heat-maps in Figure 5.4 illustrate the point of gaze, of a typical subject, corresponding to VOG data recorded during different experiments. Table 5.2 summarises the results obtained for blink and eye movement type classification. The average balanced accuracy of the classifiers, and the corresponding experimental data, for blink, fixation, smooth

(a) Experiment1: short saccade (b) Experiment2: long saccade (c) Experiment3: fixed SSVEP (d) Experiment4: smooth pursuit SSVEP

Figure 5.4: Point of gaze of a typical subject during a) short saccade, b) long saccade, c) fixed SSVEP and d) smooth pursuit SSVEP experiments, obtained from VOG data recorded by an optical eye tracker. The details of each experiment are described in section 4.2.

pursuit and saccade classification, are reported. Because each experimental paradigm is designed for classification of certain types of eye movements, classification of some eye movement types are not applicable using all of the experimental data. Despite the fact that fixation and blink are common in all experiments, and the timestamps of both events are annotated in all of the experimental data.

Table 5.2: Obtained BA for Blink and eye movement classification, using data recorded during different experiments. Dash-line represents the cases where, using the corresponding data, classification of specific types of eye movement is not applicable.

Experiment	Blink (%)	Fixation (%)	Smooth Pursuit (%)	Saccade (%)
Exp. 1	83.20	90.26	–	80.11
Exp. 2	79.01	95.70	–	85.23
Exp. 3	85.00	96.30	–	–
Exp. 4	82.04	94.33	76.00	–
Average	82.31	94.14	76.00	82.67

As is evident from the results, fixation classification achieved the highest BA, 94.14%, when compared to blink and other eye movement types. This could be due to the fact that fixation segments have more stereotyped behavior than blink and other types of eye movement. Additionally, according to the experimental paradigms, the training samples for fixation classification are more than blink and other eye movement types. It can be confirmed by looking at BA of fixation classification through different experiments. As is

shown in the results, fixation's BA is highest in experiment 3, where subjects are asked to attend to a fixed SSVEP stimulus at the centre of the screen and avoid other types of eye movements.

With 82.31% average BA, blink classification achieved approximately 12% lower BA than fixation classification. This might be due to imperfect labeling of blink segments in the data. Based on the sampling rate of the employed optical eye tracker and as is mentioned in the eye tracker's manual, some of rapid and large saccades might not be captured by the eye tracker, resulting in missing points (gaps) in the VOG data. The resulting gaps might be misinterpreted as blinks, and degrade the quality of blink ground truth. This can be confirmed by the obtained BA of blink classification, which is the worst in experiment 2 (79.01%), where subjects are asked to perform large saccades.

The average BA of saccade classification (82.67%) is similar to blink classification (82.31%). Based on the experimental paradigms, saccade classification is only evaluated using the data captured in experiments 1 and 2. As is shown in the results (Table 5.2), saccade classification is highest in experiment 2 (approximately 85%), where subjects perform large saccades, and it is worst in experiment 1 (approximately 80%), where subjects perform short saccades. This is due to the fact that, large saccades have larger amplitudes and are more distinguishable, from other types of eye movements, than short saccades.

Smooth pursuit classification is only evaluated using data captured in experiment 4. Between all eye movement types, smooth pursuit achieved the worst BA (76%). By looking at the predicted labels of the classifier, it is found that low BA of smooth pursuit classification might be due to miss-classification of short saccades as smooth pursuit. This suggests that, using the selected features, smooth pursuit is less distinguishable from short saccades.

Table 5.3 shows the results obtained for classification of saccade amplitude. The results shows, how accurate the system discriminates large saccades from short saccades. The result presents the BA of saccade amplitude classifier, when it is applied on the output

feature instances of saccade classification (discriminating saccades from non-saccades), and when it is applied on the concatenated feature instances extracted from short and large saccade experiment data (experiments 1 and 2, respectively). As is shown in the results, the amplitude of saccades can be classified with 95.22% BA, when saccade classification is not performed beforehand. However, the BA of saccade amplitude classification decreases by approximately 22% when it is applied on the data labeled as saccade using saccade classifier. According to the results, when saccade classification is applied beforehand, the BA of large saccade classification in experiment 2 (BA= 73.50%), is 2% higher than short saccade classification in experiment 1. Therefore, if saccade amplitude classification is applied on the output of saccade classifier, using both data in experiment 1 and 2, the average BA of saccade classification is 72.41%. Imperfect saccade classification resulted in misclassification of some non-saccade instances as saccades; consequently, the saccade amplitude classifier misclassified some non-saccade instances as either short or long saccades.

The obtained results of eye movement direction classification are presented in Table 5.4. The BA and RMSE of eye movement direction classification are reported. Results are compared when eye movement direction classification is applied on the feature instances previously classified as smooth pursuit or saccade, and when it is applied on the unlabeled feature instances. The results show that the highest BA and lowest RMSE are obtained for direction classification of smooth pursuit eye movements from unlabeled

Table 5.3: Saccade amplitude classification result, when it is applied directly on the data (Before Saccade Classification) or it is applied on the saccade instances obtained using saccade classification (After Saccade Classification).

Experiment	**Saccade Amplitude Classification**	
	Before Saccade Classification	After Saccade Classification
Exp.1	95.22 %	71.33 %
Exp.2		73.50 %
Average	95.22 %	72.41 %

data in experiment 4 (BA=81.64% and RMSE=11.51°). The performance is decreased by almost 10% when feature instances classified as smooth pursuit are used for eye movement direction classification. Eye movement direction classification for short and large saccades achieved similar results (approximately BA=74% and RMSE=19°), when unlabeled data is used. The result is degraded by almost 4% when feature instances labeled as saccade or smooth pursuit are used for eye movement classification. Similar to saccade amplitude classification, the eye movement direction classification is degraded due to imperfect saccade and smooth pursuit classification.

5.4.2 SSVEP Frequency Classification and Stimulus Detection

Table 5.5 summarises the results obtained for SSVEP frequency classification and stimulus detection during fixations and smooth pursuits (experiments 3 and 4, respectively). The BA of the classifiers are reported. Results suggests that the SSVEP response during smooth pursuit movements is no harder to detect than fixations despite the potential for more EEG signal contamination due to eye-related artefacts. Surprisingly, the result shows that SSVEP frequency classification and stimulus detection increased by almost 3% and 1%, respectively; during smooth pursuit (Exp. 4). The lower performance obtained for fixed SSVEP might be due to habituation effects (see section 6.5.3 for more details).

Table 5.4: Eye movement classification result, when it is applied directly on the data (Before Saccade and Smooth Pursuit Classification) or it is applied on the classified saccade or smooth pursuit instances (After Saccade and Smooth Pursuit Classification).

Experiment	**Eye Movement Direction Classification**			
	Before Saccade and Smooth Pursuit Classification		After Saccade and Smooth Pursuit Classification	
	RMSE(°)	**BA(%)**	**RMSE(°)**	**BA(%)**
Exp. 1	19.02	73.84	23.80	69.73
Exp. 2	19.30	73.45	24.51	68.07
Exp. 4	11.51	81.64	20.61	72.00
Average	16.61	76.31	22.97	69.93

Table 5.5: SSVEP frequency classification and stimulus detection results.

Experiment	SSVEP Frequency Classification	SSVEP Stimulus Detection
Exp. 3	83.87 %	91.38 %
Exp. 4	86.59 %	92.27 %
Average	82.23 %	91.82 %

Table 5.6: FoA estimation results, when SSVEP response detection is present (SSVEP Present) and when it is not present (No SSVEP).

Experiment	FoA Estimation			
	No SSVEP		SSVEP Present	
	RMSE (°)	**BA (%)**	**RMSE (°)**	**BA (%)**
Exp. 4	11.51	81.64	10.87	84.00

Overall, on average BA of SSVEP frequency classification is 82.23% and BA of detecting whether subjects are attending on SSVEP stimuli or not, is approximately %6 higher (BA=91.82). The better performance on SSVEP stimulus detection is due to the fact that there are fewer classes (2 classes) for SSVEP stimulus detection than for SSVEP frequency classification (4 classes).

5.4.3 Hybrid SSVEP-EOG for FoA estimation

The result of using SSVEP as an extra source of information to improve eye movement direction classification is reported in Table 5.6. Results demonstrate that the presence of the SSVEP in the visual field not only does not hinder the classification of smooth pursuit direction classification, but it also significantly (p-value=0.04) improves classification of BA by almost 3% and reduces RMSE to 10.87°. Overall, the BA of eye movement direction classification is the best (i.e. 84.00%) with the least RMSE (i.e. 10.87°), when both SSVEP detection and EOG features are used for direction classification.

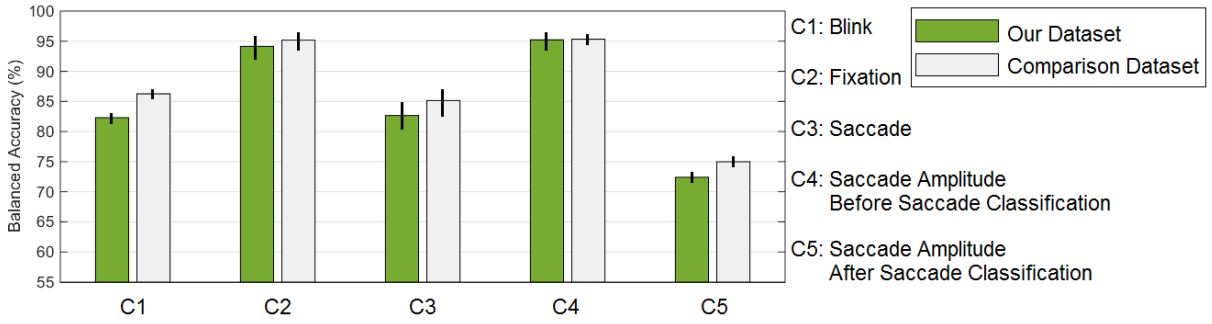

Figure 5.5: The balanced accuracy of blink (C1), fixation (C2), saccade (C3), saccade amplitude before performing saccade classification (C4) and saccade amplitude after performing saccade classification (C5); when data is collected using consumer apparatus (green bars) compared to data collected using laboratory apparatus (gray bars). The error bars represent standard errors.

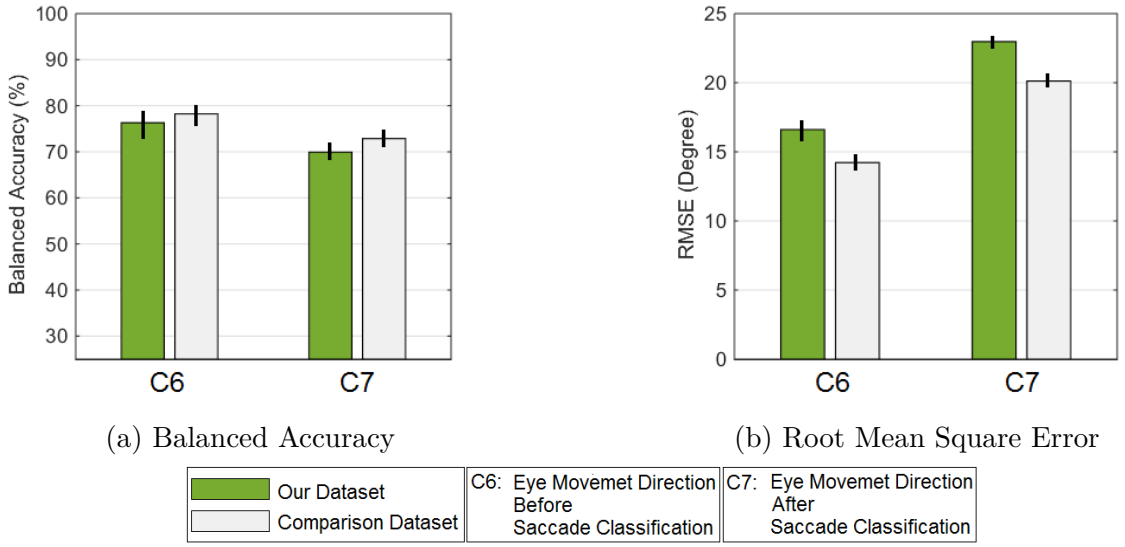

(a) Balanced Accuracy

(b) Root Mean Square Error

Figure 5.6: (a) Balanced accuracy and (b) RMSE, of the eye movement direction classification, before performing saccade classification (C6) and after performing saccade classification (C7); when data is collected using consumer apparatus (green bars) compared to data collected using laboratory apparatus (gray bars). The error bars represent standard errors.

5.4.4 Comparison Dataset - Plöchl

Figure 5.5 and 5.6 show the obtained results for blink, fixation, saccade, saccade amplitude and eye movement direction classifications, when our proposed method is applied on the data collected using laboratory based equipments (comparison dataset). The results are compared with the results obtained in section 5.4.1, where consumer-grade equipment

is used.

Results show the performance of all the classification tasks improved, with similar trend to previous results, when the comparison dataset is employed. Although, when t-test is performed, the improvement is only statistically significant (p-value=0.04) for the blink classification. According to Figure 5.5, blink classification increased by 4%, to 86.26%. The highest and the lowest obtained BA are achieved for classification of saccade amplitude, when saccade classification is not performed (BA=95.34%) and when saccade classification is performed (BA=74.98%) prior to amplitude classification, respectively.

Figure 5.6 shows the results obtained for eye movement direction classification (i.e. FoA estimation), in terms of BA and RMSE. According to the results, although using the comparison dataset, the BA of the system is not significantly improved for FoA estimation, the RMSE is significantly (p-value=0.04) improved (by approximately 3°) when saccade classification is performed prior to FoA estimation.

5.5 Summary

A signal processing scheme for extracting eye tracking data from wireless portable scalp-based EEG has been proposed and explored in this chapter. Classification results demonstrate reasonable performance of the proposed system to classify blink and different types of eye movements, as well as FoA estimation. The blink and eye movement classification can be used for human activity recognition and eye tracking applications. The result also demonstrate improved FoA estimation performance when SSVEP response detection is used along with eye movement direction classification. Consequently, FoA estimation might further improved, by improving SSVEP response detection. Additionally, the integrity and generalisability of the proposed signal processing method is shown by applying the method on a comparison dataset collected using laboratory-grade equipments.

"Do not expect goodwill from someone whom you regard with ill will; as his heart towards you is the same as your heart towards him."

Ali al-Hadi (PBUH)

6

Perfomance Improvement by VOG-based EOG Artefact Removal

6.1 Introduction

In the previous chapter, it is demonstrated how SSVEP detection can be used along eye movement direction classification to improve FoA estimation. Therefore, it is suggested that improving performance of SSVEP detection might lead to improved FoA estimation.

Blinking and eye movements are the prevalent artefacts that contaminate EEG signals, leading to less accurate SSVEP detection. In addition to the artefacts, when users are exposed to prolonged flashing stimuli there is a gradual decrement in their SSVEP response

and thus SSVEP detection - an effect known as *habituation* [14].

In the current chapter, we combine the problem of reliably detecting SSVEP for moving stimuli with that of eye movement artefact removal for robust field BCI. Moving stimuli will elicit eye movement artefacts - specifically slow moving 'pursuit' eye movement which can degrade SSVEP detection accuracy. However, moving stimuli can avoid the issue of habituation which can improve SSVEP detection accuracy.

ICA has been successfully applied on EEG data to separate blink and eye movement artefacts from other sources of activity [11]. Although ICA can estimate independent sources, it does not label them. In this chapter we proposed 'BVOG-ICA'- an automatic EOG artefact removal algorithm based on ICA that uses VOG information from an eye-tracker.

The proposed artefact removal method is evaluated using a matched VOG-EEG dataset designed specifically to elicit EOG artefacts arising from pursuit eye movements, fixations and saccades.

The datasets described in section 4.2 and 4.3 are used to evaluate the proposed method. The results are compared with the state-of-art artefact rejection method proposed by Plöchl et al [13] (named Plöchl).

6.1.1 Related Work

As was mentioned in section 2.5.1, most automatic IC labeling methods rely on the frequential, temporal and spatial characteristic of the artefacts. Most of these methods were successful in removing artefacts with distinct spectral or statistical properties. However, there is no distinct properties for eye movement artefacts, specially in case of small saccades or smooth pursuit eye movements. Different types of eye movements have their specific statistical and spectral properties. Additionally, eye movement artefacts may be distributed into multiple ICs. Most of the proposed eye-related artefact removal methods can only detect blink and vertical and horizontal saccades, and consider only one IC for each type of eye-related artefact. Additionally, they can only perform well when the arte-

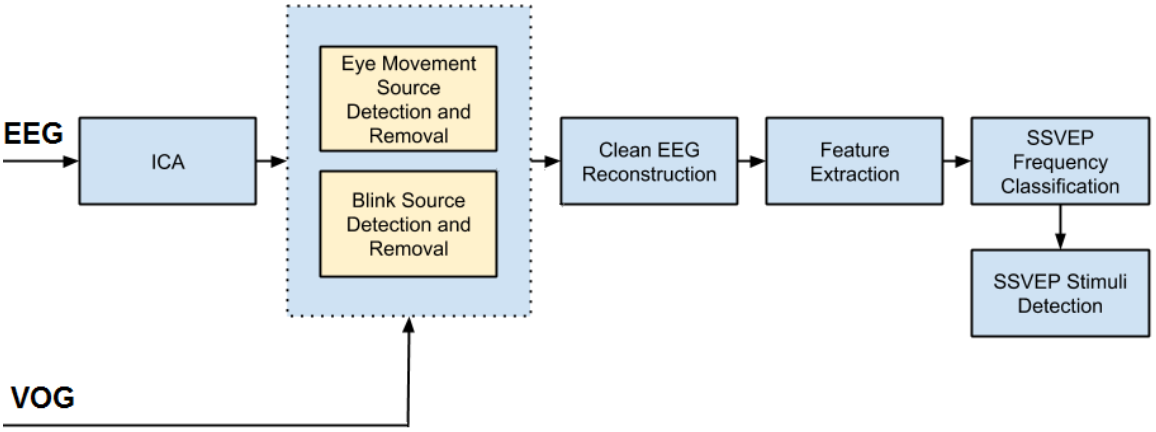

Figure 6.1: Block diagram of the proposed ICA-based artefact removal method.

facts are strongly presented in the data. To solve this problem most recently [13] and [113] considered using optical eye tracking information for handling eye-related artefacts. [113] used optical eye tracking information to detect ERP trials containing EOG artefacts, and exclude them from analysis. This way a large amount of data is lost. However, [13] used eye tracking information to label the artefacts arising from saccades. According to [13], first the saccade and fixation events are detected in the eye tracking data, then the ICs that their mean variance in the saccade durations is 10% larger than their fixation durations, are taken as eye-related artefact. Their method is not properly evaluated and have three major draw backs. First, the method is highly dependent on accuracy of detecting saccade events in the eye tracking data. Secondly, their method can only detect saccade artefacts. Finally, they used a fixed threshold, which limits the generalisation of the method over other datasets.

6.2 Methodology

The block diagram of the proposed method is depicted in Figure 6.1. Different steps of the proposed method for EOG artefact removal and SSVEP response classification are shown. Input to the processing chain are the EEG and VOG signals. In the first step ICA is applied to decompose the EEG data into independent sources, corresponding to artefacts and non-artefacts. Then, optical information form VOG are used to detect and

remove sources corresponding to blink and eye movements. In the next steps, clean EEG data is reconstructed from remaining sources and is used to extract SSVEP features for SSVEP frequency classification. Finally, the presence of SSVEP stimuli is detected via the SSVEP frequency classification results.

Additionally, the habituation effect is investigated by comparing the performance of SSVEP classification when users are exposed to fixed SSVEP stimuli with when they are exposed to moving SSVEP stimuli.

6.2.1 EOG Artefact Identification based on VOG-enhanced ICA

The Extended-Infomax ICA algorithm is employed to separate EOG sources from non-EOG sources (i.e. other EEG activity). According to the ICA assumptions, the N dimensional observed scalp EEG signal $E(t) = [e_1(t)\ e_2(t)\ \cdots\ e_N(t)]$ is a linear combination of independent sources. The independent sources can be originated from cerebral or non-cerebral origins. Here, we divided the independent sources into two parts, sources corresponding to EOG artefact $S_{EOG}(t)$ and all other sources (including cerebral and non-cerebral sources), $S_{nEOG}(t)$. Therefore, according to Equation 2.5, the observed EEG signal of the channels $E(t)$, can be expressed as follows:

$$E(t) = [A_{EOG}\ A_{nEOG}]_{N,N} \begin{bmatrix} S_{EOG}(t) \\ \\ S_{nEOG}(t) \end{bmatrix} \tag{6.1}$$

where A_{EOG} and A_{nEOG} are the corresponding mixing matrices for $S_{EOG}(t)$ and $S_{nEOG}(t)$, respectively. Thus, if there are k number of EOG artefact sources, the observed EEG signal for each channel $e_i(t)$ $(i = 1, 2, \cdots, N)$ can be expressed as a linear combination of EOG

artefact sources and other activity sources as follows:

$$\begin{bmatrix} e_1(t) \\ e_2(t) \\ \vdots \\ e_N(t) \end{bmatrix} = \begin{bmatrix} \overbrace{a_{1,1}\ s_1(t) + \cdots + a_{1,k}\ s_k(t)}^{\text{EOG artefactual sources}} + \overbrace{a_{1,k+1}\ s_{k+1}(t) + \cdots + a_{1,N}\ s_N(t)}^{\text{other activity sources}} \\ a_{2,1}\ s_1(t) + \cdots + a_{2,k}\ s_k(t) + a_{2,k+1}\ s_{k+1}(t) + \cdots + a_{2,N}\ s_N(t) \\ \vdots \\ a_{N,1}\ s_1(t) + \cdots + a_{N,k}\ s_k(t) + a_{N,k+1}\ s_{k+1}(t) + \cdots + a_{N,N}\ s_N(t) \end{bmatrix} \tag{6.2}$$

Considering the limitation of ICA algorithm in separating EOG sources in the case of small and rare eye movements in the EEG recordings, the value of k may vary between 0, i.e. no EOG source, to $N-1$, i.e. there is at least one source other than EOG artefact.

Eye Movement Source Detection

After applying ICA and source separation, we need to detect the EOG artefact sources. In section 2.2.2, it is discussed that horizontal and vertical eye movements can be observed by placing a set of electrodes around the eyes. Additionally, from Chapter 5 we know that VOG recording gives the time-variant signals $x(t)$ and $y(t)$ representing the horizontal and vertical coordinates of the gaze at time t, respectively. We therefore hypothesise that if EEG and VOG signals are recorded simultaneously, the independent sources highly correlated with $x(t)$ and $y(t)$ can be assumed to be EOG artefact sources corresponding to horizontal and vertical eye movements, respectively.

Employing the Pearson product-moment correlation coefficient (PCC) is suggested to show the strength of correlation between the sources estimated by ICA and horizontal and vertical gaze coordinates. The PCC is a statistical measure of the linear dependence between two time-variant signals X and S. The PCC value ranges from -1 to $+1$, where -1 indicates perfect negative correlation, 0 indicates no correlation and $+1$ indicates perfect positive correlation. The formula for PCC between two time-variant signals X

and S, $\rho_{X,S}$, is as follows:

$$\rho_{X,S} = \frac{E[(X - \mu_X)(S - \mu_S)]}{\sigma_X \sigma_S} \tag{6.3}$$

where $E[...]$ is the expected value and σ_X and σ_S refer to the standard deviation of X and S, respectively.

From section 2.5, we know that ICA does not guarantee the sign of its estimated sources, and the sign of the sources may change through each run of ICA. Consequently, it is not possible to predict whether the correlation coefficient values, between an EOG source S and gaze position X (or Y), is positive or negative. Hence, obtaining the absolute value of PCC is of interest (i.e. $|\rho_{X,S}|$). The greater the value of $|\rho_{X,S}|$, the higher the linear relationship between X and S. According to our hypothesis we can say that, the highest $|\rho_{X,S}|$ and $|\rho_{Y,S}|$ values correspond to the sources with most information about horizontal and vertical eye movements, respectively. We have to consider that our hypothesis is only true if the EEG and VOG acquisition equipment have the same temporal resolution and the output signals are perfectly synchronised, which is an ideal case. Even if VOG and EEG data are acquired at the same sampling rates, since independent clocks are usually used in each recording device, the collected data may not be perfectly synchronised and are considered asynchronous.

Figure 6.2 shows a typical example of saccade eye movement captured by synchronised EEG and VOG data (see section 4.2.4 for synchronisation details). Based on the EOG data recorded in EEG, the subject performed the saccade $100ms$ after the presentation of saccade cue; however, based on the VOG data, the saccade is performed $20ms$ later. When checked on our data, the duration of this time lag is not consistent through subjects.

The synchronisation issue can be addressed by calculating the cross-correlation [114] of the sources S, with $x(t)$ and $y(t)$. Basically, the cross-correlation of two time-variant signals S and X, measures the correlation between the two signals as a function of time. This is done by sliding signal S along time and calculating the integral of their dot product

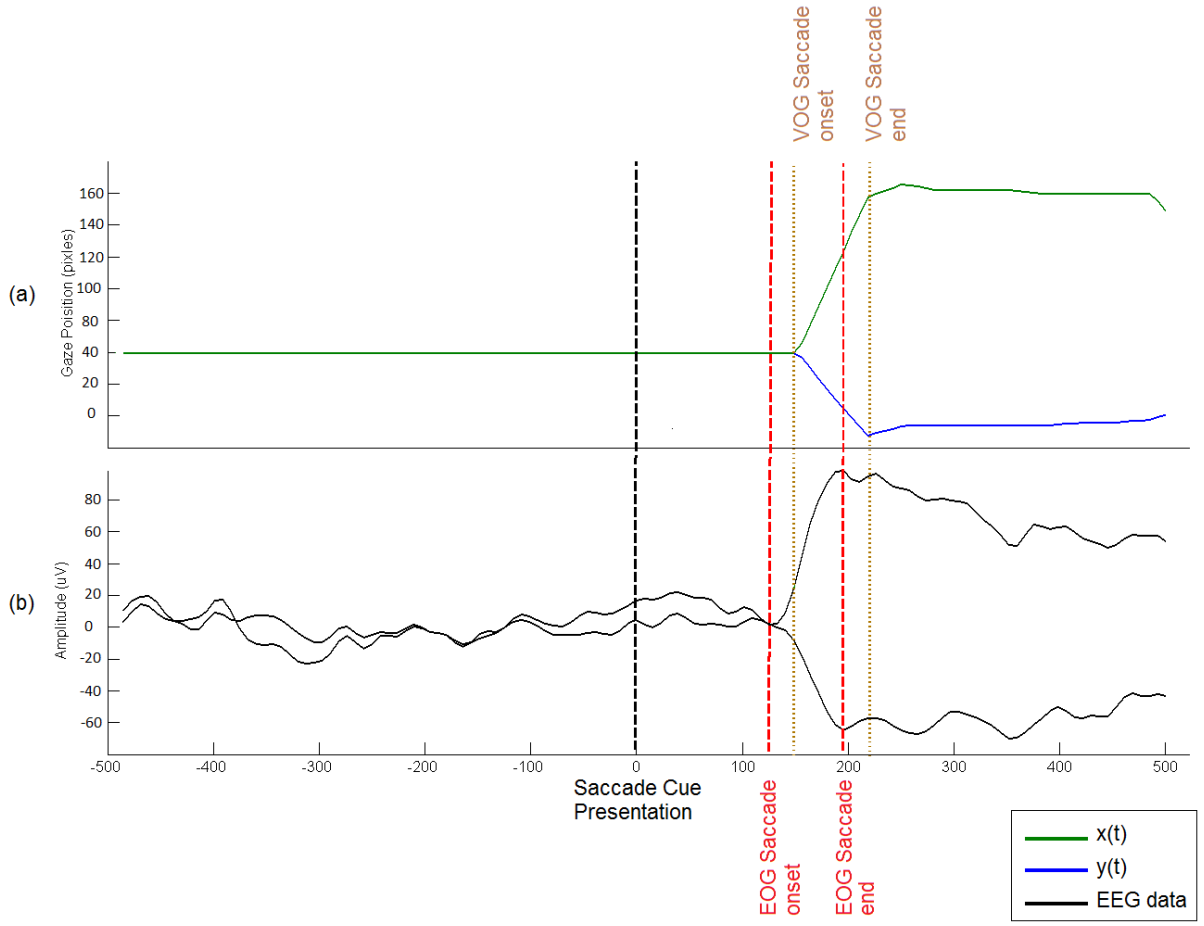

Figure 6.2: Typical example of synchronised (a) VOG and (b) EEG data, when a subject performs a long saccade. The solid black signals in (b) are the EOG activity recorded at channels $F7$ and $F8$ using the consumer-grade EEG device. The black, red and orange dashed lines represent onset and end of saccade cue, EOG saccade response (recorded in EEG) and VOG saccade response events, respectively.

at each time t.

$$(X \star S)(\tau) \stackrel{\text{def}}{=} \int_{-\infty}^{+\infty} X^*(t)\ S(t-\tau)\mathrm{d}t \tag{6.4}$$

where X^* is the complex conjugate of X and τ is the time lag. As mentioned earlier, we are looking for absolute correlation, so the absolute value of the cross-correlation is of interest. The maximum value of cross-correlation indicates the time where the signals S and X are best correlated (aligned). In addition to solve the synchronisation problem, the cross-correlation can be used to determine the time lag between the EEG and VOG recordings. This may help to understand the factors which might affect the synchronisation of two signals (e.g. between experiment or subject variations). The

time lag between two signals $\tau_{\mathbf{lag}}$ is determined by calculating the time which maximum correlation happens:

$$\tau_{\mathbf{lag}} = \arg\max_{t}((X \star S)(\tau) \tag{6.5}$$

Therefore, for EOG artefact labelling, all of the sources are scored according to the maximum absolute values of their cross-correlation with $x(t)$ and $y(t)$, independently:

$$\gamma_{X,i} = \max_{t}(|(S_i * X)(\tau)|) \tag{6.6}$$

$$\gamma_{Y,i} = \max_{t}(|(S_i * Y)(\tau)|) \tag{6.7}$$

where $\gamma_{X,i}$ and $\gamma_{Y,i}$ refer to the maximum absolute values of the cross-correlation between the i^{th} source, $S_i(t)$, and signals $X(t)$ and $Y(t)$, respectively.

In order to generalise our method on different types of datasets collected from different subjects and recording apparatus, and to eliminate the scaling effect, all of the obtained scores are normalised. For normalisation, Z-scores (normal scores) of $\gamma_{X,i}$ and $\gamma_{Y,i}$ for each source are calculated as follows:

$$Z\gamma_{X,i} = \frac{\gamma_{X,i} - E[\gamma_{X,i}]}{\sigma(\gamma_{X,i})} \tag{6.8}$$

$$Z\gamma_{Y,i} = \frac{\gamma_{Y,i} - E[\gamma_{Y,i}]}{\sigma(\gamma_{Y,i})} \tag{6.9}$$

where $E[...]$ and $\sigma(...)$ refer to the expected value and standard deviation of $\gamma_{X,i}$ (and $\gamma_{Y,i}$), respectively. The Z-score of a source indicates the distance (deviation) of that source from the distribution mean of all the sources. If score values of the sources are normally distributed, approximately 95% of the sources should have Z-scores between -2 and $+2$ (i.e. -2 and $+2$ standard deviations away from the distribution mean) (see Figure 6.3). If the Z-score of a source does not fall within this range, it means that score of that

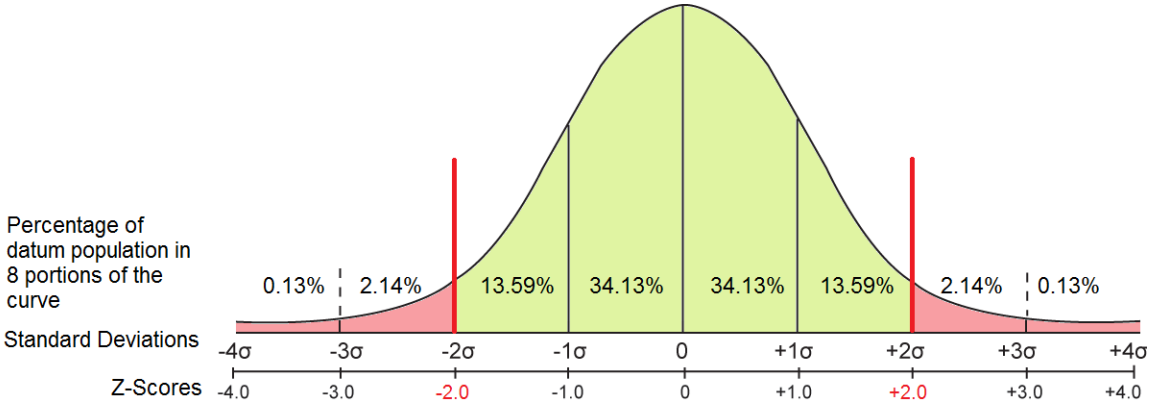

Figure 6.3: Visualisation of z-scores and standard-deviations in a normal distribution. Almost 95% of datum population lies between the red solid lines (the green area), corresponding to the z-scores=±2.

source is significantly away from the mean and that source may have a less typical pattern than other sources. Considering our hypothesis it means, sources with Z-scores above the threshold, $Z\gamma_{X,i} = 2.0$ or $Z\gamma_{Y,i} = 2.0$, are highly correlated with eye movements and are detected as EOG artefacts. As we are only calculating the absolute values of maximum cross-correlation, there could not be a negative Z-score less than -2.0.

Gap Fill in

In VOG recordings, occurrence of data loss is unavoidable and usually some data samples cannot be collected. The data loss often occurs when eye-trackers cannot identify eyes mainly due to blinking or looking away so that the eye-trackers' scene of the eyes is obscured. Data loss in eye tracking usually results in gaps of hundred milliseconds or more in the VOG data. Therefore, prior to eye movement source detection, employing a gap fill algorithm is needed. Interpolation is performed as a gap fill algorithm to cover segments of lost data. During the interpolation, the average of the last value prior to the gap and the first value after the gap are calculated and substituted as the first lost value in the gap, for x and y coordinates. The procedure is continued forward until the last missing value is substituted and the gap is filled.

6.2.2 Blink Source Detection

Similar to the section 5.3.3, we exploited the gaps in the VOG data and derived a third signal $b(t)$, representing occurrence of the blink at time t. The blink trigger signal $b(t)$ is derived so that, the times when gaps, lasting between 100 to $400ms$, occurred in the VOG data, they are substituted with a large value (i.e. $Blink - On$) and all other times are substituted with zero (i.e. $Blink - Off$).

Similar to eye movement source detection (section 6.2.1), ICs are scored according to the maximum absolute values of their cross-correlation with $b(t)$, and Z-Scores of the obtained score by the sources are calculated. ICs with Z-scores above the threshold, $Z\gamma_{b,i} = 2.0$, are highly correlated with eye blinks and are detected as blink artefactual sources.

6.2.3 EOG Artefact Removal

All of the detected eye movement and blink artefacts are removed by making the weight of the detected sources equal to zero, $A_{EOG} = 0_{k,k}$, where k is the number of sources detected as EOG artefacts. The cleaned EEG signals $E^{'}(t)$ is reconstructed as follow:

$$E^{'}(t) = [0_{k,k}\ W_{nEOG}]_{N,N} \begin{bmatrix} S_{EOG}(t) \\ \\ S_{nEOG}(t) \end{bmatrix} \tag{6.10}$$

Thus, according to equation 6.2, each cleaned EEG channel $e_i^{'}(t)$ can be expressed as follow:

$$\begin{aligned} e_i^{'}(t) = 0\ s_1(t) + 0\ s_2(t) + \cdots + 0\ s_k(t) + a_{i,k+1}\ s_{k+1}(t) + \cdots + a_{i,N-1}\ s_{N-1}(t) + a_{i,N}\ s_N(t) \\ = a_{i,k+1}\ s_{k+1}(t) + \cdots + a_{i,N-1}\ s_{N-1}(t) + a_{i,N}\ s_N(t) \end{aligned} \tag{6.11}$$

6.2.4 Improved FoA estimation

In section 5.2.3 we described how SSVEP response detection (derived from SSVEP classification) is used as an extra source of information to improve classification of directional pursuit eye movements. The same method is applied here for classification of directional pursuit eye movements, however this time, prior to SSVEP classification (and detection), the proposed EOG artefact removal method is applied to improve accuracy of SSVEP detection.

6.2.5 Habituation

In order to investigate the effect of user habituation on the SSVEP responses, the amplitude of the SSVEP response during SSVEP stimulation is observed. The SSVEP amplitude variation and SSVEP frequency classification are performed when subjects are exposed to a fixed or moving flickering stimulus and results are compared.

6.3 Evaluation

In order to evaluate the proposed IC labeling and artefact removal system, it is applied on a matched VOG-EEG dataset, recorded during two SSVEP stimulation paradigms. IC labeling is validated using a ground truth, manually generated by visual inspection. Then, the system's SSVEP classification output is compared to the annotated events, and performance of the system is assessed using balanced accuracy. Additionally, for benchmarking, the proposed method is applied on the dataset introduced by [13]. Because the benchmarking dataset is recorded during an Event Relate-Potential paradigm, the accuracy of ERP classification is used to assess quality of the proposed artefact removal method. For comparison, the state-of-art artefact removal method, Plochl [13], is applied on both datasets and results are compared with our method.

6.3.1 The Dataset

To evaluate the VOG-ICA signal processing for EOG artefact removal, the proposed method is applied on two matched VOG-EEG datasets (introduced in Chapter 4) collected during different SSVEP experimental paradigms. In one of the experiments, subjects are asked to attend on a fixed stimulus on the screen, while in the other experiment subjects are intentionally prompt to generate pursuit eye movements, by following a moving stimulus. The stimulus in both of the experiments flickers at $7Hz$, $10Hz$ and $12Hz$. Experiments are designed to investigate the effect of eye movements on SSVEP response detection accuracy and to evaluate performance of the proposed artefact removal method based on the improvements in SSVEP detection accuracy. The same data is used for exploring the habituation effect.

6.3.2 IC Labeling Validation

In order to validate the ICs labeled as EOG artefacts, and to evaluate the performance of the proposed IC classification system, a ground truth is generated. All of the ICs are visually inspected and sources corresponding to EOG artefacts are manually labeled. Visual inspection is performed by one expert, based on the ICs time series, scalp map and power spectral density.

6.3.3 SSVEP Detection

The method described in section 5.2.2 is used to classify SSVEP stimulus frequencies and detect presence of the SSVEP stimulus. EEG channels are bandpass filtered to remove slow drifts and high frequency noise. The spectral power at the stimulus frequencies and their second harmonics are extracted from $2000ms$ temporal windows with 90% overlap, as features. A 1-NN classifier is employed for SSVEP feature classification. Finally, the feature instances classified as non-fixation are considered as SSVEP instances.

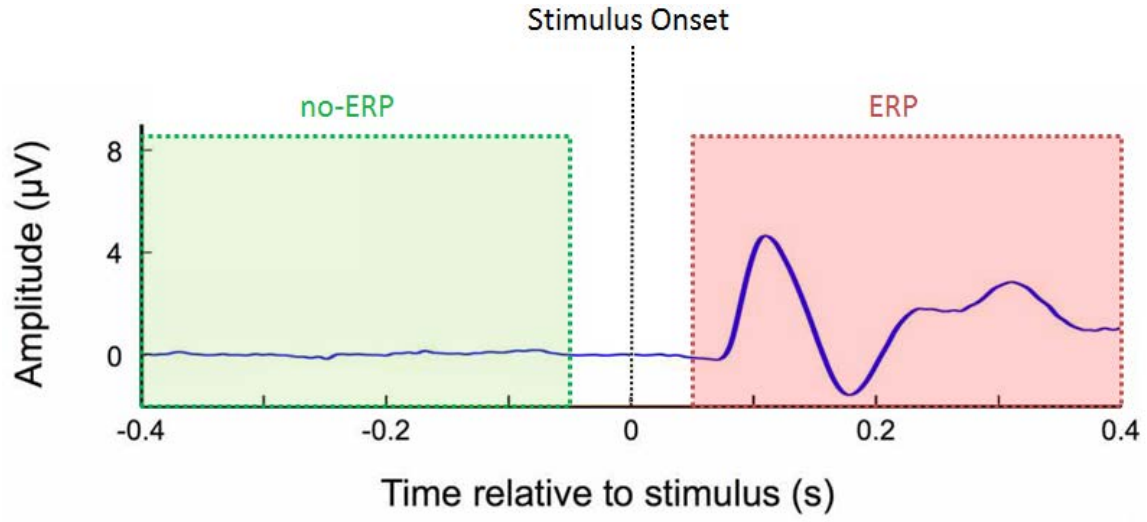

Figure 6.4: Illustration of the segments where extracted feature instances are labeled as ERP and no-ERP.

6.4 Comparison Dataset - Plöchl

In order to evaluate generalisability of the proposed BVOG-ICA over different dataset, recorded during different EEG paradigms, the proposed EOG source detection method is also applied on the dataset described in section 4.3. The dataset contains matched VOG-EEG data recorded during an ERP stimulation paradigm. Therefore, accuracy of ERP classification, before and after cleaning the EEG, is used to evaluate performance of the proposed artefact removal method in reconstructing artefact free EEG. The proposed method is then compared to the state-of-art Plöchl [13].

6.4.1 Event-Related Potential Classification

The single trial ERP detection method proposed by [56], is utilised to evaluate performance of the proposed system to remove eye-related artefacts. [13] showed in the captured dataset, strongest ERP responses are observed over occipital electrode sites. In order to avoid the curse of dimensionality, we used only 7 EEG channels placed over occipital sites for ERP analysis. First, eye-related artefacts are removed using our method and the method proposed by [13]; and cleaned EEG is reconstructed. Then, the cleaned EEG

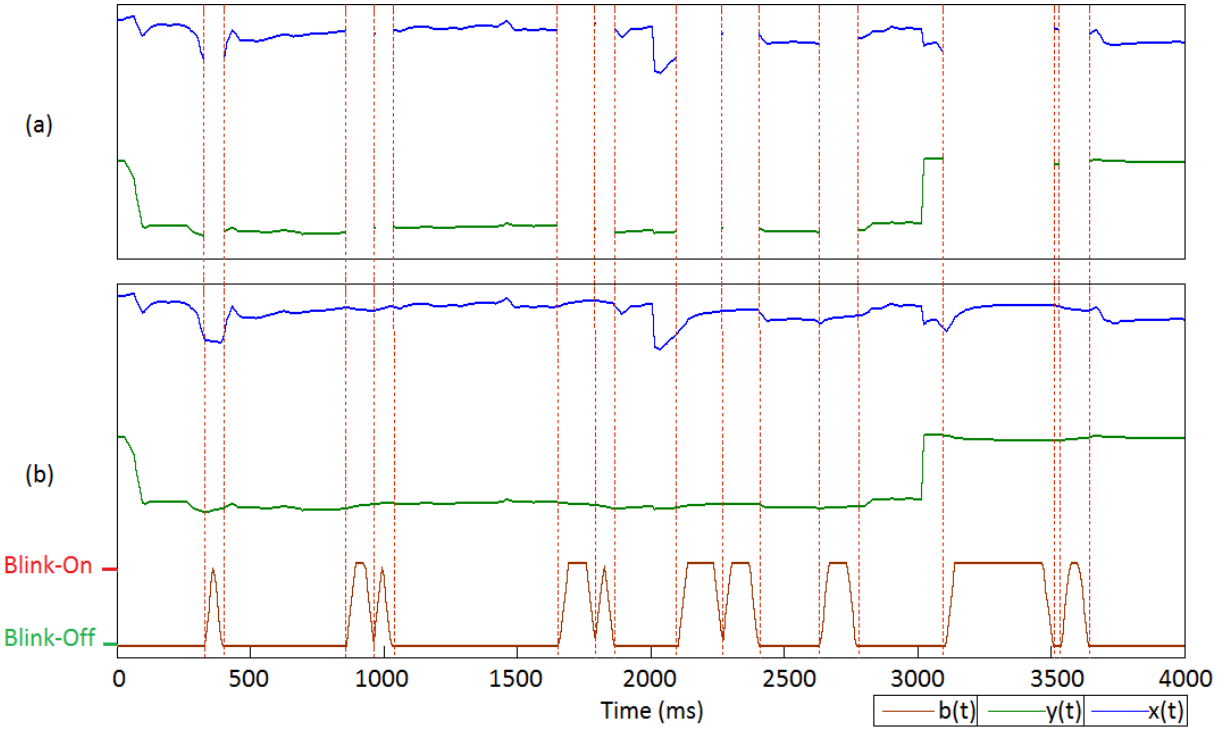

Figure 6.5: Sample processed VOG data where missing values in (a) are substituted using interpolation; (b) shows the interpolated VOG data and the blink trigger signal derived from the missing values.

data is band-pass filtered ($0.1-4Hz$). The time samples between $50ms$ to $400ms$ after the stimulus, and $50ms$ to $400ms$ before stimulus onset are considered as, ERP and no-ERP features, respectively (see Figure 6.4). To remove baseline drift, prior to feature extraction, the mean of the pre-stimulus segment (no-ERP) is subtracted from both the ERP and no-ERP segments. In order to reduce the dimensionality of data, after selecting ERP and noERP segments, the data samples are decimated with factor of 5 (for more details see [56]). Feature vector is made by concatenating ERP and no-ERP samples, extracted from each of the preselected EEG channels. In total 630 features ($90\text{samples} \times 7\text{channels}$) are extracted. The extracted features are used to train a kNN classifier with Euclidean distance (the value of k is set to 1). The accuracy of ERP classification, for each subject, is obtained using a 10-fold cross validation. Therefore, all of the obtained accuracies are averaged over all subjects, and total accuracy of the system is obtained.

6.5 Results

Figure 6.5.b illustrates an instance where interpolation described in section 6.2.1 is performed to fill the VOG gaps in Figure 6.5.a. Additionally, Figure 6.5.b depicts the blink signal $b(t)$, derived from 100 to 400ms gaps in the VOG data. As is shown in the figure, the employed gap filling method avoided the occurrence of manipulated saccades by providing a smooth transition between the last data sample before the start of a gap and the first data sample after the end of that gap. Fig. 6.6 shows the distribution of the

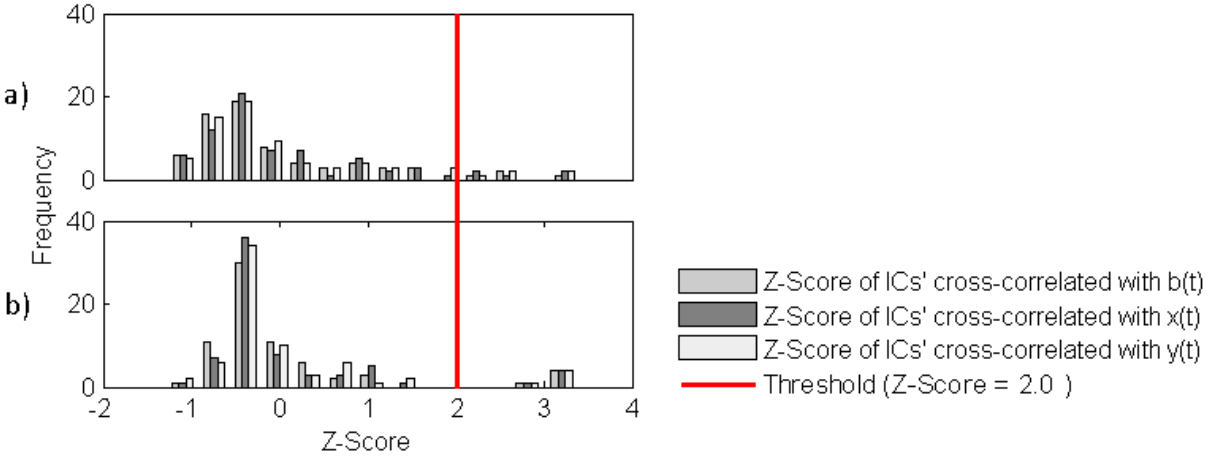

Figure 6.6: Distribution of the Z-Score values obtained by cross-correlation of each single IC with $b(t)$, $x(t)$ and $y(t)$. Scores belong to all subjects in (a) the *Fixed SSVEP* and (b) the *Smooth Pursuit SSVEP* experiments. Red lines indicate the selected threshold ($Z\gamma_{b,i}$,$Z\gamma_{x,i}$ or $Z\gamma_{y,i} = 2.0$)..

blink, horizontal and vertical eye movement Z-Scores of ICs of all subjects in fixed SSVEP (Fig. 6.6.a) and smooth pursuit SSVEP (Fig. 6.6.b). The ICs with Z-Scores higher than 2.0 are considered as EOG artefacts. As is shown in the figure, in the smooth pursuit SSVEP where there are intentional eye movements, the ICs considered as EOG artefacts are better separated from the mean distribution of all other ICs in the fixed SSVEP where subjects are instructed to avoid eye movements. It can suggest that ICA performed a better EOG source separation, when there are more eye movement activities conveying more information about behaviour of the EOG sources.

Figure 6.7 shows an example of the time series, scalp map and the power spectral

density of an IC automatically detected as the eye-related artefactual source. Considering the dipolar behaviour of the eyes, the distribution of the detected IC over the right and left frontal channels on the scalp map implies a horizontal eye movement. This is confirmed by rapid amplitude fluctuations, similar to saccade activity, in the IC's time series; and higher spectral power of the IC below $5Hz$, than all other frequencies.

The detected ICs are validated by comparing them to the ground truth. In the ground truth, from 140 ICs (2 experiments $\times 5$ subjects $\times 14$ ICs) in the SSVEP dataset, 18 ICs are labeled as eye-related artefacts (8 blink ICs and 10 eye movement ICs).

Considering both fixed and smooth pursuit SSVEP, using the proposed method, there are 11 ICs detected as blinks, 10 ICs detected as horizontal eye movements and 10 ICs detected as vertical eye movement artefacts. The 10 ICs detected as horizontal eye movements are the same ICs detected as vertical eye movements, suggesting information of both types of eye movements are concentrated in the same ICs. Additionally, there are 2 ICs mutually detected as blink and eye movement artefacts. In total, there are 19 unique ICs detected as EOG artefacts (either blink or eye movement artefacts).

Table 6.1a shows the confusion matrix of the eye-related IC detection, using our method. Based on the confusion matrix, all of the 18 artefactual ICs labeled in the ground truth, are correctly detected using the proposed method. Additionally, the method labeled another IC which is not labeled as an artefact in the ground truth. The proposed method achieved $BA = 97\%$, which indicates the reliability of the eye-related IC detection, based on the ground truth.

For comparison, Ploch's method is also applied to detect IC's corresponding to eye-movements. Because Ploch is not designed to detect blink sources, the ICs labeled as blink are excluded from the ground truth. Table 6.1b shows the confusion matrix of the eye movements source detection, using Ploch method. Ploch achieved $BA = 69\%$ for eye movement IC detection, 28% lower than our proposed method (p-value< 0.05).

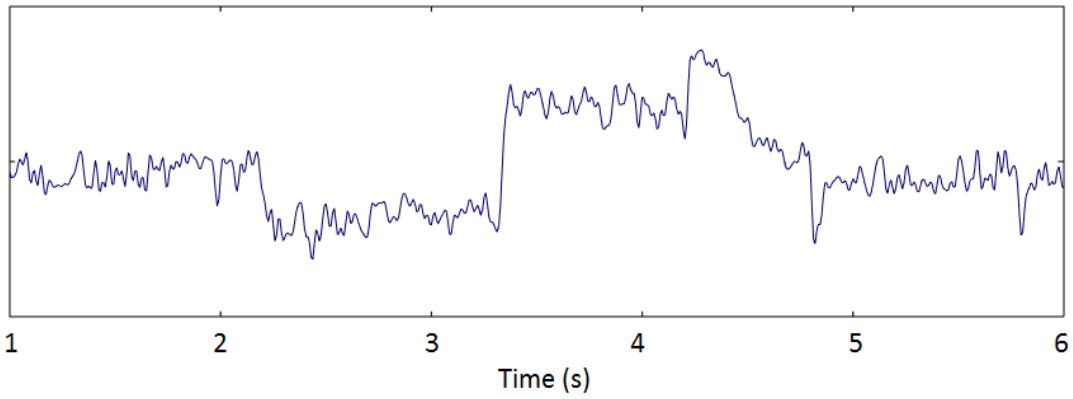

(a) Saccade time Series

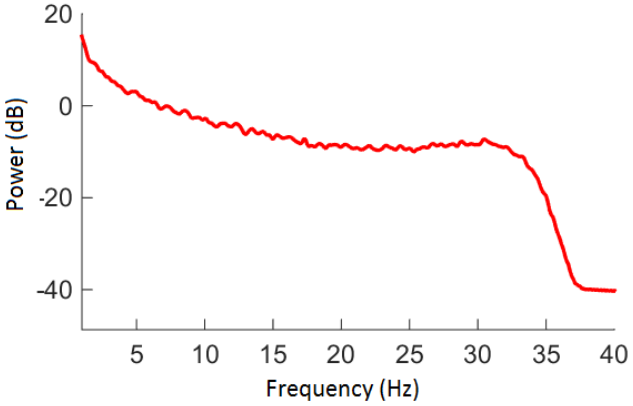

(b) Saccade PSD

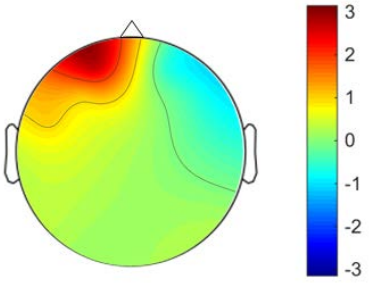

(c) Saccade topography

Figure 6.7: Typical example of (a) time series, (b) power spectral density and (c) scalp map (topography) of an IC, corresponding to the horizontal saccade, manually labeled in the validation procedure.

6.5.1 SSVEP detection

Table 6.2 summarises the SSVEP detection accuracy across all subjects, when different EOG artefact removal methods are applied. SSVEP response detection for all subjects is the highest when the BVOG-ICA is applied in both experiments (i.e Fixed SSVEP and Smooth Pursuit SSVEP). The average SSVEP classification accuracy significantly increases by 7% in fixed SSVEP, and by 4% in smooth pursuit SSVEP. There is a significant increase in the average SSVEP classification accuracy when VOG-ICA is applied as well; 4% increase in fixed SSVEP and 3% increase in smooth pursuit SSVEP. However, when comparing the SSVEP classification accuracy of the subjects individually, there are some cases where SSVEP classification accuracy is decreased when VOG-ICA is applied.

Table 6.1: Confusion matrix of eye-related artefact detection using different methods.

(a) ICs detected by BVOG-ICA.

		Prediction	
		Art	Non-Art
Truth	Art	100%	0%
	Non-Art	0.82%	99.18%

(b) ICs detected by Plöchl.

		Prediction	
		Art	Non-Art
Truth	Art	60%	40%
	Non-Art	18.03%	81.97%

The lowest averaged SSVEP classification accuracy is obtained when Plöchl is applied. As is expected from the IC validation procedure, when Plöchl is applied, the averaged SSVEP classification accuracy falls below raw data by approximately 6% (in both tasks). This might be due to false detection of EOG sources and removing the ICs containing SSVEP information (see Table 6.1). Overall, SSVEP classification accuracy is increased when VOG-ICA and BVOG-ICA are applied. However, only BVOG-ICA in fixed SSVEP achieved significantly higher results (p-value=0.02). Comparing VOG-ICA and BVOG-ICA, the latter method achieved better results; this is due to fact that in addition to the eye movement sources detected by VOG-ICA, BVOG-ICA removes the artefacts arising from eye blinks. Between all three EOG artefact removal methods, BVOG-ICA achieved less between person variations (last rows of Table 6.2a and 6.2b).

6.5.2 Improved FoA estimation

Table 6.3 summarises the result of SSVEP classification and SSVEP detection, before and after applying the proposed BVOG-ICA, for artefact removal. As is evident from the results, as BVOG-ICA increased accuracy of SSVEP frequency classification, it increased SSVEP stimulation detection as well. The result shows applying BVOG-ICA increased the accuracy (BA) of both SSVEP frequency classification and SSVEP stimulation detection by 7% in the case of fixed SSVEP. In the case of smooth pursuit SSVEP, applying BVOG-ICA improved the accuracy (BA) by 4% and 7% for SSVEP classification and SSVEP stimulation detection, respectively. The increases in the SSVEP stimuli detection is statistically significant for both fixed and smooth pursuit SSVEP (p-value = 0.03 and

Table 6.2: Performance of SSVEP classification for each subject in (a) Fixed SSVEP and (b)Smooth Pursuit SSVEP; when there is no EOG artefact removal (Orig) compared to when Plöchl, VOG-ICA and BVOG-ICA are applied for EOG artefact removal. The best obtained result is highlighted in bold.

(a) Fixed SSVEP

Subjects	Fixed SSVEP			
	Orig (%)	Plöchl (%)	VOG-ICA (%)	BVOG-ICA (%)
S01	**82.98**	68.36	81.60	**82.98**
S02	88.99	89.24	**94.02**	**94.02**
S03	80.38	76.10	90.65	**93.02**
S04	85.27	72.99	82.00	**94.01**
S05	81.76	—	**90.55**	**90.55**
Ave	83.88	77.69 *	87.76	**90.91**
std	3.37	8.08	5.62	4.65

(b) Smooth Pursuit SSVEP

Subjects	Smooth Pursuit SSVEP			
	Orig (%)	Plöchl (%)	VOG-ICA (%)	BVOG-ICA (%)
S01	89.14	—	93.47	**93.98**
S02	88.65	64.55	91.24	**92.34**
S03	89.80	83.79	85.86	**90.01**
S04	83.85	83.29	95.01	**96.00**
S05	81.54	—	80.12	**81.88**
Ave	86.60	80.46 *	89.14	**90.84**
std	3.68	9.33	6.11	5.47

* In the cases where there is no IC detected as artefact ("—"), the original accuracy is considered in calculation of the averaged accuracy.

0.04, respectively). As described in section 5.2.3, the detected SSVEP instances are employed as an extra source of information for FoA estimation based on the eye movement direction classification. Figure 6.8 compares the result of FoA estimation, when i) SSVEP response detection is not employed, ii) when SSVEP response detection is employed, but EOG artefacts are not removed and iii) when artefacts are removed using BVOG-ICA and, enhanced SSVEP response detection is used.

The results in Figure 6.8 demonstrate that when no EOG artefact removal is ap-

Table 6.3: Results of SSVEP frequency classification and stimuli detection, before and after applying BVOG-ICA, in Fixed SSVEP and Smooth Pursuit SSVEP experiments.

	SSVEP Frequency Classification		**SSVEP Stimulation Detection**	
	Before BVOG-ICA	After BVOG-ICA	Before BVOG-ICA	After BVOG-ICA
Fixed SSVEP	83.87 %	90.91 %	91.38 %	98.34 %
Smooth Pursuit SSVEP	86.59 %	90.84 %	92.27 %	98.87 %

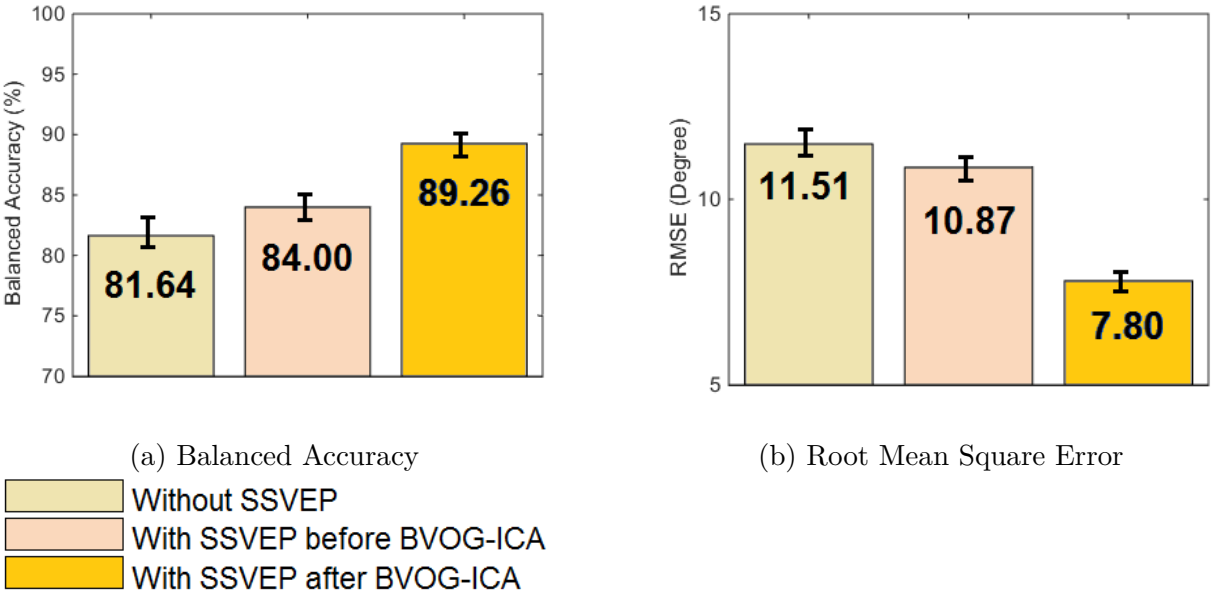

(a) Balanced Accuracy

(b) Root Mean Square Error

Figure 6.8: FoA estimation results without use of SSVEP compared to the presence of SSVEP, when there is no artefact removal and when eye-related artefacts are removed by BVOG-ICA. Results are compared in terms of obtained BA and RMSE.

plied, the presence of the SSVEP in the visual field, significantly (p-value=0.04) improves classification BA by almost 3% and reduces RMSE to 10.87°. Result also suggest that, removing EOG artefacts, using the proposed EOG artefact removal method, significantly (p-value=0.04) increases the FoA estimation by 5%, and reduces RMSE to 7.80°. Overall, the BA of eye movement direction classification is best (i.e. 89.26%) with the least RMSE (i.e. 7.80°), when both prior to SSVEP detection, BVOG-ICA is applied for EOG artefact removal, and both SSVEP response detection and EOG features are used for direction classification.

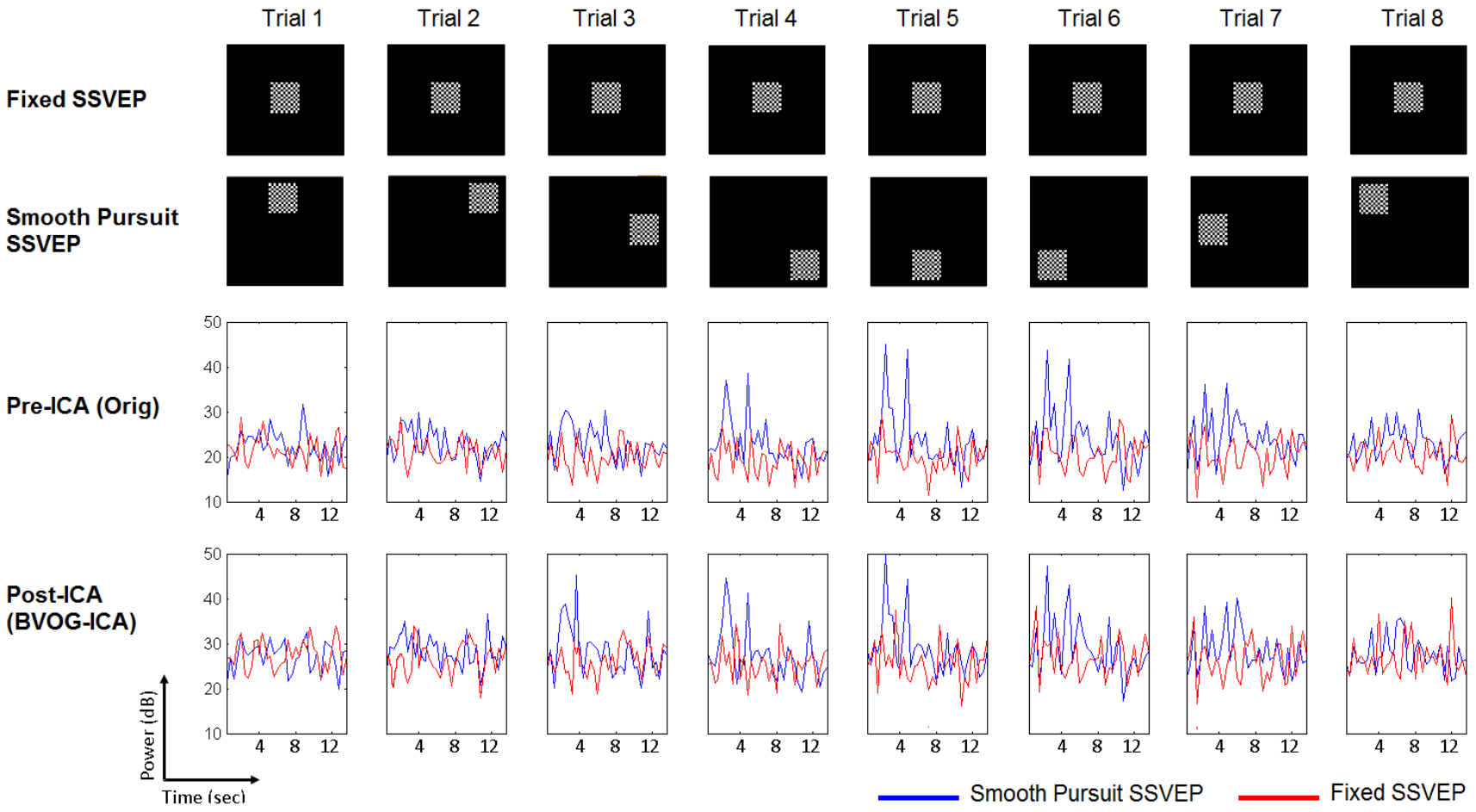

Figure 6.9: A typical example of SSVEP response amplitude variation during different trials recorded in the Fixed SSVEP and Smooth Pursuit SSVEP experiments; when eye-related artefacts are removed using BVOG-ICA (Post-ICA) and when no artefact removal is applied (Orig). First two illustrate the location of the stimuli in the fixed SSVEP and direction of stimuli movement in the Smooth Pursuit SSVEP.

6.5.3 Habituation

As is shown in Table 6.3, SSVEP classification accuracy in smooth pursuit SSVEP is approximately 3% higher than fixed SSVEP. And the classification results for fixed and smooth pursuit SSVEP is increased by 7% and 4%, respectively; when BVOG-ICA is applied. The reason could be a gradual decrement in SSVEP amplitude responses due to habituation of the subjects under the fixed SSVEP stimulation. In contrast, when subjects follow the moving stimuli in *Pursuit SSVEP*, they are constantly exposing to a new stimulation also paying more attention, therefore habituation is avoided. It can be confirmed by looking at the SSVEP responses depicted in Figure 6.9.

Figure 6.9 illustrates a typical example of the amplitude of SSVEP responses during fixed and smooth pursuit SSVEP stimulation (flickering at $10Hz$). As is shown in the figure, in most of the cases the amplitude of SSVEP responses to fixed SSVEP is lower than smooth pursuit SSVEP where stimuli moves in different directions. It is also evident that the SSVEP response amplitudes increased, in both fixed and smooth pursuit SSVEP, when BVOG-ICA is applied to remove EOG artefacts.

6.5.4 Comparison Dataset - Plöchl

The BVOG-ICA and Plöchl are applied on the comparison dataset, with the aim of cleaning EOG artefacts. Table 6.4 shows the average ERP classification accuracy across all subjects, before EOG artefact removal and after applying Plöchl, VOG-ICA after and BVOG-ICA artefact removal methods. As is illustrated in the table, ERP classification for all subjects is highest when the BVOG-ICA is applied for artefact removal. The average ERP classification accuracy significantly (p-value$<$0.05) increased by 2.2% to 88.43%. There is an increase in the average ERP classification accuracy when VOG-ICA and Plöchl are applied as well; 1.77% increase by VOG-ICA (p-value$<$0.05) and 0.8% increase by Plöchl (p-value=0.26). When the ERP classification accuracy of the subjects are compared individually, there is one case where no IC is detected as an eye movement source,

Table 6.4: Performance of ERP classification for each subject; when there is no EOG artefact removal (Orig) compared to when Plöchl, VOG-ICA and BVOG-ICA are applied for EOG artefact removal. The best obtained result is highlighted in bold.

Subjects	ERP Classification			
	Orig (%)	Plöchl (%)	VOG-ICA (%)	BVOG-ICA (%)
S01	88.24	89.26	89.26	**90.17**
S02	84.23	85.33	86.43	**86.43**
S03	93.17	94.54	94.54	**95.00**
S04	94.45	**96.12**	**96.12**	**96.12**
S05	84.56	—	—	**85.64**
S06	91.43	91.83	93.46	**93.87**
S07	82.87	83.00	83.92	**84.35**
S08	76.96	80.00	80.34	**81.35**
S09	80.01	**83.56**	**83.56**	**83.56**
S10	86.43	82.12	**87.82**	**87.82**
Ave	86.23	87.03 *	88.00*	**88.43**
std	5.67	5.55	5.26	5.13

* In the cases where there is no IC detected as artefact ("—"), the original accuracy is considered in calculation of the averaged accuracy.

using VOG-ICA and Plöchl (i.e. S05); and there is one subject where ERP classification accuracy is decreased when Plöchl is applied (i.e. S10). The lowest averaged ERP classification accuracy is obtained when Plöchl is applied (accuracy = 87.03). Overall, ERP classification accuracy is increased when Plöchl,VOG-ICA and BVOG-ICA are applied. However, BVOG-ICA achieved significantly (p-value<0.05) better results due to fact that Plöchl and VOG-ICA do not remove the artefacts arising from eye blinks. Additionally, again between all three EOG artefact removal methods, BVOG-ICA achieved less between person variations (last row of Table 6.4).

6.6 Summary

In this chapter, we proposed a VOG-based automatic method for the detection and removal of eye movement and blink artefacts from EEG. The VOG signal from an optical

eye tracker is used to assist in the detection of ICA components related to eye movement artefacts. The proposed method outperforms the state-of-art method Plöchl et al. [13], which does not account for blink detection explicitly by their algorithm, when evaluated on matched VOG and EEG data. Removal of EOG artefacts detected by BVOG-ICA leads to 7% and 4% improvement in SSVEP classification accuracy for fixed and moving SSVEP stimuli, respectively. This resulted in 98% SSVEP stimulation detection which is employed to improve the FoA estimation method introduced in Chapter 5. Performance of the FoA estimation is significantly improved by almost 5%, to $BA = 89.26\%$ and $RMSE = 7.80$.

Additionally, the proposed method significantly improved accuracy of the ERP classification by almost 2% to 88.43%, when applied on the dataset recorded by Plöchl (described in section 4.3.5). The result demonstrates BVOG-ICA provides a reliable automatic way for EOG artefact removal in SSVEP and ERP paradigms, using both laboratory and consumer grade EEG apparatus. Despite the fact that EEG and VOG data are recorded by separate devices, with independent sampling clocks, the proposed method can efficiently work without being affected by the synchronisation problem. Additionally, the trade-off between increasing eye movement artefacts which lowers SSVEP detection performance and reduces the effect of habituation by using moving stimuli which raises SSVEP detection performance is favourable.This study, highlights the benefits of using optical information for EOG artefact removal.

"Silence is a door among the doors of wisdom."

Ali al-Ridha (PBUH)

7

Performance Improvement by Extracting Features From Independent Sources

7.1 Introduction

Previous studies in EEG chiefly apply ICA exclusively for artefact removal rather than feature extraction. In this chapter, it is demonstrated that ICA components can be beneficial as features for blink, eye movement, SSVEP and ERP classification. We demonstrate improved performance by extracting features from source signals estimated by the blind source separation technique ICA rather than the traditionally used preprocessed EEG channels. The data introduced in Chapter 3 and 4 are used for evaluation. All of the clas-

sification tasks conducted in previous chapters are repeated, however, this time features are extracted from ICA decompositions rather than EEG channels. The results are then compared with best obtained classification results in the previous chapters.

7.2 Related Works

In most of the EEG studies ICA was used for source separation and artefact removal. However, in the field of speech and image processing it is demonstrated, by projecting the data into independent sources, ICA was useful for feature extraction. For example [115] used ICA to extract features for image analysis, and [116] used ICA to extract features for phoneme detection.

7.3 ICA-based Feature Extraction

As is described in section 2.5, ICA assumes that the observed data X, is a linear combination of statistically independent sources. The goal of ICA is to find the mixing matrix A and the independent sources S ($X = AS$). In other words, ICA represents observed data as a linear combination of maximally independent sources, corresponding to the dimensionality of the observed data.

In most EEG studies, ICA is employed to separate and remove artefactual sources from EEG signal [12, 13]. First, ICA is applied to estimate independent sources which are either artefactual or non-artefactual. Then, the artefactual sources are detected based on their stereotyped temporal, frequential and spatial characteristics[12]. However, because ICA does not solve the inverse EEG problem, the subjective artefactual source detection has no solid theoretical basis. Subjective selection of ICs based on suggestions in previous studies, may prompt risk of biasing the results to support uncertain brain functioning theories; specially in the case of removing artefacts from EEG data recorded during not well-known cognitive tasks. Additionally, subjective IC selection might be affected by introducing errors due to different EEG setups and inter-subject variations.

Here, the main idea is that instead of detecting and removing artefactual ICs, all of the independent sources estimated by ICA can be used as a set of independent features, to be used for classification of EEG patterns, relating to different tasks. It can be beneficial for classification methods such as Naïve Bayesian, which works under the assumption of independence of the features.

Fo this purpose, first the Extended-Infomax ICA algorithm is applied on all the data recorded during different experiments described in previous chapters. Then, instead of extracting feature, from raw or reconstructed clean EEG, features are extracted from estimated independent components.

7.3.1 t-Test Investigations

In order to evaluate the performance of the EEG pattern classifications based on ICA features, t-testis is performed. We are testing the following hypothesises:

- Test Hypothesis: the population means of EEG pattern classification accuracy is different when features are extracted from reconstructed EEG channels or independent components.
- Null Hypothesis: the population means of EEG pattern classification accuracy is the same when features are extracted from reconstructed EEG channels or independent components.

The $p-\text{value} = 0.05$ is considered as the level of significance; it corresponds to a 95% confidence level.

7.3.2 Evaluation

In order to test the null hypothesis, we used a simple simulated data as well as the data captured during all of the experiments in Chapter 3 and Chapter 4. The best results obtained in previous chapters, for each task, are compared to the new results where

features are extracted from ICs. Results are compared in terms of BA; and RMSE where possible.

7.3.3 Simulated Data

A simple simulated dataset is generated to evaluate the proposed feature extraction approach. Suppose we are collecting data during a visual stimulation paradigm, stimulating subjects at times t_1 and t_2, and we want to use a classifier and find the time segments when stimulation occurred.

Assume, the two known signals in Figure 7.1a are original brain responses generated within the brain. The cosine signal $s(1)$ is considered as background EEG activity, generated from a part of the brain not responding to the task; and step signal $s(2)$ is considered as brain impulses to a specific cognitive task.

We know that, the EEG data collected from the scalp, is a mixture of the original sources generated within the brain. Here we assume, the original source signals, $s(1)$ and $s(2)$, are linearly mixed using the following (randomly generated) mixing matrix and build up the observation signals $x(1)$ and $x(2)$, in Figure 7.1b.

$$W_{Orig} = \begin{bmatrix} 0.8 & 0.2 \\ 0.7 & 0.3 \end{bmatrix}$$

We used a $50ms$ sliding window and extracted mean amplitude of each window from each signal as a feature to train a classifier. There are two sets of features, mean amplitude extracted from two observation signals $x(1)$ and $x(2)$ and mean amplitude extracted from two estimated ICs $u(1)$ and $u(2)$. ICs are estimated using Extended-Infomax ICA algorithm. In the training data, the feature instances extracted from durations in which step impulses occurred are labeled as target and all other instances are labeled as non-target. The extracted features, from observation signals and ICs, are separately used to train a RBF-SVM classifier, a 1-NN classifier and a Naive Bayesian classifier. The classification performance is assessed using a 5-fold cross-validation technique.

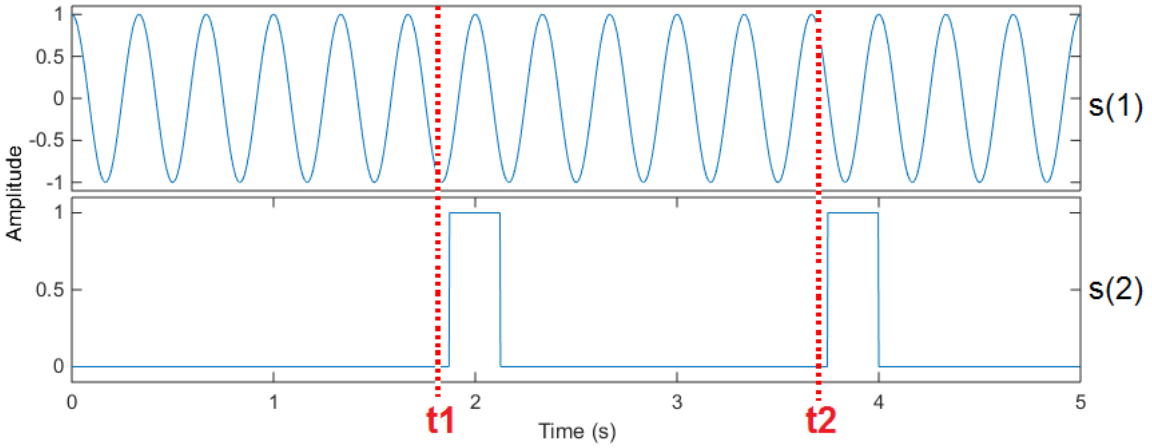

(a) Original sources

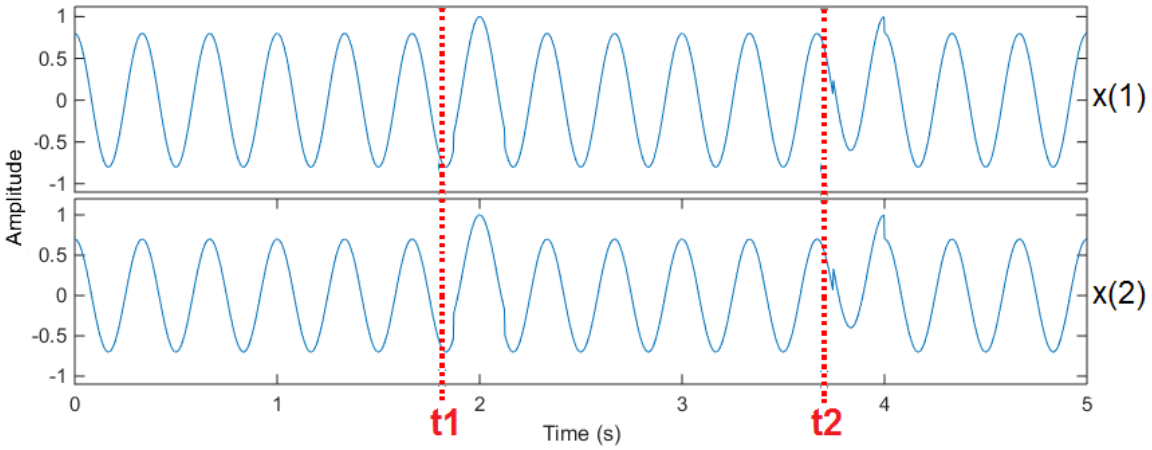

(b) Observation

Figure 7.1: An illustration of the simulated data. a) Simulation of the original responses generated within the brain. b) The observed simulated EEG data on the scalp. The red dashed lines represents the hypothetical stimulation onsets at times t_1 and t_2.

7.3.4 Real Data

All the data described in Chapter 3 and Chapter 4, are used for evaluation in this chapter. In Chapter 3 three types of data are recorded during three different experiments; namely, Cognitive Load, Motor Imagery and SSVEP Classification. Additionally, a pilot dataset is collected for classification of eye blinks and directional eye movements. In Chapter 4, four types of data are captured during four experiments; namely, Short Saccade, Long Saccade, Fixed SSVEP and Smooth Pursuit SSVEP. Additionally, a comparison dataset is described which includes ERP stimulation.

All the above datasets are employed for classification problems described in the ex-

perimental Chapters 3 to 6. The best obtained classification results in each chapter are compared with new results obtained by the proposed ICA-based feature extraction.

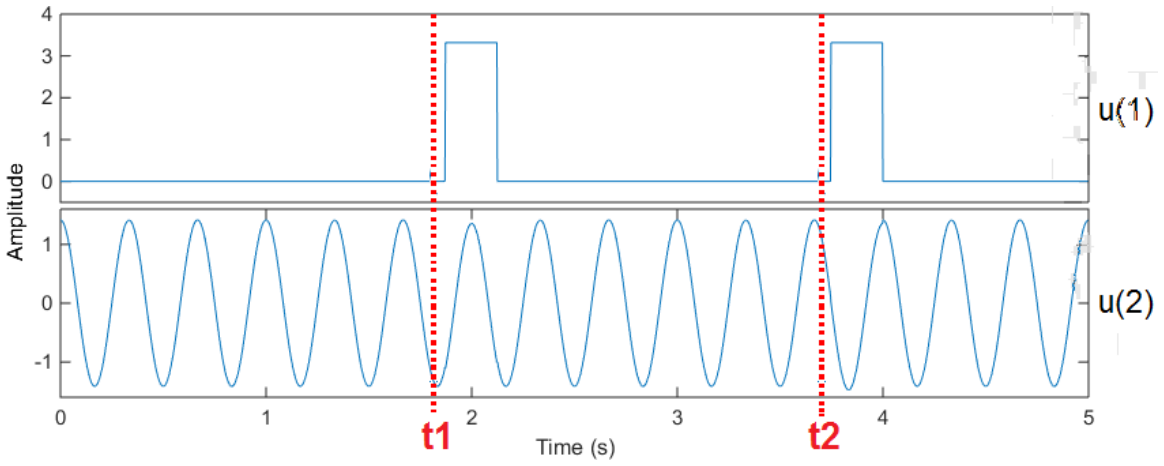

Figure 7.2: The time series of the ICs estimated from simulated data.

7.4 Results

The effect of the proposed feature extraction approach on the classification performances for both simulated and real data are reported.

7.4.1 Simulated Data

Figure 7.2 shows the independent sources estimated by the Extended-Infomax algorithm. As is evident from Figure 7.1b, brain responses are not easily detectable by visually inspecting observation signals $x(1)$ and $x(2)$, however, we can easily detect the times when brain responses occurred, by looking at the time series of the estimated sources.

Figure 7.3a and 7.3b show the distribution of the feature instances extracted from observation signals and independent components, respectively. The distribution of two feature sets suggest that, features extracted from ICs are more independent and discriminated than the features extracted from observation signals.

Table 7.1 depicts the obtained confusion matrix when RBF-SVM or 1-NN classifiers are trained using features extracted from observation signals. Table 7.2 depicts the obtained

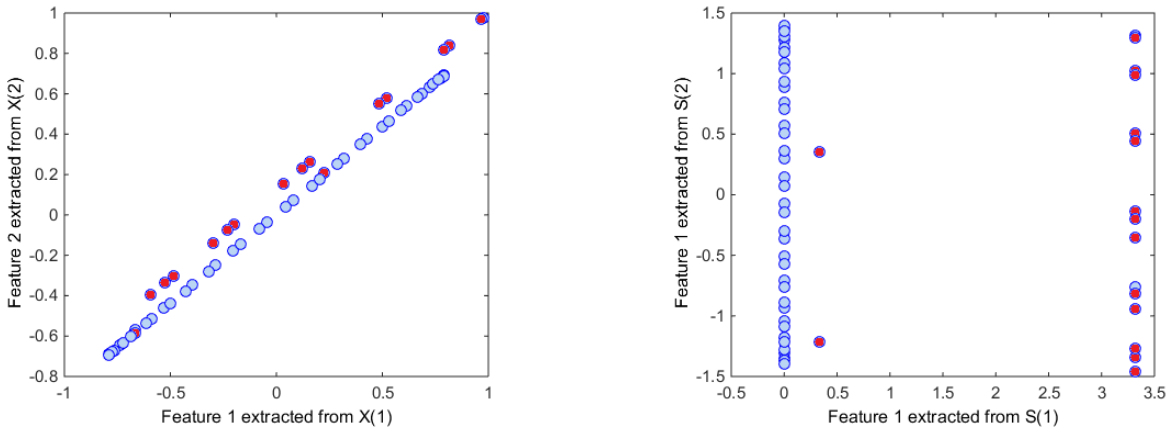

(a) Original sources (b) Observation signals

Figure 7.3: Distribution of the features extracted from a) simulated EEG observations, b) ICs estimated from observation data.

confusion matrices when Naive Bayesian classifier is trained using the same features. As is evident in the results, the Naive Bayesian classifier could not classify any true brain responses, while around half (54%) of the true brain responses are correctly classified by 1-NN and RBF-SVM. RBF-SVM and 1-NN performed the same and achieved $BA = 90.16\%$, however, the NB classifier achieved $BA = 44.47\%$.

Table 7.3 shows the obtained confusion matrices the three classifiers are trained using features extracted from ICs. The same confusion matrix is obtained for all three classifiers. As is shown in the results, performance of all the classifiers is improved and they achieved the same BA, 93.88%. Comparing the obtained classification BA, across the cross-validation folds with previous results, suggests significant improvement ($p < 0.05$) in the performance of all classifiers, when features are extracted from ICs.

Table 7.1: Confusion matrix obtained by 1-NN and RBF-SVM classifiers.

	Target	**Non-Target**
Target	0.54	0.45
Non-Target	0.02	0.98

Table 7.2: Confusion matrix obtained by NB classifier.

	Target	**Non-Target**
Target	0	1.00
Non-Target	0.01	0.99

Table 7.3: Confusion matrix obtained by 1-NN, RBF-SVM and NB classifier.

	Target	**Non-Target**
Target	0.82	0.18
Non-Target	0.02	0.98

7.4.2 Real Data

Table 7.4, summarises the classification accuracy obtained in different experiments, using the data described in Chapter 3. As is shown in the results, when ICA-based feature extraction is used, performance of all the classification tasks is improved. However, the improvement is only significant (p-value=0.03) for classification of blink and eye movement direction, in the pilot dataset. From the results, it is also evident that blink and eye movement direction classification, benefit more from ICA-based feature extraction.

In Table 7.5, the results of blink and different types of eye movement classification, as well as FoA estimation based on SSVEP classification are shown. The results are obtained by applying the methods described in Chapter 5 on the data in Chapter 4. The best obtained results are compared to ICA-based feature extraction. As is expected, the highest accuracies are obtained when ICA-based features are used. All of the classifica-

Table 7.4: The best obtained results for classification of different tasks described in Chapter 3 are compared to new results obtained by extracting features from ICs (ICA Features). The best obtained result is highlighted in bold.

Description	Accuracy (%)	
	Normal Features	ICA Features
Cognitive Load Classification	97.65	**98.22**
Motor Imagery Movement Classification	98.99	**99.10**
SSVEP Frequency Classification	97.22	**97.95**
Pilot Blink Classification	89.95	**97.15**
Pilot Eye Movement Direction Classification	89.48	**94.33**

Table 7.5: Classification results obtained for blink, eye movement and SSVEP classification, when features are extracted from normal EEG compared to when features are extracted from ICs (ICA Features). The best obtained result is highlighted in bold.

Description	Accuracy (%)	
	Normal Features	ICA Features
Blink Classification	82.31	**85.16**
Fixation Classification	94.14	**98.12**
Smooth Pursuit Classification	76.00	**80.03**
Saccade Classification	82.67	**85.22**
Saccade Amplitude Classification	95.22	**97.33**
Eye movement Direction Classification	76.31	**91.39**
SSVEP Frequency Classification	85.23	**96.21**
SSVEP Stimuli Detection	91.82	**97.85**

tion accuracies significantly improved ($p - value < 0.05$). The results suggest that, eye movement direction classification achieved the highest percentage of improvement (15% improvement in BA) and benefited most from ICA-based feature extraction. The lowest BA increase is achieved for saccade amplitude classification (2% improvement in BA).

Table 7.6 summarises the result of SSVEP classification during fixed SSVEP and smooth pursuit SSVEP experiments, when features are extracted from original EEG data compared to when BVOG-ICA (proposed in Chapter 6) is used for cleaning EEG data, and when no cleaning is performed and features are extracted from ICs rather than EEG channels. Result shows that, the SSVEP classification for all subjects is higher when features are extracted from ICs rather than EEG channels. It is also evident that, using ICA-based features significantly (p-value< 0.05) increases average SSVEP classification performance, and decreases the between-person variation.

The results of ERP classification, using the comparison dataset described in Chapter 4 (and analysed in Chapter 6) is reported in Table 7.7. Similar to SSVEP classification, the results suggest significant improvement in ERP classification, and lower between person variations, when ICA-based features are used. The new result is significantly higher than the original data and the data cleaned using BVOG-ICA.

Table 7.6: Performance of SSVEP classification for each subject in (a) Fixed SSVEP and (b) Smooth Pursuit SSVEP; when features are extracted from original EEG data (Orig), EEG data cleaned by BVOG-ICA and independent components (ICA Features). The best obtained result is highlighted in bold.

(a) Fixed SSVEP

Subjects	Fixed SSVEP		
	Orig (%)	BVOG-ICA (%)	ICA Features(%)
S01	82.98	82.98	**96.69**
S02	88.99	94.02	**96.84**
S03	80.38	93.02	**96.08**
S04	85.27	94.01	**96.57**
S05	81.76	90.55	**95.72**
Ave	83.88	90.91	**96.38**
std	3.37	4.65	0.46

(b) Smooth Pursuit SSVEP

Subjects	Smooth Pursuit SSVEP		
	Orig (%)	BVOG-ICA (%)	ICA Features(%)
S01	89.14	93.98	**96.87**
S02	88.65	92.34	**95.25**
S03	89.80	90.01	**95.03**
S04	83.85	96.00	**96.91**
S05	81.54	81.88	**96.21**
Ave	86.60	90.84	**96.05**
std	3.68	5.47	0.88

Finally, Figure 7.4 illustrated the improvement of FoA estimation when BVOG-ICA described in Chapter 6 is applied compared to when ICA-based features are used for FoA estimation. Again the results shows significant (p-value=0.01) improvement in FoA estimation (by 8.31% to 97.57%) and significant (p-value=0.01) decrease in RMSE (by 6.17° to 1.63°), when ICA-based features are used.

Overall, as it is evident from the results, the accuracy of all classifiers is improved and the between-person variation decreased significantly if features are extracted from ICA components. Considering the RMSE, similar trend is obtained. This might be due to

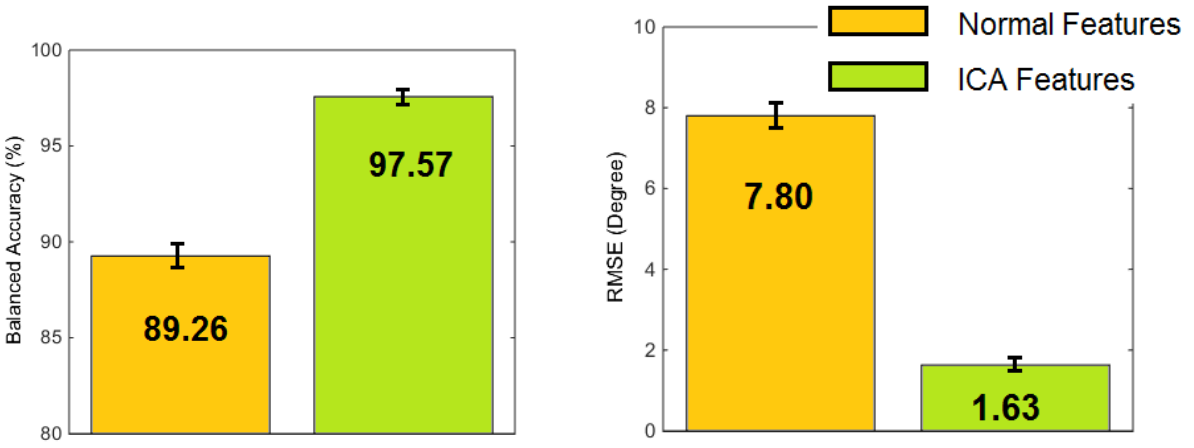

(a) Original sources (b) Observation

Figure 7.4: FoA estimation results with the presence of SSVEP, when features are extracted from EEG channels compared to when features are extracted from ICA components. Results are compared in terms of obtained BA and RMSE.

Table 7.7: Performance of ERP classification for each subject; when features are extracted from original EEG data (Orig), EEG data cleaned by BVOG-ICA and independent components (ICA Features). The best obtained result is highlighted in bold.

Subjects	ERP Classification		
	Orig (%)	BVOG-ICA (%)	ICA Features(%)
S01	88.24	90.17	**92.33**
S02	84.23	86.43	**89.54**
S03	93.17	95.00	**96.35**
S04	94.45	96.12	**99.92**
S05	84.56	85.64	**90.89**
S06	91.43	93.87	**95.83**
S07	82.87	84.35	**89.10**
S08	76.96	81.35	**85.80**
S09	80.01	83.56	**88.86**
S10	86.43	87.82	**91.61**
Ave	86.23	88.43	**92.02**
std	5.67	5.13	4.22

the maximal independence of estimated sources by ICA meaning that the mixed source signals in the EEG can be well separated. Thus, the information extracted as a feature from each IC can represent maximum possible information of the dominant source signal

within that IC.

7.5 Summary

In this chapter we showed how ICA can be used as a feature extraction technique to significantly improve different classification tasks conducted in this thesis. Most importantly, we demonstrated how ICA-based feature extraction improves eye movement classification and SSVEP stimulus detection; which lead to enhanced FoA estimation. The performance of eye movement classification and SSVEP stimulus detection increased by 15% and 6%, respectively. As a result, FoA estimation BA is improved by 8% to 97.57% and RMSE decreased to 1.63°.

"Knowledge is a great treasure which does not come to an end."

Ali ibn Abi Talib (PBUH)

8

Conclusion

This thesis evaluated the feasibility of employing a consumer-grade EEG device for eye-tracking and FoA estimation. First, the integrity of a consumer-grade EEG device (i.e. Emotiv EPOC) for common BCI paradigms is assessed, and reliability of the device to be used in BCI applications is demonstrated. Then, novel matched VOG/EEG data is introduced to explore blinking and eye movement patterns in the EEG data, and investigate the effect of eye-related artefacts and habituation on the performance of SSVEP response detection. Afterwards, a signal processing method is proposed to classify blink, saccade, fixation and smooth pursuit eye movement; in addition to saccade amplitude and eye movement direction. The FoA is estimated by a hybrid of SSVEP detection and eye movement direction classification. In the next step, performance of the proposed hybrid

FoA estimation is improved by improving accuracy of SSVEP detection via BVOG-ICA- a fully automated artefact removal method which employs VOG data to detect and remove ICA components corresponding to blink and eye movements. Additionally, the habituation effect on the SSVEP response detection is explored. Finally, FoA estimation is improved by extracting eye movement direction and SSVEP classification features from ICA components rather than EEG channels.

8.1 Summary of Results

In this research we first focused on the evaluation of Emotiv EPOC, a consumer EEG headset. The evaluation is performed by conducting 3 experiments - cognitive task, Imagery movement and SSVEP classification. The consumer EEG device showed remarkable performance and achieved above 97% accuracy in the classification of the tasks in each experiment. Additionally, the effect of varying window and overlap size as well as ICA-based artefact removal methods and classification methods are investigated. The optimum window and overlap size, best performing ICA algorithm to remove artefacts, and best classification method are reported. Moreover, the feasibility of using the EEG headset to classify blink and eye movements into different directions are assessed in a pilot study. In the pilot study, using the device blink and directional eye movements are classified with accuracy above 89%.

After demonstrating the integrity of the consumer-grade EEG device, the device is used along a consumer-grade eye-tracking glasses to record a matched VOG/EEG dataset in a set of experiments. In the designed experiments, participants perform saccade and smooth pursuit eye movements while looking at SSVEP stimuli. This way, on the one hand, EEG patterns corresponding to different eye movements can be observed in the data, on the other hand, the effect of eye-related artefacts on the SSVEP classification performance can be explored.

A signal processing approach is proposed to classify blink and different types of eye

movements, including fixation saccade and smooth pursuit, as well as saccade amplitude and direction of eye movements. The matched VOG/EEG dataset is used for evaluation. Using the proposed approach, blink, fixation, smooth pursuit, saccade, saccade direction and eye movement direction can be classified with 82.31%, 94.14%, 76.00%, 82.67%, 95.22%, 76.31% balanced-accuracy. Additionally, a hybrid of SSVEP detection and eye movement direction classification is used to estimated the focus of foveal attention (FoA). FoA is estimated with 84.00% balanced-accuracy, and RMSE less than 11°.

Afterwards, the FoA estimation is improved by improving the accuracy of SSVEP detection, via artefact removal. A fully automated ICA-based artefact removal method is proposed which employs VOG information to detect and remove ICA components corresponding to blink and eye movements. The proposed artefact removal method increased SSVEP detection by 4% to 98%, which resulted in more than 5% improvement in FoA estimation (BA=89.26% and RMSE=7.80°). The ERP classification performance is also improved by 2% to 88.43%, when the proposed method is applied on the dataset recorded by Plöchl. The proposed method outperforms the state-of-art method Plöchl.

Finally, it is demonstrated that performance of all the classification problems conducted in the thesis, as well as FoA estimation, improved significantly when features are extracted from ICA components rather than EEG data. The eye movement direction classification improved the most, with 15% BA improvement to 91.39%. Using the new features, FoA estimation is also significantly improved, by 8% increase in BA (BA=97.57%) and 6° decrease in RMSE (RMSE=1.63°).

8.2 Future Work

Eternally, there are countless number of ways in which the current work can be extended. In the following, some of the possible extensions and future works are pointed out.

- The proposed EEG artefact removal method is evaluated on only ERP and SSVEP paradigms. The generality of the proposed artefact removal method can be evaluated

by recording matched VOG/EEG data during other BCI paradigms such as imagery movements, or P300 spellers.

- The evaluation datasets introduced in this work are collected from normal and healthy subjects. In order to assess the generality and usability of the proposed signal processing methods, collecting a database from people with sever motor disabilities is of interest.

- All the data is collected in controlled conditions, where subjects are asked to remain as still as possible. To be able to extend the work for real-life applications, collecting a dataset recorded during less controlled conditions where subjects can freely move is of interest. To this aim, similar to VOG, use of different types of on-body sensors (e.g. MEG, accelerometer, etc) to record and detect different types of body movements can be beneficial.

- The use of Augmented Reality to modulate the visual field with flashing stimuli potentially promises eye tracking technologies utilising SSVEP detection.

- The proposed blink and eye movement classification in addition to the FoA estimation method, can be used for human activity recognition. The number of blink, saccade, fixation and duration of smooth pursuit eye movements, as well as patterns of eye movements can be employed to discriminate different activities.

- The data recorded using the EEG headset's 2D gyroscope can be used to extend the proposed EEG artefact removal method and eye movement classification in the presence of EEG artefacts arising from head movement.

- In this work, VOG information is used to label the ICA sources corresponding to eye-related artefacts. An interesting question would be the use of VOG information and other information recorded using different sensors, to optimally estimate sources with most amount of VOG (or information from types of artefact), using ICA.

- All the experiments in this study are conducted in an offline manner. Proposing a real-time ICA technique for online artefact removal is on interest for online BCI applications.

The ultimate goal of this study is to explore the feasibility of using non-intrusive and user-friendly EEG apparatus for BCI and eye-tracking applications at the same time. Therefore, proposing an integrated hardware and software system which records EEG data and at the same time removes different types of artefacts from EEG is of interest. The proposed system could use real-time ICA for optimised estimation of eye-related sources. Then, the eye-related sources can be used for eye-tracking applications and all other non-artefactual sources can be used for BCI applications.

Appendices

"No servant is a scholar unless he does not envy the superior (over himself) and does not degrade the inferior (than himself)."

Muhammad al-Baqir (PBUH)

A

List of Publications

1 Mohammad Reza Haji Samadi, Zakeri, Z. and Cooke, N., 2016, February. VOG-enhanced ICA for removing blink and eye-movement artefacts from EEG. In 2016 IEEE-EMBS International Conference on Biomedical and Health Informatics (BHI) (pp. 603-606). IEEE.

2 Zakeri, Z., Haji Samadi, M.R., Cooke, N. and Jancovic, P., 2016, February. Automatic ERP classification in EEG recordings from task-related independent components. In 2016 IEEE-EMBS International Conference on Biomedical and Health Informatics (BHI) (pp. 288-291). IEEE.

3 Mohammad Reza Haji Samadi, Neil Cooke, "VOG-enhanced ICA for SSVEP response

detection from consumer-grade EEG", In Signal Processing Conference (EUSIPCO), 2013 Proceedings of the 22nd European, pp. 2025-2029, 2014.

4 Mohammad Reza Haji Samadi, Neil Cooke, "EEG signal processing for eye tracking", In Signal Processing Conference (EUSIPCO), 2013 Proceedings of the 22nd European, pp. 2030-2034, 2014.

5 Mohammad Reza Haji Samadi, Neil Cooke, "A novel approach for adaptive eeg artefact rejection and eog gaze estimation", In HCI International 2013, Springer, pp. 603-607, 2013.

List of References

[1] Sharma C, Dubey SK. Analysis of eye tracking techniques in usability and HCI perspective. In: Computing for Sustainable Global Development (INDIACom), 2014 International Conference on. IEEE; 2014. p. 607–612.

[2] Jeunet C, Vi C, Spelmezan D, N'Kaoua B, LOTTE F, Subramanian S. Continuous Tactile Feedback for Motor-Imagery based Brain-Computer Interaction in a Multitasking Context. In: INTERACT; 2015. .

[3] Baecker RM, Buxton WA. Readings in human-computer interaction. Elsevier Science; 2014.

[4] Nicolas-Alonso LF, Gomez-Gil J. Brain computer interfaces, a review. Sensors. 2012;12(2):1211–1279.

[5] Rosch JL, Vogel-Walcutt JJ. A review of eye-tracking applications as tools for training. Cognition, technology & work. 2013;15(3):313–327.

[6] Bradbury JW, Vehrencamp SL. Principles of animal communication. 1998;.

[7] Bulling A, Ward JA, Gellersen H, Tröster G. Eye movement analysis for activity recognition using electrooculography. Pattern Analysis and Machine Intelligence, IEEE Transactions on. 2011;33(4):741–753.

[8] Liu Y, Sourina O, Nguyen MK. Real-time EEG-based human emotion recognition and visualization. In: Cyberworlds (CW), 2010 International Conference on. IEEE; 2010. p. 262–269.

[9] Morimoto CH, Mimica MR. Eye gaze tracking techniques for interactive applications. Computer Vision and Image Understanding. 2005;98(1):4–24.

[10] Middendorf M, McMillan G, Calhoun G, Jones KS. Brain-computer interfaces based on the steady-state visual-evoked response. Rehabilitation Engineering, IEEE Transactions on. 2000;8(2):211–214.

[11] Vigário RN. Extraction of ocular artefacts from EEG using independent component analysis. Electroencephalography and clinical neurophysiology. 1997;103(3):395–404.

[12] Mognon A, Jovicich J, Bruzzone L, Buiatti M. ADJUST: An automatic EEG artifact detector based on the joint use of spatial and temporal features. Psychophysiology. 2011;48(2):229–240.

[13] Plöchl M, Ossandón JP, König P. Combining EEG and eye tracking: identification, characterization, and correction of eye movement artifacts in electroencephalographic data. Frontiers in human neuroscience. 2012;6.

[14] Sharpless S, Jasper H. Habituation of the arousal reaction. Brain. 1956;79(4):655–680.

[15] Vidal JJ. Toward direct brain-computer communication. Annual review of Biophysics and Bioengineering. 1973;2(1):157–180.

[16] Mihajlovic V, Grundlehner B, Vullers R, Penders J. Wearable, wireless EEG Solutions in daily life applications: what are we missing? Biomedical and Health Informatics, IEEE Journal of. 2015;19(1):6–21.

[17] Lopez A, Rodriguez I, Ferrero F, Valledor M, Campo J. Low-cost system based on electro-oculography for communication of disabled people. In: Multi-Conference on Systems, Signals & Devices (SSD), 2014 11th International. IEEE; 2014. p. 1–6.

[18] Mantiuk R, Kowalik M, Nowosielski A, Bazyluk B. Do-it-yourself eye tracker: Low-cost pupil-based eye tracker for computer graphics applications. Springer; 2012.

[19] Li D, Babcock J, Parkhurst DJ. openEyes: A Low-cost Head-mounted Eye-tracking Solution. In: Proceedings of the 2006 Symposium on Eye Tracking Research &Amp; Applications. ETRA '06. New York, NY, USA: ACM; 2006. p. 95–100. Available from: `http://doi.acm.org/10.1145/1117309.1117350`.

[20] Kim KN, Ramakrishna R. Vision-based eye-gaze tracking for human computer interface. In: Systems, Man, and Cybernetics, 1999. IEEE SMC'99 Conference Proceedings. 1999 IEEE International Conference on. vol. 2. IEEE; 1999. p. 324–329.

[21] Klin A, Jones W, Schultz R, Volkmar F, Cohen D. Visual fixation patterns during viewing of naturalistic social situations as predictors of social competence in individuals with autism. Archives of general psychiatry. 2002;59(9):809–816.

[22] Ettinger U, Kumari V, Crawford TJ, Davis RE, Sharma T, Corr PJ. Reliability of smooth pursuit, fixation, and saccadic eye movements. Psychophysiology. 2003;40(4):620–628.

[23] Fischer B, Ramsperger E. Human express saccades: extremely short reaction times of goal directed eye movements. Experimental Brain Research. 1984;57(1):191–195.

[24] Fischer B, Boch R. Saccadic eye movements after extremely short reaction times in the monkey. Brain research. 1983;260(1):21–26.

[25] Marg E. Development of electro-oculography: Standing potential of the eye in registration of eye movement. AMA archives of ophthalmology. 1951;45(2):169–185.

[26] Clarke AH, Teiwes W, Scherer H. Videooculography—an alternative method for measurement of three-dimensional eye movements. Oculomotor control and cognitive processes Amsterdam: Elsevier. 1991;p. 431–43.

[27] Bulling A, Roggen D, Tröster G. It's in your eyes: towards context-awareness and mobile HCI using wearable EOG goggles. In: Proceedings of the 10th international conference on Ubiquitous computing. ACM; 2008. p. 84–93.

[28] Wijesoma WS, Wee KS, Wee OC, Balasuriya AP, San KT, Soon LK. EOG based control of mobile assistive platforms for the severely disabled. In: Robotics and Biomimetics (ROBIO). 2005 IEEE International Conference on. IEEE; 2005. p. 490–494.

[29] Ubeda A, Ianez E, Azorín JM. Wireless and portable EOG-based interface for assisting disabled people. Mechatronics, IEEE/ASME Transactions on. 2011;16(5):870–873.

[30] Cleveland D, Cleveland JH, Norloff PL. Eye tracking method and apparatus. Google Patents; 1993. US Patent 5,231,674.

[31] Duchowski AT. A breadth-first survey of eye-tracking applications. Behavior Research Methods, Instruments, & Computers. 2002;34(4):455–470.

[32] Nieuwenhuys R, Voogd J, Van Huijzen C. The human central nervous system: a synopsis and atlas. Springer Science & Business Media; 2007.

[33] Horwitz B, Poeppel D. How can EEG/MEG and fMRI/PET data be combined? Human brain mapping. 2002;17(1):1–3.

[34] Berger H. Über das elektrenkephalogramm des menschen. European Archives of Psychiatry and Clinical Neuroscience. 1929;87(1):527–570.

[35] Sanei S, Chambers JA. EEG signal processing. John Wiley & Sons; 2013.

[36] Evans JR, Abarbanel A. Introduction to quantitative EEG and neurofeedback. Elsevier; 1999.

[37] Homan RW, Herman J, Purdy P. Cerebral location of international 10–20 system electrode placement. Electroencephalography and clinical neurophysiology. 1987;66(4):376–382.

[38] Teplan M. Fundamentals of EEG measurement. Measurement science review. 2002;2(2):1–11.

[39] Rockstroh B. Slow cortical potentials and behaviour. Urban & Schwarzenberg; 1989.

[40] Haynes JD, Rees G. Decoding mental states from brain activity in humans. Nature Reviews Neuroscience. 2006;7(7):523–534.

[41] Pfurtscheller G, Lopes da Silva F. EEG event-related desynchronization (ERD) and event-related synchronization (ERS). Electroencephalography: basic principles, clinical applications and related fields,. 1999;958.

[42] Farwell LA, Donchin E. Talking off the top of your head: toward a mental prosthesis utilizing event-related brain potentials. Electroencephalography and clinical Neurophysiology. 1988;70(6):510–523.

[43] Shah AS, Bressler SL, Knuth KH, Ding M, Mehta AD, Ulbert I, et al. Neural dynamics and the fundamental mechanisms of event-related brain potentials. Cerebral cortex. 2004;14(5):476–483.

[44] Lin Z, Zhang C, Wu W, Gao X. Frequency recognition based on canonical correlation analysis for SSVEP-based BCIs. Biomedical Engineering, IEEE Transactions on. 2006;53(12):2610–2614.

[45] Demos JN. Getting started with neurofeedback. WW Norton & Company; 2005.

[46] Klimesch W. EEG alpha and theta oscillations reflect cognitive and memory performance: a review and analysis. Brain research reviews. 1999;29(2):169–195.

[47] Craig A, McIsaac P, Tran Y, Searle A, et al. Alpha wave reactivity following eye closure: a potential method of remote hands free control for the disabled. Technology and Disability. 1999;10(3):187–194.

[48] Wolpaw JR, McFarland DJ, Vaughan TM. Brain-computer interface research at the Wadsworth Center. Rehabilitation Engineering, IEEE Transactions on. 2000;8(2):222–226.

[49] Bashashati A, Fatourechi M, Ward RK, Birch GE. A survey of signal processing algorithms in brain–computer interfaces based on electrical brain signals. Journal of Neural engineering. 2007;4(2):R32.

[50] Croft R, Barry R. Removal of ocular artifact from the EEG: a review. Neurophysiologie Clinique/Clinical Neurophysiology. 2000;30(1):5–19.

[51] Woestenburg J, Verbaten M, Slangen J. The removal of the eye-movement artifact from the EEG by regression analysis in the frequency domain. Biological psychology. 1983;16(1):127–147.

[52] Van den Berg-Lenssen M, Brunia C, Blom J. Correction of ocular artifacts in EEGs using an autoregressive model to describe the EEG; a pilot study. Electroencephalography and clinical Neurophysiology. 1989;73(1):72–83.

[53] Jung TP, Humphries C, Lee TW, Makeig S, McKeown MJ, Iragui V, et al. Extended ICA removes artifacts from electroencephalographic recordings. Advances in neural information processing systems. 1998;p. 894–900.

[54] Viola FC, Thorne J, Edmonds B, Schneider T, Eichele T, Debener S. Semi-automatic identification of independent components representing EEG artifact. Clinical Neurophysiology. 2009;120(5):868–877.

[55] Mayeli A, Zotev V, Refai H, Bodurka J. An automatic ICA-based method for removing artifacts from EEG data acquired during fMRI in real time. In: Biomedical Engineering Conference (NEBEC), 2015 41st Annual Northeast. IEEE; 2015. p. 1–2.

[56] Ghaderi F, Kim SK, Kirchner EA. Effects of eye artifact removal methods on single trial P300 detection, a comparative study. Journal of neuroscience methods. 2014;221:41–47.

[57] Subha DP, Joseph PK, Acharya R, Lim CM. EEG signal analysis: a survey. Journal of medical systems. 2010;34(2):195–212.

[58] Pfurtscheller G, Neuper C, Brunner C, da Silva FL. Beta rebound after different types of motor imagery in man. Neuroscience letters. 2005;378(3):156–159.

[59] Yazdani A, Ebrahimi T, Hoffmann U. Classification of EEG signals using Dempster Shafer theory and a k-nearest neighbor classifier. In: Neural Engineering, 2009. NER'09. 4th International IEEE/EMBS Conference on. IEEE; 2009. p. 327–330.

[60] Costantini G, Casali D, Todisco M. An SVM based classification method for EEG signals. In: Proceedings of the 14th WSEAS International Conference on Circuits, Corfu Island, Greece. vol. 2224; 2010. .

[61] Subasi A, Gursoy MI. EEG signal classification using PCA, ICA, LDA and support vector machines. Expert Systems with Applications. 2010;37(12):8659–8666.

[62] Haselsteiner E, Pfurtscheller G. Using time-dependent neural networks for EEG classification. Rehabilitation Engineering, IEEE Transactions on. 2000;8(4):457–463.

[63] Chiappa S, Bengio S. HMM and IOHMM modeling of EEG rhythms for asynchronous BCI systems. IDIAP; 2003.

[64] Tzallas AT, Tsipouras MG, Fotiadis D, et al. Epileptic seizure detection in EEGs using time–frequency analysis. Information Technology in Biomedicine, IEEE Transactions on. 2009;13(5):703–710.

[65] Bouchard G, Triggs B. The tradeoff between generative and discriminative classifiers. In: 16th IASC International Symposium on Computational Statistics (COMPSTAT'04); 2004. p. 721–728.

[66] Lotte F, Congedo M, Lécuyer A, Lamarche F. A review of classification algorithms for EEG-based brain–computer interfaces. Journal of neural engineering. 2007;4.

[67] Bishop CM. Pattern recognition and machine learning. springer; 2006.

[68] Cortes C, Vapnik V. Support-vector networks. Machine learning. 1995;20(3):273–297.

[69] Hyvärinen A, Karhunen J, Oja E. Independent component analysis. vol. 46. John Wiley & Sons; 2004.

[70] Cardoso JF. Infomax and maximum likelihood for blind source separation. 1997;.

[71] Lee TW, Girolami M, Sejnowski TJ. Independent component analysis using an extended infomax algorithm for mixed subgaussian and supergaussian sources. Neural computation. 1999;11(2):417–441.

[72] Bingham E, Hyvärinen A. A fast fixed-point algorithm for independent component analysis of complex valued signals. International journal of neural systems. 2000;10(01):1–8.

[73] Delorme A, Palmer J, Onton J, Oostenveld R, Makeig S, et al. Independent EEG sources are dipolar. PloS one. 2012;7(2):e30135.

[74] Langlois D, Chartier S, Gosselin D. An introduction to independent component analysis: InfoMax and FastICA algorithms. Tutorials in Quantitative Methods for Psychology. 2010;6(1):31–38.

[75] Zakeri Z, Assecondi S, Bagshaw A, Arvanitis TN. Influence of signal preprocessing on ICA-based EEG decomposition. In: XIII Mediterranean Conference on Medical and Biological Engineering and Computing 2013. Springer; 2014. p. 734–737.

[76] Moghimi S, Kushki A, Marie Guerguerian A, Chau T. A review of EEG-based brain-computer interfaces as access pathways for individuals with severe disabilities. Assistive Technology. 2013;25(2):99–110.

[77] Zhao Q, Zhang L, Cichocki A. EEG-based asynchronous BCI control of a car in 3D virtual reality environments. Chinese Science Bulletin. 2009;54(1):78–87.

[78] Al Mamun SA. Emotiv EPOC Bengali brain computer interface controlled by single emokey. In: International Conference on Emerging of Networking, Communication and Computing Technologies (ICENCCT 2014) Co-jointed with International Conference on Emerging Trends of Computer Science with Educational Technology (ICETCSET 2014)–Zurich, Switzerland on February; 2014. p. 22–23.

[79] Wang D, Mo F, Zhang Y, Yang C, Liu J, Chen Z, et al. Auditory evoked potentials in patients with major depressive disorder measured by Emotiv system. Bio-Medical Materials and Engineering. 2015;26(s1):917–923.

[80] Holewa K, Nawrocka A. Emotiv EPOC neuroheadset in brain-computer interface. In: Control Conference (ICCC), 2014 15th International Carpathian. IEEE; 2014. p. 149–152.

[81] Guneysu A, Akin HL. An SSVEP based BCI to control a humanoid robot by using portable EEG device. In: Engineering in Medicine and Biology Society (EMBC), 2013 35th Annual International Conference of the IEEE. IEEE; 2013. p. 6905–6908.

[82] Liu Y, Jiang X, Cao T, Wan F, Mak PU, Mak PI, et al. Implementation of SSVEP based BCI with Emotiv EPOC. In: Virtual Environments Human-Computer Interfaces and Measurement Systems (VECIMS), 2012 IEEE International Conference on. IEEE; 2012. p. 34–37.

[83] Bobrov P, Frolov A, Cantor C, Fedulova I, Bakhnyan M, Zhavoronkov A. Brain-computer interface based on generation of visual images. PloS one. 2011;6(6):e20674.

[84] Brennan C, McCullagh P, Lightbody G, Galway L, Trainor D. Quantifying brain activity for task engagement. In: Bioinformatics and Biomedicine (BIBM), 2014 IEEE International Conference on. IEEE; 2014. p. 8–11.

[85] Chowdhury P, Kibria Shakim S, Karim MR, Rhaman MK. Cognitive efficiency in robot control by Emotiv EPOC. In: Informatics, Electronics & Vision (ICIEV), 2014 International Conference on. IEEE; 2014. p. 1–6.

[86] Gull MA, Iqbal J, Tiwana MI. Spatial Temporal based Classification for Antebrachium and Carpus Movement of EEG Data Using Emotive Head set. Journal of Biomedical Engineering and Medical Imaging. 2015;1(6).

[87] Chowdhury P, Shakim SK. Optimizing cognitive efficiency of emotiv EPOC and controlling wheelchair through it. BRAC University; 2014.

[88] Friedrichs F, Igel C. Evolutionary tuning of multiple SVM parameters. Neurocomputing. 2005;64:107–117.

[89] Anderson CW, Stolz EA, Shamsunder S. Multivariate autoregressive models for classification of spontaneous electroencephalographic signals during mental tasks. Biomedical Engineering, IEEE Transactions on. 1998;45(3):277–286.

[90] Palaniappan R. Brain computer interface design using band powers extracted during mental tasks. In: Neural Engineering, 2005. Conference Proceedings. 2nd International IEEE EMBS Conference on. IEEE; 2005. p. 321–324.

[91] Garcia G, Ebrahimi T, Vesin JM. Classification of EEG signals in the ambiguity domain for brain-computer interface applications. EUSIPCO; 2002. .

[92] del R Millan J, Mourino J, Abiloni F, Cincotti F, Varsta M, Heikkonen J. Local neural classifier for EEG-based recognition of mental tasks. In: Neural Networks, 2000. IJCNN 2000, Proceedings of the IEEE-INNS-ENNS International Joint Conference on. vol. 3. IEEE; 2000. p. 632–636.

[93] Haselsteiner E, Pfurtscheller G. Using time-dependent neural networks for EEG classification. Rehabilitation Engineering, IEEE Transactions on. 2000;8(4):457–463.

[94] Lemm S, Schäfer C, Curio G. BCI competition 2003-data set III: probabilistic modeling of sensorimotor μ rhythms for classification of imaginary hand movements. Biomedical Engineering, IEEE Transactions on. 2004;51(6):1077–1080.

[95] Cincotti F, Scipione A, Timperi A, Mattia D, Marciani M, Millan J, et al. Comparison of different feature classifiers for brain computer interfaces. In: Neural Engineering, 2003. Conference Proceedings. First International IEEE EMBS Conference on. IEEE; 2003. p. 645–647.

[96] Felzer T, Freisieben B. Analyzing EEG signals using the probability estimating guarded neural classifier. Neural Systems and Rehabilitation Engineering, IEEE Transactions on. 2003;11(4):361–371.

[97] LaFleur K, Cassady K, Doud A, Shades K, Rogin E, He B. Quadcopter control in three-dimensional space using a noninvasive motor imagery-based brain–computer interface. Journal of neural engineering. 2013;10(4):046003.

[98] Tello RM, Muller SM, Bastos-Filho T, Ferreira A. A comparison of techniques and technologies for SSVEP classification. In: Biosignals and Biorobotics Conference (2014): Biosignals and Robotics for Better and Safer Living (BRC), 5th ISSNIP-IEEE. IEEE; 2014. p. 1–6.

[99] Müller-Putz GR, Scherer R, Brauneis C, Pfurtscheller G. Steady-state visual evoked potential (SSVEP)-based communication: impact of harmonic frequency components. Journal of neural engineering. 2005;2(4):123–130.

[100] Wass SV, Smith TJ, Johnson MH. Parsing eye-tracking data of variable quality to provide accurate fixation duration estimates in infants and adults. Behavior Research Methods. 2013;45(1):229–250.

[101] Delorme A, Makeig S. EEGLAB: an open source toolbox for analysis of single-trial EEG dynamics including independent component analysis. Journal of neuroscience methods. 2004;134(1):9–21.

[102] Lalor EC, Kelly SP, Finucane C, Burke R, Smith R, Reilly RB, et al. Steady-state VEP-based brain-computer interface control in an immersive 3D gaming environment. EURASIP journal on applied signal processing. 2005;2005:3156–3164.

[103] Riccio A, Mattia D, Simione L, Olivetti M, Cincotti F. Eye-gaze independent EEG-based brain–computer interfaces for communication. Journal of neural engineering. 2012;9(4):045001.

[104] Brunner P, Joshi S, Briskin S, Wolpaw J, Bischof H, Schalk G. Does the'P300'speller depend on eye gaze? Journal of neural engineering. 2010;7(5):056013.

[105] Manabe H, Fukumoto M, Yagi T. Direct Gaze Estimation Based on Non-linearity of EOG. 2015;.

[106] Belkacem AN, Hirose H, Yoshimura N, Shin D, Koike Y. Classification of four eye directions from EEG signals for eye-movement-based communication systems. Journal of Medical and Biological Engineering. 2014;34(6):581–588.

[107] Belkacem AN, Shin D, Kambara H, Yoshimura N, Koike Y. Online classification algorithm for eye-movement-based communication systems using two temporal EEG sensors. Biomedical Signal Processing and Control. 2015;16:40–47.

[108] Ramli R, Arof H, Ibrahim F, Mokhtar N, Idris MYI. Using finite state machine and a hybrid of EEG signal and EOG artifacts for an asynchronous wheelchair navigation. Expert Systems with Applications. 2015;42(5):2451–2463.

[109] Ma J, Zhang Y, Cichocki A, Matsuno F. A Novel EOG/EEG Hybrid Human–Machine Interface Adopting Eye Movements and ERPs: Application to Robot Control. Biomedical Engineering, IEEE Transactions on. 2015;62(3):876–889.

[110] Johns M, Crowley K, Chapman R, Tucker A, Hocking C. The effect of blinks and saccadic eye movements on visual reaction times. Attention, Perception, & Psychophysics. 2009;71(4):783–788.

[111] Welch P. The use of fast Fourier transform for the estimation of power spectra: a method based on time averaging over short, modified periodograms. Audio and Electroacoustics, IEEE Transactions on. 1967;15(2):70–73.

[112] García V, Mollineda RA, Sánchez JS. Index of balanced accuracy: A performance measure for skewed class distributions. In: Pattern Recognition and Image Analysis. Springer; 2009. p. 441–448.

[113] Savage SW, Potter DD, Tatler BW. Does preoccupation impair hazard perception? A simultaneous EEG and Eye Tracking study. Transportation research part F: traffic psychology and behaviour. 2013;17:52–62.

[114] Buck JR, Daniel MM, Singer AC. Computer explorations in signals and systems using MATLAB. Prentice-Hall, Inc.; 1997.

[115] Hoyer PO, Hyvärinen A. Independent component analysis applied to feature extraction from colour and stereo images. Network: Computation in Neural Systems. 2000;11(3):191–210.

[116] Kwon OW, Lee TW. Phoneme recognition using ICA-based feature extraction and transformation. Signal Processing. 2004;84(6):1005–1019.